Measurements of HONO in Southern Ontario using Long Path Absorption Photometry

Jeremy JB Wentzell

A DISSERTATION SUBMITTED TO THE FACULTY OF GRADUATE STUDIES

IN PARTIAL FULFILMENT OF THE REQUIREMENTS

FOR THE DEGREE OF

DOCTOR OF PHILOSOPHY

GRADUATE PROGRAMME IN CHEMISTRY

YORK UNIVERSITY

TORONTO, ONTARIO

November 2009

Your file Votre référence
ISBN: 978-0-494-64971-8
Our file Notre référence
ISBN: 978-0-494-64971-8

Abstract

A highly sensitive Long Path Absorption Photometer (LOPAP) was constructed and used to investigate HONO chemistry at rural and urban sites in Southern Ontario. The instrument utilizes liquid core waveguides (LCW's) to achieve part per trillion (pptv) sensitivities. The 3σ detection limit of the instrument was determined to be 5 pptv. The only interference of note was NO_2 and it was quantitatively removed by the subtraction of the signal due to NO_2 in a second channel.

The instrument was deployed in Southern Ontario for the measurement of HONO at three different measurement sites, one urban (Toronto), one forested (Borden) and one semi-rural (BAQS-Met, Harrow super site). High concentrations of HONO were observed at the urban site, which was located next to a major highway. These concentrations can largely be explained by traffic emissions from the highway. While the largest HONO mixing ratios measured were found at the urban sampling site, high $HONO/NO_2$ ratios were observed at the forested site (as high as 16%, mean=1.9%). The forested site (Borden, Ontario) was a very clean site with mean NO_x concentrations of only 1.5 ppbv. The mean first order conversion rate of NO_2 to HONO during the night-time hours at this site was found to be 1.4×10^{-6} s^{-1}, two orders of magnitude smaller than HONO photolysis at midday. Since measurable amounts of HONO were present during the midday hours this lead to the conclusion that there was a very efficient conversion process of NO_2 to HONO in the forested environment. High daytime concentrations of HONO were also observed at the Harrow supersite during the BAQS-Met campaign. These

concentrations were also well in excess of predicted HONO values using traditional HONO chemistry,

Analysis of the daytime data from both the forested site and BAQS-Met suggests a HONO source with a dependence on UV radiation, NO_2 and H_2O mixing ratio. The data set at Harrow, a site impacted by different pollution sources depending on wind direction, produced a variety of apparent rate constants for HONO production in the range of 2.9-7.8 x 10^{-13} $cm^3molec^{-1}s^{-1}$, which suggests that the HONO production was heterogeneous. In contrast at the forested site at Borden the apparent rate constants varying from only 1.2x10^{-13} to 1.6 x 10^{-13} $cm^3molec^{-1}s^{-1}$. These are similar to one reported (but disputed) value for a gas phase process involving photoexcited NO_2 in a reaction with water vapour which may yield HONO, but the small variation in rate is more likely a result of the lack of dependence of the nature of the fetch on wind direction at Borden.

ACKNOWLEDGEMENTS

There are many people who helped to make this work possible and for this I owe them a debt of gratitude.

My supervisor, Prof. Geoff Harris, without his help, guidance and support with this work, it would not have been possible.

My supervisory committee, Prof. Don Hastie and Prof. Rob McLaren for their helpful comments and advice.

A very special thank you is necessary for Dr. Corinne Schiller, for her helpful advice about research, writing and life in general. Without her support (and thesis editing) I don't know where I'd be.

I would like to thank my many lab mates over the years (Ian, J.F., Kristin, Andrew and many others) for assistance with experiments and making the lab such a great place to work. I would also like to thank all of the members at CAC over the years that provided helpful discussion and loaned me equipment. The most important member of CAC is and always has been Carol. Thank you for making everything easier than it otherwise would have been.

There are many individuals at both the Ontario Ministry of the Environment and Environment Canada who helped make this research possible by providing measurements and helpful comments. Thank you to Dr. Nick Karellas and Al Melanson at O.M.E. and Dr. Ralf Staebler and Kathy Hayden at E.C. for their help.

A special thank you to my family (Mom, Dad, Jess, Nana, Ron and Colleen) for their support and always telling me my thesis would be completed when I thought it wouldn't.

The most important thank you goes to my "better half" Karen for her unwavering support and patience during my degree. I can honestly say I would not be where I am now without her.

TABLE OF CONTENTS

LIST OF TABLES

LIST OF FIGURES

1 Introduction

1.1 Nitrous Acid (HONO)

Nitrous acid plays an important role in the atmospheric chemistry of the troposphere. It usually follows a diurnal cycle where the concentration of HONO increases at night and is destroyed in the morning through photolysis (R 1). The photolysis of HONO results in the production of the hydroxyl radical and may be the dominant early morning source of the hydroxyl radical [Platt et al., (1980); Harris et al., (1982); Lammel and Cape, (1996); Alicke et al., (2003); Kleffmann et al., (2005)].

$$\mathbf{HONO + h\upsilon(300 - 400\ nm) \rightarrow NO + OH} \qquad \mathbf{R\ 1}$$

Reaction 1 can cause a morning spike in hydroxyl radical concentrations, which begins the oxidation of hydrocarbons. Besides HONO photolysis, OH can be produced by photolysis of ozone and formaldehyde (followed by the reaction of HO_2 with NO). It is also a secondary product of the ozonolysis of alkenes. Table 1 lists the reactions involved in OH production. During the day the OH production is dominated by O_3 photolysis however in the morning, O_3 concentrations (due to loss by dry deposition during the night) and photolysis rates are low, formaldehyde and nitrous acid photolysis become the dominant sources. Thus HONO can have a large impact on the morning OH production rates.

Table 1: Reactions leading to OH production in the troposphere [Finlayson-Pitts and Pitts, (2000)].

Chemical Processes
$O_3 + h\nu\ (\lambda < 340\ nm) \rightarrow O(^1D) + O_2(^1\Delta_g)$
$O(^1D) + H_2O \rightarrow OH + OH$
$HONO + h\nu\ (\lambda < 400\ nm) \rightarrow OH + NO$
$HCHO + h\nu\ (\lambda < 370\ nm) \rightarrow H + HCO$
$\rightarrow H_2 + CO$
$H + O_2 + M \rightarrow HO_2 + M$
$HCO + O_2 \rightarrow HO_2 + CO$
$HO_2 + NO \rightarrow OH + NO_2$
$Alkene + O_3 \rightarrow \ldots \rightarrow OH + other\ products$

In urban environments night-time HONO mixing ratios can reach several parts per billion (ppbv), while in rural or remote environments 10's to 100's of parts per trillion (pptv) are reached. A recent study of HONO in a German forest found that 33% of the daytime OH budget was attributed to HONO, surpassing all other OH formation pathways [Kleffmann et al., (2005)]. Similar results have been found to be widespread now that very sensitive methods are available. Nitrous acid also has an indirect effect on other oxidants. A modelling study [Harris et al., (1982)] found large increases in O_3 formation earlier in the day when a given amount of HONO was included in the model. Their study showed that the inclusion of an initial 5 ppbv of HONO led to a given amount of ozone 45 minutes earlier in the day than when HONO was not included. When 10 ppbv of HONO was included, the same ozone level was reached 75 minutes earlier than in the absence of HONO in the model. While the addition of HONO did not affect the overall ozone maximum,

which is governed by the overall amounts of NO_x and hydrocarbons in the system and is dependent on whether the regime is NO_x or hydrocarbon limited, HONO was found to have a large effect on the integrated dose of ozone received by an exposed population. The influence of HONO on oxidants in plumes in less polluted environments has also been investigated [Staffelbach et al., (1997a); Staffelbach et al., (1997b)]. They determined that while HONO was important to early morning oxidant formation only small overall changes to OH and O_3 were found.

Nitrous acid is not only important in atmospheric chemistry, it has been suggested that it may be harmful to human health or may react to produce products harmful to human health. Nitrous acid can react with amines to produce carcinogenic nitrosamines (R 2) [Hanst et al., (1977); Pitts et al., (1978)].

$$\mathbf{R_2NH + HONO \rightarrow R_2NNO + H_2O} \qquad \mathbf{R\ 2}$$

In addition, chamber studies have shown HONO can adversely affect lung function and tear fluid in the eye [Rasmussen et al., (1995)]. Studies of HONO in indoor environments have also suggested that HONO produced from gas cooking appliances could lead to decreased lung function [Jarvis et al., (2005)].

1.2 Sources of HONO

The sources of HONO in the atmosphere are not fully understood. Measurements indicate that the sources of HONO have been underestimated [Kleffmann et al., (2005)]. Daytime measurements of HONO have found concentrations well in excess of what can be explained by classical HONO chemistry. In this section the current understanding of HONO sources is examined.

Nitrous acid can be formed homogeneously from the recombination of NO and OH and a third body (R 3).

$$NO + OH + M \rightarrow HONO + M \qquad \text{R 3}$$

This reaction can be relevant during periods of high OH, however in the absence of other sources HONO mixing ratios would only be expected to be a few pptv. Another gas phase reaction which appears to be too slow to produce significant amounts of HONO is the NO_2 reaction with water (R4).

$$NO_2 + H_2O \rightarrow HONO + OH \qquad \text{R 4}$$

$$NO_2^* + H_2O \rightarrow HONO + OH \qquad \text{R 5}$$

Svensson et al., (1987) found the reaction of NO_2 with water vapour (R 4) to be too slow in the gas phase to be atmospherically relevant [Svensson et al., (1987)]. Crutzen (cited in Crowley and Carl, (1997)) suggested that the reaction might occur more rapidly when NO_2 is photo-excited (R 5). Reaction 5 was examined by Crowley and Carl, (1997) using NO_2 that had been photo-excited to the red of the dissociation threshold at 432-449 nm and 532 nm. The photoexcited NO_2 is a mix of the B^2B_1 and A^2B_2 excited electronic states in addition to the X^2A_1 ground electronic state [Thornton et al., (2000)]. They determined an upper limit of for the rate constant of 1.2×10^{-14} cm^3 $molec^{-1}$ s^{-1} implying that R 5 is too slow to be relevant under atmospheric conditions. However the

reaction was re-examined by Li et al., (2008) using excitation of the NO_2 in the region between 560 and 640 nm. Their results showed the reaction proceeding at a rate an order of magnitude larger than the upper limit reported by Crowley and Carl, (1997). This discrepancy has yet to be resolved, but if the Li et al., (2008) report is correct, R5 may be very important under some conditions.

Nitrous acid has been shown to be formed heterogeneously on surfaces in the presence of NO_2 and H_2O (R 6, R 7) [Lammel and Perner, (1988); Junkermann and Ibusuki, (1992); Ammann et al., (1998); Barney and Finlayson-Pitts, (2000)].

$$\mathbf{NO_2(g) + NO(g) + H_2O(l) \rightarrow 2HONO(g)} \qquad \textbf{R 6}$$

$$\mathbf{2NO_2(g) + H_2O(l) \rightarrow HONO(g) + HNO_3(ads)} \qquad \textbf{R 7}$$

Chamber experiments have also shown HONO production to be first order in NO_2 and H_2O, [Svensson et al., (1987); Jenkin et al., (1988); Kleffmann et al., (1998)] but independent of NO, suggesting that R 7 is more important that R 6 in the formation of HONO. While HONO production from (R 7) is second order in the bulk aqueous phase [Lee and Schwartz, (1981)] as the stoichiometry suggests, production of HONO from the heterogeneous reaction is found to be first order in NO_2 due to limitations by physical mass transfer of the reactant.

Nitrous acid may also be directly emitted from combustion. Several traffic studies have been performed and the measured ratio of $HONO/NO_x$ emitted was found to be between ~0.03-1.0%.[Kirchstetter et al., (1996); Kurtenbach et al., (2001); Kleffmann et al., (2003)] Some part of the variability in the measured emission ratios is likely due to differences in automobile fleets between Europe and North America. Kirchstetter et al., (1996) found the $HONO/NO_x$ ratios to be 0.06% in experiments performed in North America, significantly lower than that found by Kurtenbach et al., (2001) in the European fleet which is comprised of a larger number of diesel

engines. Nitrous acid has also been detected by Fourier Transform Infrared Spectroscopy (FTIR) as an important product of biomass burning (private communication I. Burling. (2009)).

In recent years it has become apparent that there are other daytime sources of HONO. During the 2003 ECHO study [Kleffmann et al., (2005)] relatively large daytime mixing ratios were measured under a forest canopy. When compared with modelled data of known classical HONO chemistry (R 1, R 3, R 6) it was determined that an additional daytime HONO source of approximately 500 pptv hr^{-1} would be needed to explain the observed concentrations. George et al., (2005) suggested that production of HONO from the uptake of NO_2 on organic surfaces encountered in the troposphere is highly enhanced when the system is irradiated by light between 300-420 nm if electron donors such as phenolic compounds are present.

In experiments performed by George et al., (2005) 4-benzoylbenzoic acid (4-BBA) was used as the light absorbing species and excited to a triplet state. The 4-BBA then underwent an electron transfer reaction with the phenol shown in Figure 1. Nitrogen dioxide then acted as an electron acceptor leading to production of HONO and regeneration of the 4-BBA. The reaction was performed in a flow reactor coated with the phenol and the absorber molecule, in this case 4-BBA. Nitrogen dioxide was then introduced to the reactor in a flow of zero air at 20% relative humidity. The yield of HONO from this reaction using 4-BBA as the photo absorber was found to be very high (between 80-100% relative to NO_2) for NO_2 mixing ratios between 0 and 20 ppbv, while there was no yield from the dark reaction. Their proposed reaction is shown in Figure 1.

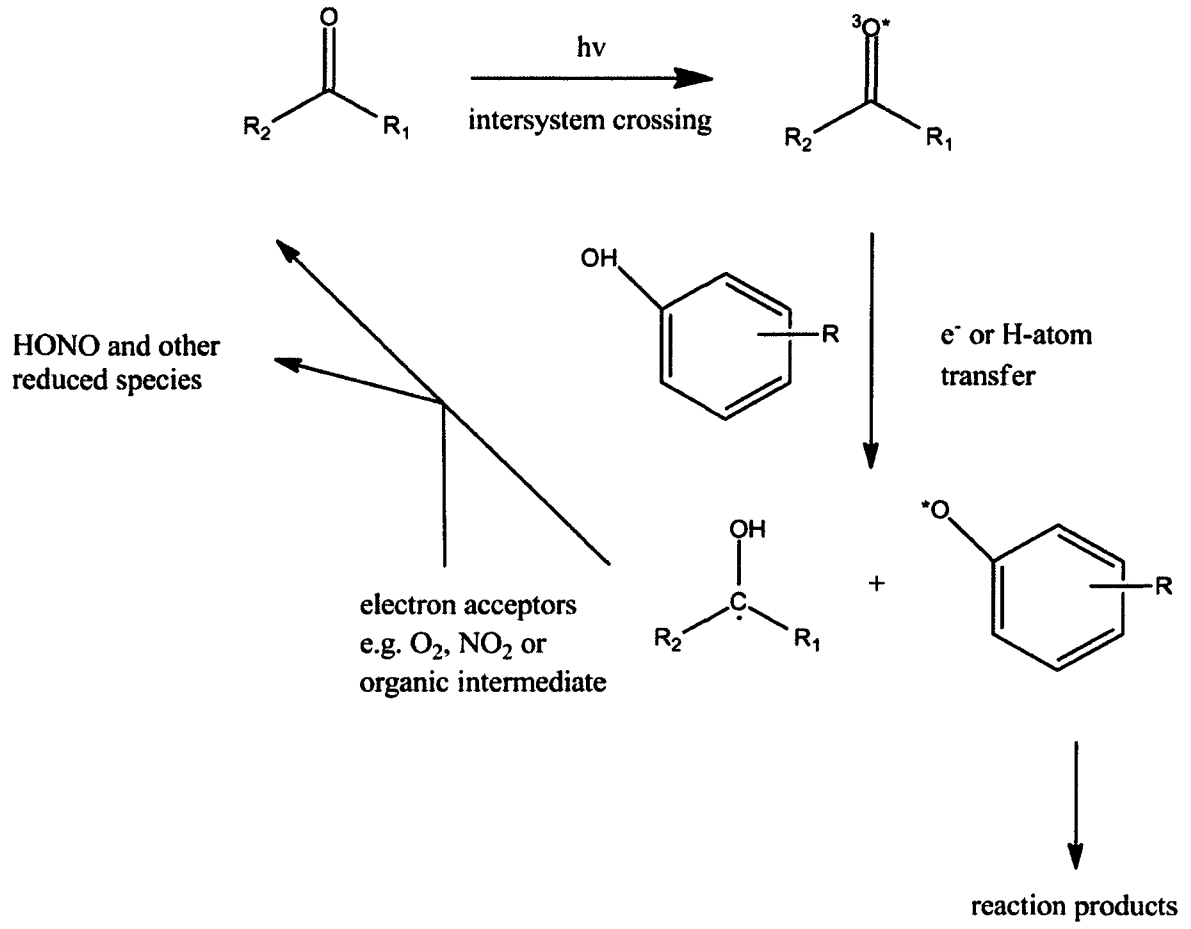

Figure 1: Proposed reaction mechanism for the photoreduction of NO_2 to HONO in the presence of 4-BBA (absorbing photosensitizer) and substituted phenol (electron donor) [George et al., (2005)].

Other laboratory studies have suggested possible HONO sources from organic surfaces. Stemmler et al., (2006) suggested photo reduction of NO_2 on humic acid type compounds could be a potential surface source of HONO, with the mechanism for the reaction being similar to that of George et al., (2005). They demonstrated that NO_2 could be very efficiently converted into HONO on humic acid surfaces. Humic acids are ubiquitous in soils and while NO_2 (17 ppbv) reacting on humic surfaces in the dark yielded only small quantities of HONO (2.5×10^{10} molec $cm^{-2}s^{-1}$), when irradiated with UV radiation (300-420 nm), HONO formation increased by a factor of 30. Stemmler et al., (2006) described the mechanism of formation with the following three reactions.

$$HA + h\nu \rightarrow A^{RED} + X \qquad \text{R 8}$$

$$A^{RED} + X \rightarrow A' \qquad \text{R 9}$$

$$A^{RED} + NO_2 \rightarrow HONO + A' \qquad \text{R 10}$$

The humic acid (HA) has it's reductive centres activated (A^{RED}) by the UV radiation, (R 8). At this point two routes are possible, either the centres are deactivated (R 9) or they can react with NO_2 to form HONO (R 10). The compound X represents any reducible compound other than NO_2 that could inhibit the photolytically excited reductive centres of the humic acid from reacting with NO_2. The analogous reaction on humic acid aerosol was found to be unimportant under most atmospheric conditions [Stemmler et al., (2007)] as uptake coefficients for NO_2 were found to smaller than that for a humic acid bulk sample.

Bejan et al., (2006) suggested a mechanism of HONO production involving photolysis of ortho-nitrophenols. The proposed reaction is shown in Figure 2. The formation of HONO was found to be linearly dependant on photolysis light intensity and the reactant concentration. Nitrophenols can be found in both the gas and liquid phase [Harrison et al., (2005)] and are produced by direct emission, hydrolysis of pesticides and secondary formation through nitration of phenols, which can occur in either the gas or liquid phase. Another proposed secondary source of nitrophenols is the transformation of benzaldehyde under photochemical smog conditions. It is believed that atmospheric formation accounts for over one-third of the nitrophenols in the atmosphere and likely a higher fraction in remote regions. Photolysis has been shown to be a dominant process for removal of nitrophenols during the daytime [Vione et al., (2009)].

Ndour et al., (2008) found that NO_2 could efficiently be taken up on mineral dust and converted into HONO. Mixed TiO_2-SiO_2 Saharan dust and Arizona Test Dust were exposed to NO_2

in an illuminated flow reactor (light source 300-420 nm, 24% relative humidity).The conversion efficiency of NO_2 to HONO (up to 100%) appeared to vary with the content of TiO_2 in the dust. Exposure of 24 ppbv of NO_2 to a sample of ground Saharan sand (5 wt.% TiO_2), irradiated with UV radiation (300-420 nm) produced an 80% yield of HONO. The exact mechanism of NO_2 reduction to HONO on TiO_2 surfaces is as yet unknown.

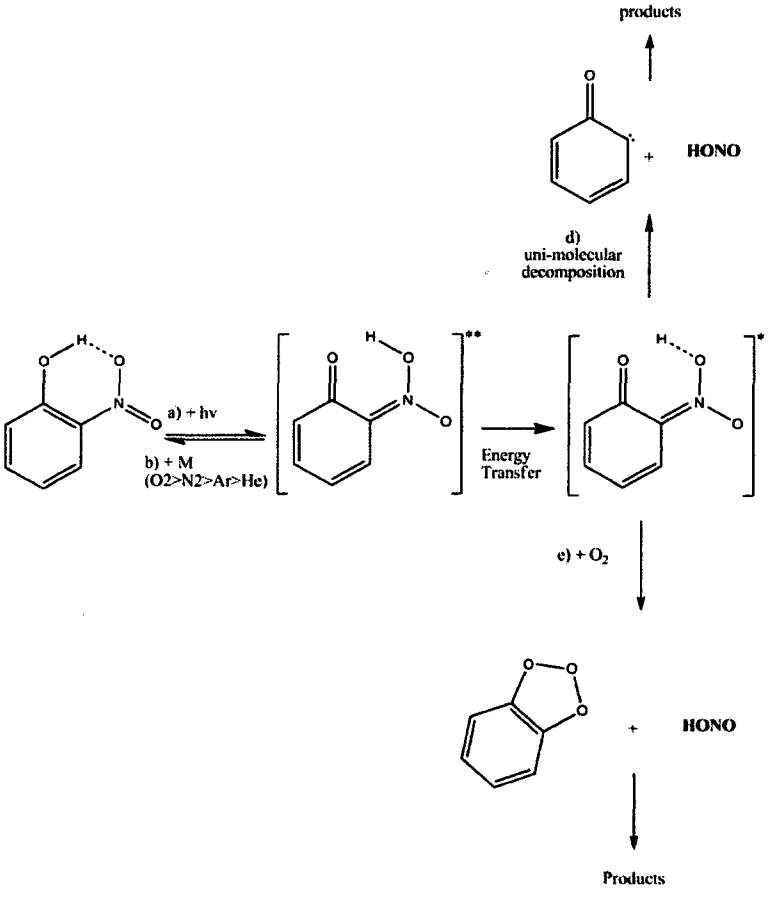

Figure 2: Proposed mechanism of ortho-nitrophenol photolysis to form HONO [Bejan et al., (2006)].

With a large number of important new daytime HONO formation mechanisms proposed in the past several years, further laboratory and field work need to be done to determine the relative importance of each, as well as determine any other potential missing sources.

1.3 Nitrous Acid Loss Processes

The dominant loss process for HONO during the daytime hours is photolysis (R 1). Typical lifetimes vary from 10 to 20 minutes at midday during the summer months at mid latitude [Stutz et al., (2002)]. Lifetimes can be significantly extended on heavily cloudy days by the attenuation of solar radiation.

Nitrous acid may also be lost by the homogeneous reaction with OH radicals (R 11).

$$HONO + OH \rightarrow H_2O + NO_2 \qquad \text{R 11}$$

This reaction can be important near midday however the rate constant is too small for it to be competitive with photolysis [Jenkin and Cox, (1987)] accounting for at most 10% of the total loss rate. Nitrous acid may also be lost by the gas phase self reaction (R 12) [Kaiser and Wu, (1977)].

$$HONO + HONO \rightarrow NO_2 + NO + H_2O \qquad \text{R 12}$$

While R 12 may be relevant during laboratory experiments, where HONO concentrations are high, it is not significant under atmospheric conditions [Kaiser and Wu, (1977); Mebel et al., (1998)].

In addition to the loss of HONO due to homogeneous reactions in the atmosphere, it may also be lost to dry and wet deposition. Dry deposition has been observed over grass surfaces, [Stutz et al., (2002); Harrison and Kitto, (1994); Harrison et al., (1996)]. Stutz et al., (2002) estimated the deposition velocity of HONO to be 0.3 cm s^{-1} from gradient measurements using DOAS over a grass surface. Nitrous acid uptake by cloud water has also been shown to be an important sink [Cape et al., (1992)] or at least a reservoir [Cape et al., (1997)] making the measurement of HONO during foggy conditions challenging. Increased moisture on sampling inlet surfaces makes HONO measurement difficult due to artefact formation under conditions of high liquid water content (private communication M. Sörgel University Bayreuth, 2008). While HONO

can be lost to deposition, deposition of NO_2 on plant stomata has also been suggested as a possible daytime source of HONO. However, laboratory studies indicate that HONO uptake on plant stomata [Schimang et al., (2006)] is a net loss process. Many types of plants quickly metabolize the NO_2^- produced when HONO is taken up, creating a net sink. The uptake of HONO by plants also appears to have a negative effect on their photosynthetic ability. Experiments performed specifically on the Scots Pine [Sakugawa and Cape, (2007)] under conditions simulating an urban environment showed a negative effect on the photosynthetic ability of the pine needles caused by both HONO uptake onto the needles and OH oxidation from HONO photolysis.

1.4 Nitrous Acid measurement techniques

Nitrous acid in the atmosphere was initially unambiguously measured by Perner and Platt in the late 1970's using differential optical absorption spectroscopy (DOAS) [Platt et al., (1980); Perner and Platt, (1979)]. Since that time, numerous techniques have been developed to measure HONO. Table 2 outlines the various techniques, investigators and detection limits achieved by their technique.

Table 2: List of techniques for measuring HONO with detection limits.

Technique	Gas Phase or Liquid Sampling	Detection Limit (DL)	Reference
DOAS	Gas Phase	≥ 100 pptv (pathlength dependant)	Platt et al., (1980); Harris et al., (1982); Alicke et al., (2003); Stutz et al., (2002); Perner and Platt, (1979); Stutz et al., (2000); Alicke et al., (2002); Stutz et al., (2004)
Tunable Diode Laser Absorption Spectroscopy (TDLAS)	Gas Phase	500 pptv, 200 pptv	Schiller et al., (2001); Li et al., (2008)
Long Path Absorption Spectroscopy (LOPAP)	Liquid Sampling	≥ 1 pptv	Heland et al., (2001); Kleffmann et al., (2002)
Photofragmentation Laser Induced Fluorescence (PF-LIF)	Gas Phase	10 pptv	Rogers and Davis, (1989); Liao et al., (2006-05-10); Liao et al., (2006)
Chemical Ionization Mass Spectrometry (CIMS)	Gas Phase	60 pptv	Longfellow et al., (1998); Hirokawa et al., (2009)
Cavity Ringdown Spectroscopy	Gas Phase	~1 ppbv	Wang and Zhang, (2000)
2,4-Dinitrophenylhydrazine (DNPH) Derivitization HPLC Measurement	Liquid Sampling	≤ 5 pptv	Zhou et al., (1999)
Denuder Sampling IC Measurement	Liquid Sampling	1-10 pptv	Genfa et al., (2003); Febo et al., (1995b); Vecera and Dasgupta, (1991)
Proton Transfer Mass Spectrometry (PTR-MS)	Gas Phase	~100 pptv	Wisthaler et al., (2003)
SA/NED HPLC Measurement	Liquid Sampling	1 pptv	Huang et al., (2002); Wall et al., (2006)

The most established of the techniques for measuring HONO is Differential Optical Absorption Spectroscopy. It has excellent selectivity and since it is open path it is free of sampling artefacts. The main limitation of DOAS is its sensitivity, with a detection limit of ~ 100 pptv. The high detection limits make ambient measurements possible only at night-time and in polluted urban environments, as daytime HONO mixing ratios in non-urban environments are typically below the DOAS detection limit.

Tunable Diode Laser Absorption Spectroscopy (TDLAS) has been used successfully on two occasions to measure HONO. Like DOAS, the usefulness of TDLAS is limited by detection limit ≥200 pptv [Li et al., (2008)]. Schiller et al., (2001) also noted that sampling lines need to be used, leading to possible artefact formation. Cavity Ring Down (CRD) is a spectroscopic technique which has recently been tested in the laboratory [Wang et al., (2007)]. Detection limits attained were only ~1 ppbv, limiting the usefulness of CRD to highly polluted environments.

In addition to the optical absorption techniques discussed above, laser induced fluorescence has also been employed as a technique to measure HONO. The technique involves photolysis of HONO and measures OH by laser induced fluorescence, resulting in an excellent detection limit of a few pptv [Rogers and Davis, (1989); Liao et al., (2006)]. The technique does however suffer the shortcoming of using a 282 nm excitation laser which can also photolyze O_3. The O^1D product can then react with water to form artefact OH. This interference limits the usefulness of the technique to regions with low humidity such as polar environments or the upper troposphere. Changing the probe beam wavelength to 308 nm has been suggested as a method for decreasing the O_3 interference.

Chemical Ionization Mass Spectrometers (CIMS) and Proton-Transfer Mass Spectrometers (PTR-MS) have been successfully used to measure HONO. Proton-Transfer Mass Spectrometry is a

technique that uses H_3O^+ as the ion source. When used in conjunction with a Selective Ion Flow Drift Tube (SIFDT) the detection limit of the technique was found to be~100 pptv measured as NO^+ [Wisthaler et al., (2003)]. Chemical Ionization Mass Spectrometry (CIMS) measurements of HONO have been performed in the laboratory using an SF_6^- reagent ion, to measure HONO solubility [Longfellow et al., (1998)]. A recent laboratory study has also shown SO_2Cl^- to be a suitable reagent ion for the atmospheric measurement of HONO with reported detection limits of 60 pptv [Hirokawa et al., (2009)].

Liquid sampling techniques have become common for measurement of HONO where HONO is stripped from the gas phase and is detected as NO_2^- in solution. Denuder Ion Chromatography (IC), High Pressure Liquid Chromatography (HPLC), and Long Path Absorption Photometry (LOPAP) measurements all detect HONO as NO_2^-. The denuder IC systems rely on the solubility of HONO (and other acidic gases) in a neutral or alkaline solution on the surface of the denuder. This liquid is collected and pre-concentrated using a column to assure a suitable detection limit. The NO_2^- ion concentrations are then analyzed by ion chromatography. Unlike the IC technique, in the HPLC system NO_2^- is not measured directly. HONO is sampled in a neutral or alkaline solution as with denuder technique followed by derivitization of the NO_2^- into a compound such as an azo dye which can be measured by the HPLC's UV/VIS detector. Both chromatographic detection systems suffer from varying interferences such as NO_2 which can react with the sampling solutions to form HONO. The LOPAP is another liquid sampling technique and will be discussed in detail in the next section.

2 Long Path Absorption Photometer (LOPAP)

The long path absorption photometer (LOPAP) was developed in the Kleffmann group at the University of Wuppertal, Germany [Heland et al., (2001); Kleffmann et al., (2002)]. It is a liquid scrubbing technique that relies on the reaction of NO_2^- in solution with sulfanilamide (SA) to form a diazonium ion, which can then be reacted with 1-napthylethylene-diamine (NED) to form a highly absorbing azo-dye (Figure 3).

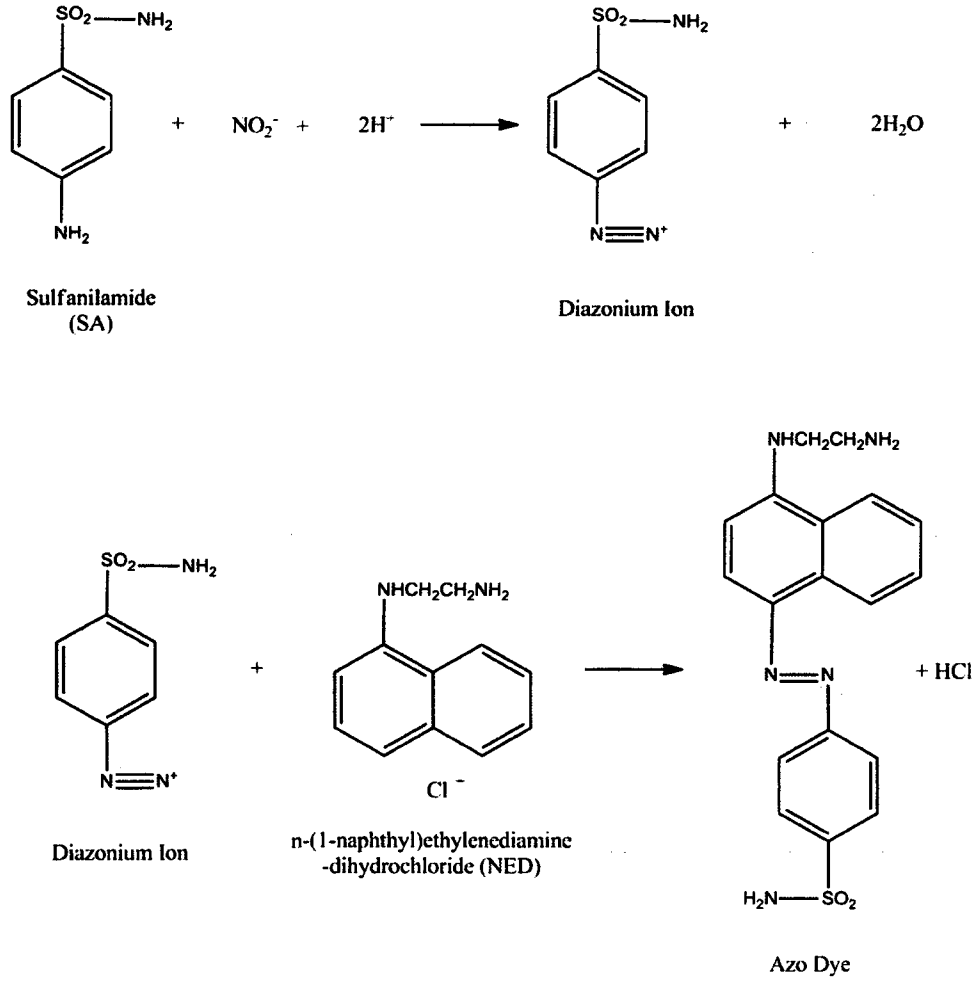

Figure 3: LOPAP chemistry that converts NO_2^- (aq) into an azo-dye.

This dye can then be measured by photometry using a UV/VIS light source and a spectrometer as its absorption follows Beer's Law (Eq. 1).

$$ABS = \log\left(\frac{I_{background}}{I_{abs}}\right) = k_\lambda \times l \times c \qquad \text{(Eq. 1)}$$

The background intensity ($I_{background}$) is the measured light intensity with no absorber present while I_{abs} is the intensity in the presence of the absorber. The log of the ratio of the two is linearly related to the concentration (c) of the absorber. The slope will be equal to the product of the wavelength dependant absorption coefficient k_λ, and the pathlength (l) the light travels through the absorber. The absorption coefficient (k_λ) for the azo dye is $5x10^4$ L $mol^{-1}cm^{-1}$ at the absorption maximum, 544 nm [Grasshoff et al., (1983)].

When performing a traditional Beer's Law experiment a blank measurement is performed to account for any absorption by materials other than the absorber. In the LOPAP application a reference wavelength is used so that a blank measurement need not be taken for each measurement. The intensity of light at a second wavelength is measured simultaneously with that at the absorption wavelength. The absorption wavelength used in the LOPAP experiment is between 544 and 590 nm, while a reference wavelength of 710 nm is used where the absorption cross section is ~0. Since the starting materials used to form the azo dye also absorb slightly at 544 nm a constant is added to the equation. This yields (Eq. 2) where I_{ref} was the intensity at 710 nm and I_{abs} is the intensity at 544 nm.

$$ABS = \log\left(\frac{I_{ref}}{I_{abs}}\right) = k_\lambda \times l \times c + \log(const.) \qquad \text{(Eq. 2)}$$

The value of the constant is dependent on the batches of SA and NED. Therefore a background measurement of the starting material must be performed whenever a new batch is used.

As with any absorption technique lower detection limits can be achieved by increasing the pathlength. The LOPAP technique uses a liquid core waveguide to increase the pathlength, which will be discussed in detail in the following section.

2.1 Liquid Core Waveguides

The use of liquid core waveguides (LCW) as absorption cells can increase the sensitivity of an instrument by orders of magnitude due to the increase in pathlength. A LCW is effectively an optical fibre with a liquid core and like an optical fibre it relies on total internal reflection [Dress and Franke, (1996); Diemer et al., (1997); Gooijer et al., (1998); Dress et al., (1998); Dasgupta et al., (1998); Belz et al., (1998); Manor et al., (2003); Dallas and Dasgupta, (2004); Altkorn et al., (1997); Dress et al., (1998)]. An optical fibre consists effectively of two parts, a core (typically glass or polymer) and a cladding. The cladding needs only to be thick enough to provide the desired isolation for the necessary application. In order to achieve total internal reflection Snell's law must be satisfied [Hecht, (1998)].

$$\beta_c = \cos^{-1}\left[\frac{n_c}{n_f}\right] \qquad \text{(Eq. 3)}$$

Light will undergo total internal reflection when going from one medium (refractive index=n_c) to another (refractive index=n_f) with an angle (β) which is less than the critical angle (β_c). The angle is measured with respect to the axial direction of the core. For a LCW the refractive index of the cladding (n_c) must be less than that of the core (n_f). This is particularly challenging when using an aqueous core since water has a low refractive index (n_w) equal to 1.33. Thus requiring n_c to be <1.33. Teflon AF 2400 is typically used in these applications as it has a refractive index of 1.29, allowing for total internal reflection with an aqueous core [Dallas and Dasgupta, (2004)]. For a LCW made with Teflon AF and an aqueous core the critical angle is 14.1°, meaning total internal reflection will occur for all angles less than 14.1°. Teflon AF can either be formed into capillaries by itself or can be coated on the inside or outside of glass tubing. The Teflon AF capillary is cut to give the desired pathlength for the application. In the case of the LOPAP a 2

metre pathlength was chosen. A schematic showing the theoretical light transmission through a LCW is shown in Figure 4.

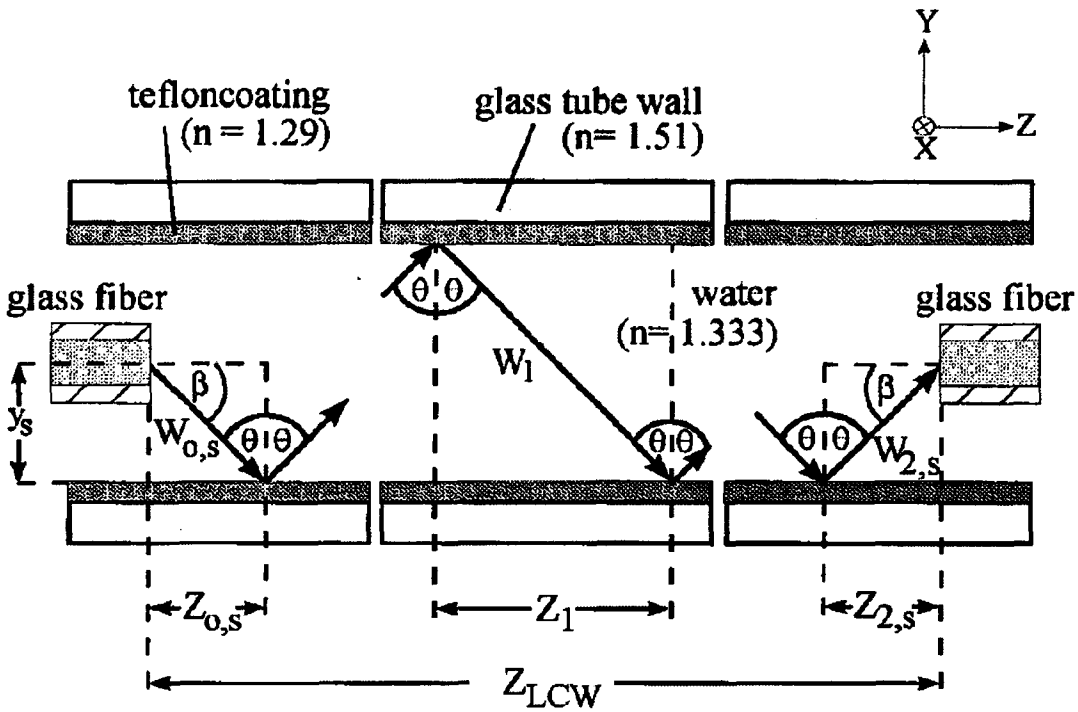

Figure 4: Schematic taken from Dress and Franke, (1997) showing the theoretical transmission of light through a liquid core waveguide.

Dress and Frank, (1997) use this simple model to divide the waveguide into three important geometric regions. These are, the in-coupling region with the characteristics $Z_{0,S}$,$W_{0,S}$,β, θ, the middle region of the LCW with the parameters $Z_{1,S}$,W_1, θ and the out coupling region with the parameters $Z_{2,S}$,$W_{2,S}$,β, θ . In all three regions Z defines the length of the region with the sum of all three equal to Z_{LCW}, the overall length of the waveguide; W refers to the length of a ray in that particular region before it reflects off the surface of the waveguide; θ is the angle of reflection, between the ray of light and a line perpendicular to the surface of the waveguide; β is the angle between the propagating ray of light and the centre of the in-coupling or out-coupling glass fibre.

2.2 LOPAP in Operation

The LOPAP instrument used in this work was a homebuilt version of the instrument described by Heland et al., (2001). The instrument is composed of two sections, a sampling unit, and a detection unit. The sampling section is composed of two glass coils (17 cm of glass each) in series, one for each channel. A 0.06 M SA solution is pumped to and from each coil at a flow rate of 0.4 mL min^{-1} using an ISMATEC roller pump. Air is pulled through the coils at a flow rate of 1 L min^{-1}. No liquid is carried from channel 1 to channel 2. The liquid is quantitatively pumped from the coil to the debubbler where any small air bubbles are separated from the liquid. The process in channel 2 is identical. It was shown in this work that nitrous acid is sampled nearly quantitatively in the first channel (99%). Other slightly soluble species are sampled in both channels with the interference in the 1^{st} channel removed by the subtraction of the signal in the 2^{nd} channel. The interferences will be discussed in a later section. The diazonium ion is formed from reaction of the HONO with the SA. Once the diazonium ion is formed, the solution is pumped through the debubbler and is mixed with a 0.2 mM solution of NED, (also pumped at 0.4 mL min^{-1} using the ISMATEC roller pump) where it forms the azo dye. The azo dye is pumped from each channel into separate liquid core waveguides (LCW).

The optical fibres were connected to the LCW's using PEEK HPLC tees. The bare optical fibre (OF) was fed straight through the tee, using PEEK tightening sleeve (TS) to ensure an effective seal, into the Teflon AF tubing (CT). The liquid was pumped in through the top of the tee using standard PEEK tubing (PT) and flowed around the bare fibre (OF) into the Teflon AF waveguide (TAF) as shown in the Figure 5.

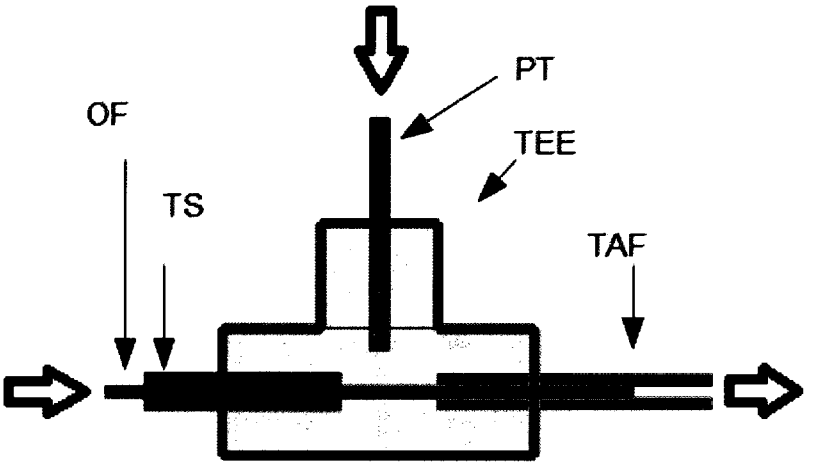

Figure 5: Diagram of liquid and light input for a Teflon AF 2400 liquid core waveguide. The abbreviations are as follows OF is the optical fibre, TS is a tightening sleeve around the fibre to ensure a seal. PT is standard 1/16" PEEK tubing for carrying the liquid. TEE is a standard 1/16" PEEK HPLC tee. TAF is the liquid core waveguide.

The numerical aperture (NA) of the bare fibres was matched to that of the Teflon AF (0.22) to minimize light losses. The fibres carrying light from the LCW's to the spectrometer were set up in an identical manner.

Initially the LCW's used were made from Teflon$^{(R)}$ AF 2400 capillary tubing similar to the original Heland et al., (2001) instrument. However the Teflon AF 2400 LCW's posed a problem. Since the azo dye was in direct contact with the Teflon, adsorption of the dye to the surface over time became a problem. After a period of use the adsorption of the dye to the surface significantly reduced the amount of light transmitted in the absorbing region of the azo dye. This had a negative effect on instrument sensitivity and stability, reducing the benefits of the extra pathlength provided by a LCW. It was decided that for durability, these LCW's would be replaced in favour of a glass lined LCW. The LCW's used were Liquid Waveguide Capillary Cells from World

Precision Instruments [Belz et al., (1999)]. In this LCW a quartz capillary is coated in Teflon AF so that the dye does not come into contact with the Teflon. This prevents the Teflon from dirtying, and eases the cleaning process. A schematic of the LWCC core and cladding is shown in Figure 6 taken from D'Sa et al., (1999).

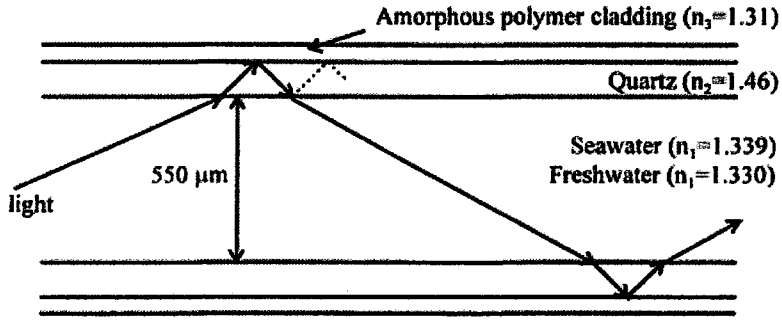

Figure 6: Schematic of WPI LWCC, showing internal reflection inside the cell. The refractive index of the Teflon cladding is 1.31 instead of 1.29 as the Teflon used by D'Sa et. al. (1999) was Teflon AF 1600.

The light source for the LOPAP is a LS-1 tungsten halogen lamp from Ocean Optics. Light from the lamp is directed into the two LCW's using a pigtailed Y optical fibre (Ocean Optics, 600 μm, NA=0.22). The output light is directed from each channel using two optical fibres (Ocean Optics, 600 μm, NA=0.22) into a two channel mini-CCD spectrometer (S2000) from Ocean Optics. The S2000 contains a high-sensitivity 2048 element linear CCD array. The usable detector range is between 350-1000 nm. The spectrometer had a slit width of 50 μm and a resolution of 1.5 nm. The analog-to-digital converter for the spectrometer was an Ocean Optics ADC1000-USB, which allowed the spectrometer to be connected to a laptop using a simple USB cable. The spectrometer is controlled using Ocean Optics OOIBase32 spectrometer software. Spectra are recorded on a laptop PC and analysed. A schematic of the instrument is shown in Figure 7

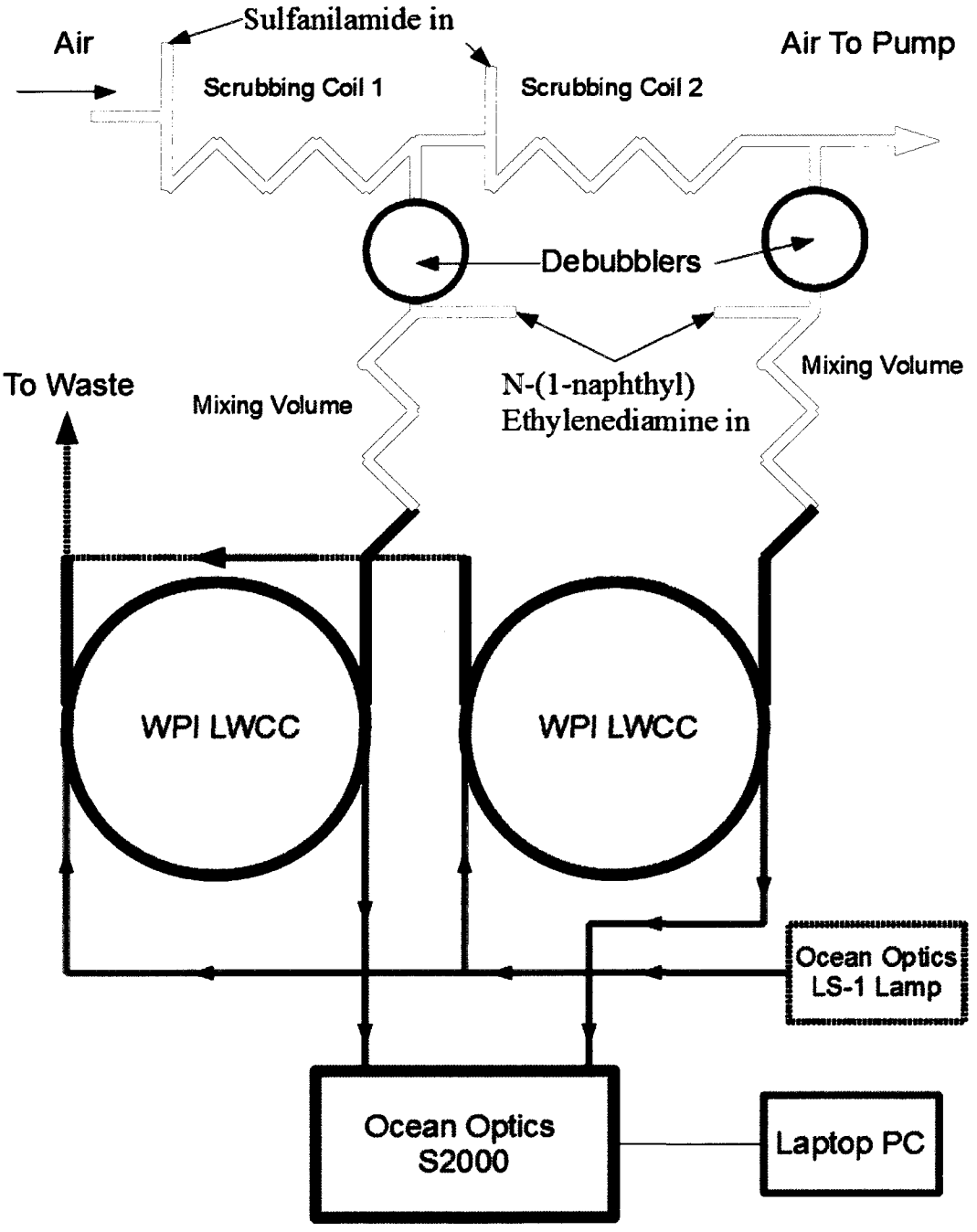

Figure 7: Schematic of LOPAP Instrument. Glass is shown in magenta, PFA tubing is shown in blue, input optical fibres are shown in green, output optical fibres are shown in red.

The instrument is calibrated using either a liquid nitrite standard or by using a gas phase HONO calibration source, the same source used by Wall et al., (2006) and first described by Febo et al., (1995a). The gas phase source uses humidified HCl gas which is passed over a bed of solid sodium nitrite giving a quantitative production of HONO from the HCl (R 13).

$$\mathbf{HCl(g) + NaNO_2(s) \rightarrow NaCl(s) + HONO(g)} \qquad \textbf{R 13}$$

The gas is humidified since the reaction will only proceed in the presence of water vapour [Febo et al., (1995a)]. Under dry condition the outside of $NaNO_2$ crystals becomes coated with NaCl preventing the reaction from continuing. The stability of the HONO generation system is dependent on the relative humidity since at high relative humidity deliquescence is a problem. Under typical operating conditions the relative humidity of system is ~60%. The LOPAP instrument demonstrated excellent linearity as can be seen from the gas phase calibration curve (Figure 8).

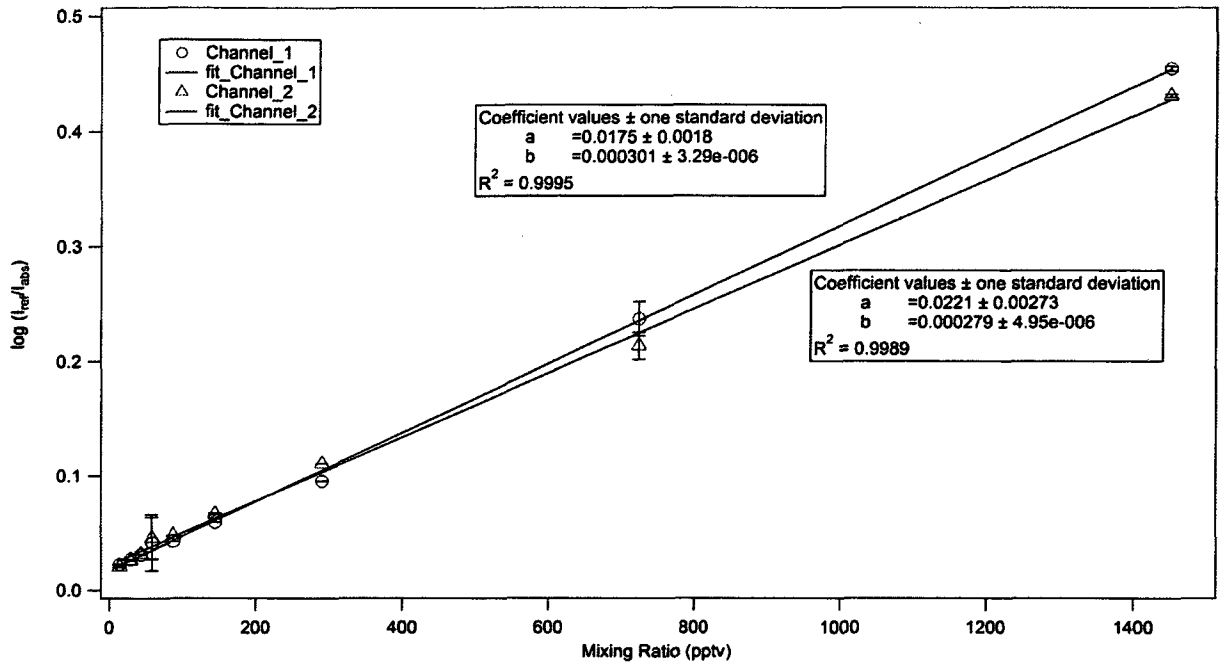

Figure 8: LOPAP calibration curve. The coefficients b and a are the slope and y intercept (respectively) of the fit of each line.

As stated earlier, the scrubbing efficiency of the instrument was found to be 99%. Since the scrubbing was quantitative, calibrations by either a liquid standard or gas standard are equally quantitative. During field experiments a liquid calibration was used due to the relatively complicated nature of the gas calibration system. The relative uncertainties for each channel are calculated from the sum of uncertainties of the gas flow rate, the liquid flow rate, and the uncertainty of the slope of the calibration fit. The total uncertainty is ~10%. The detection limit is calculated as three times the standard deviation of the measurement of the signal resulting from the absorption of the starting materials, (equivalent to the intercept of the calibration curve). It is typically 5 pptv. The absorption signal due to the starting materials (SA and NED) is obtained by performing background measurements sampling a flow of zero air with no HONO present.

2.3 Interferences

Interference tests were undertaken as part of the validation process of the instrument. During these interference tests all tubing was kept as short as possible to minimize the potential of artefact HONO formation and to eliminate potential interferences.

NO_2: The interference resulting from NO_2 was closely studied since it has been found to be an interference with other wet chemical methods [Huang et al., (2002)]. NO_2 calibration gas (2 ppmv in N_2, B.O.C.) was diluted with zero air and sampled with the LOPAP sampling coil. The interference was found to be 0.05 ± 0.03% per channel, in good agreement with Heland et al., (2001), who determined a per channel interference of 0.06 ± 0.02%. NO_2 is only slightly soluble (H_{NO2}=0.014 M/atm at 298 K, [Cheung et al., (2000)], while H_{HONO} is 49 M atm^{-1} at 298 K, [Park and Lee, (1988)]). NO_2 is therefore sampled equally in both scrubbing coils. The signal from channel 2 is thus simply subtracted from channel 1 to correct for the effect of NO_2. In a typical case of 10 ppbv NO_2, and 100 pptv of HONO (1% HONO/NO_2 ratio) the NO_2 interference would result in a per channel interference that is roughly equivalent to 6 pptv of HONO. The first channel of the LOPAP would measure the signal equivalent to 106 pptv HONO (HONO+NO_2) while the second channel would measure a signal corresponding to 6 pptv of HONO. In an extreme case, for example 500 ppbv of NO_2, it would result in an equivalent signal of 300 pptv of HONO per channel. If one considers a low real world HONO/NO_2 ratio at that concentration of NO_2 e.g. 0.5%, the LOPAP would still be measuring 2.5 ppbv of HONO in the first channel. Thus the signal in the first channel would be equivalent to 2.8 ppbv of HONO (89% of which is due to HONO) and the signal in the second channel would be equivalent to 0.3 ppbv HONO.

NO: The pure NO interference was measured by diluting an NO calibration gas (2 ppmv in N_2, B.O.C.) in zero air and sampling the diluted flow with the LOPAP. The true interference (channel 1 – channel 2) was found to be < 0.006%.

O_3: Ozone mixing ratios were examined between 10 and 100 ppbv. Ozone was generated from zero air using a UV light source in a flow tube and measured with an O_3 analyser. The true interference was found to be < 0.004%.

HNO_3: Nitric acid was examined as a potential interference. Solutions of aqueous HNO_3 (Sigma Aldrich) equivalent to up to 150 ppbv were pumped into each channel of the LOPAP sampling coil sampling coil. No signal above that of the background was observed.

O_3 + HONO: The interference due to O_3 + HONO was examined by producing O_3 as discussed above and mixing it with HONO produced from the gas phase source discussed in the previous section. The tests were performed to determine if the presence of O_3 would result in a negative HONO interference. The interference was found to be negligible as there was no discernable difference between this signal (with the ozone present) and the signal from pure HONO.

NH_3: Ammonia (Sigma Aldrich) was analysed as a potential interference. Liquid ammonia samples equivalent to several ppbv of ammonia were mixed with each channel of the LOPAP. The interference was found to be negligible as the signal produced was below the detection limit of the instrument.

Organics: Three organics, acetone, formaldehyde and benzene were also examined as potential interferences. The liquid organics were individually mixed in the LOPAP sampling coils at concentrations equivalent to up to 5 ppbv. The resulting signals from formaldehyde and acetone

were below the detection limit of the instrument while the signal from benzene yielded an interference of <0.008%.

Other interferences have been examined by other groups such as PAN, ethane, toluene and n-butane [Heland et al., (2001)] and were found to be negligible in all but the most polluted of conditions. A summary of the interference tests in this work can be found in Table 3.

Table 3: List of measured LOPAP interferences using a gas flow rate of 1L/min and a liquid flow rate of 0.4 mL/min.

Component	Interference (channel 1- channel 2)
NO_2	Below detection limit
NO	<0.004%
O_3	<0.004%
HNO_3	Below detection limit
O_3 + HONO	<0.004%
$CH_3C(O)CH_3$	Below detection limit
HCHO	Below detection limit
C_6H_6	<0.008%
NH_3	Below detection limit.

2.4 Particulate Nitrite

One of the issues when using liquid sampling for HONO measurement is whether or not particles containing nitrite are detected as well as gas phase HONO. Measurements of HONO where filters are used have been found to be unreliable due to artefact HONO formation on the filters and other surfaces [Gutzwiller et al., (2002); Zhou et al., (2002)); Kleffmann et al., (1998)] and so it is not possible to simply use a filter to remove the particles from ambient air. According to Bröske et al., (2003) and Kleffmann et al., (2006) the LOPAP did not sample particles and only measured gaseous HONO. It was unclear however whether or not there was in fact any nitrite on the particles measured in those studies, (in a private communication with J. Kleffmann he stated there was nitrite on the particles). While particulate nitrite was not believed to be an interference Kleffmann et al., (2006) suggested that the lack of interference might not hold true for particles smaller than 50 nm in diameter due faster diffusion of these particles or for particles larger than 1 μm due to impaction. While Kleffmann et al., (2006)suggested smaller particles may be an interference, they believed the particle interference would be corrected by the second LOPAP channel.

A comparison of some LOPAP field measurements with those of an Ambient Ion Monitor Ion Chromatograph (AIM-IC URG 9500) belonging to the group of Professor J.G. Murphy of the University of Toronto was performed as part of this work during the BAQS-Met study. The AIM-IC draws air in through a PM-2.5 sharp-cut cyclone at a volumetric-flow controlled rate of 3 L min^{-1} to remove the large particles from the air stream. The sample is then drawn through a Liquid Diffusion Denuder where acidic gases are removed. In order to achieve high collection efficiencies, the particle-laden air stream next enters the Aerosol Super-Saturation Chamber to enhance particle growth. An Inertial Particle separator collects these enlarged particles, which are then

injected into an Ion Chromatograph [Dionex URG 9000A. (2009)]. The HONO measurements of the AIM-IC and LOPAP were compared to check the agreement of the two instruments. Figure 9 shows that there was little correlation between the HONO measurements performed by LOPAP and those for gas phase (Total NO_2^--particle NO_2^-) HONO of the AIM-IC. When the LOPAP HONO measurements were compared with the measurements of sum nitrite [particulate NO_2^-+HONO] a significantly stronger correlation was observed, (Figure 10).

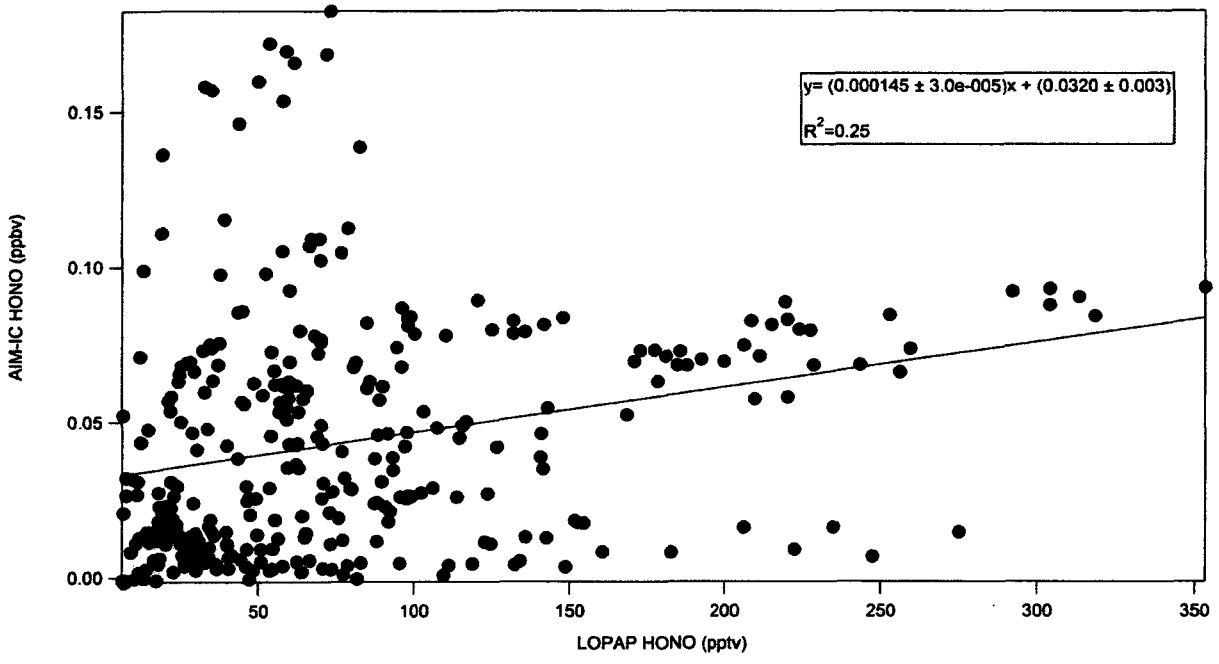

Figure 9: Plot of the correlation between AIM-IC HONO measurement and LOPAP HONO measurement.

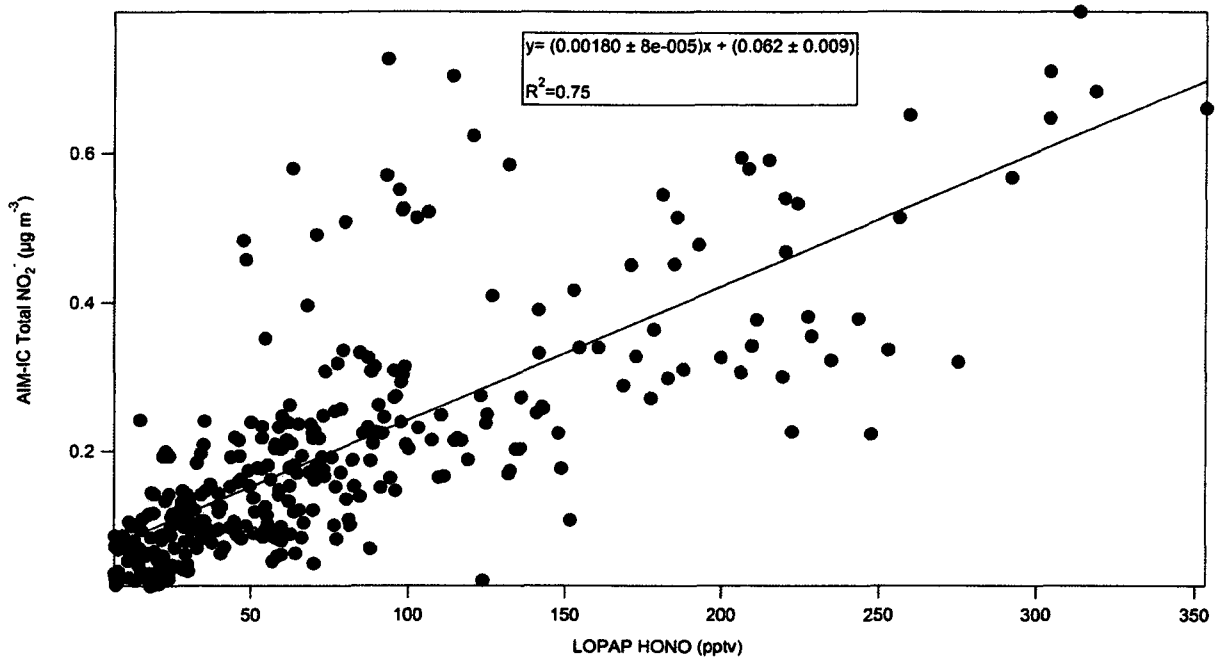

Figure 10: Correlation of LOPAP HONO and AIM-IC sum nitrite data.

Based on this, it appeared possible that LOPAP may be sampling particle nitrite as well as gaseous HONO. However, it should be noted that at this time gas phase calibration of the AIM-IC has not been performed and the collection efficiency of gaseous HONO was unknown, thus at the time the measurements were performed the AIM-IC had not been rigorously tested. It is likely that HONO is passing through the denuder and appearing as "particle nitrite".

To investigate the effect of NO_2^- particles on gas phase HONO measurements, particles of various sizes were sampled by the LOPAP instrument in the lab. Sodium nitrite aerosols were produced using a variety of sodium nitrite solutions and a nebulizer. Particles were size selected using a differential mobility analyser (DMA). An initial qualitative experiment was performed where a solution of $NaNO_2$ was nebulized and size selected to 5 nm using a DMA. The number density of the particles was $2x10^3$ cm^{-3}. The sampling of particles this size in the atmosphere might

be irrelevant since they do not contain a significant mass fraction of the aerosol. Figure 11 shows a time series of the apparent HONO mixing ratios showing that particulate nitrite is being taken up by the first channel of the LOPAP.

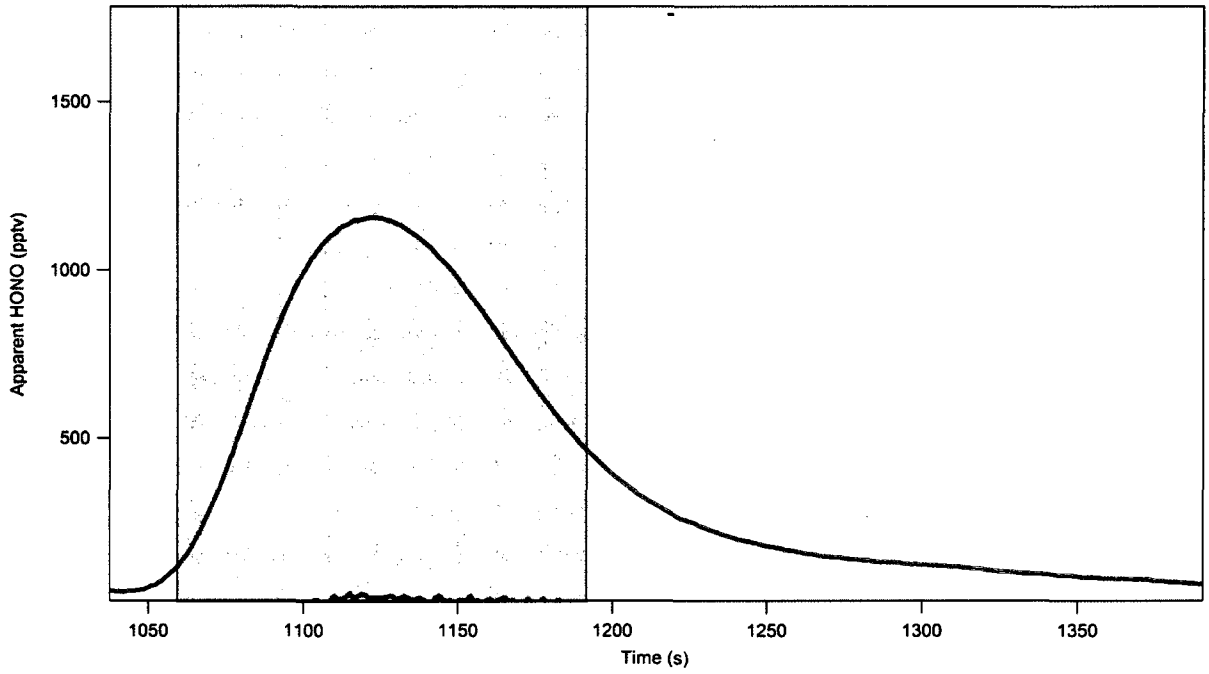

Figure 11: A plot of a nitrite particle interference test with the LOPAP. Sodium nitrite particles, size resolved to 5 nm in diameter, were measured with the LOPAP. The shaded region shows the period of time where nitrite particles were sampled. For the rest of time room air was sampled. The apparent HONO signal from channel 1 is displayed in red, while the signal from channel 2 is displayed in blue.

Uptake of the particles was nearly quantitative in the first channel (shown in red), with only a small amount of breakthrough to the second channel (shown in blue). This contradicts the suggestion by Kleffmann et al., (2006) that particles smaller than 50 nm taken up by the LOPAP would be corrected by the second channel, i.e. the particles would be sampled equally in each of the two LOPAP channels. Filter experiments (using a 100 nm filter) were performed in order to determine if a filter would be to remove particle nitrite from a flow. Figure 12 shows an

experiment where a flow of $NaNO_2$ particles (500 nm, number density $2x10^3$ cm^{-3}) where removed by a filter. A time series is shown in Figure 12.

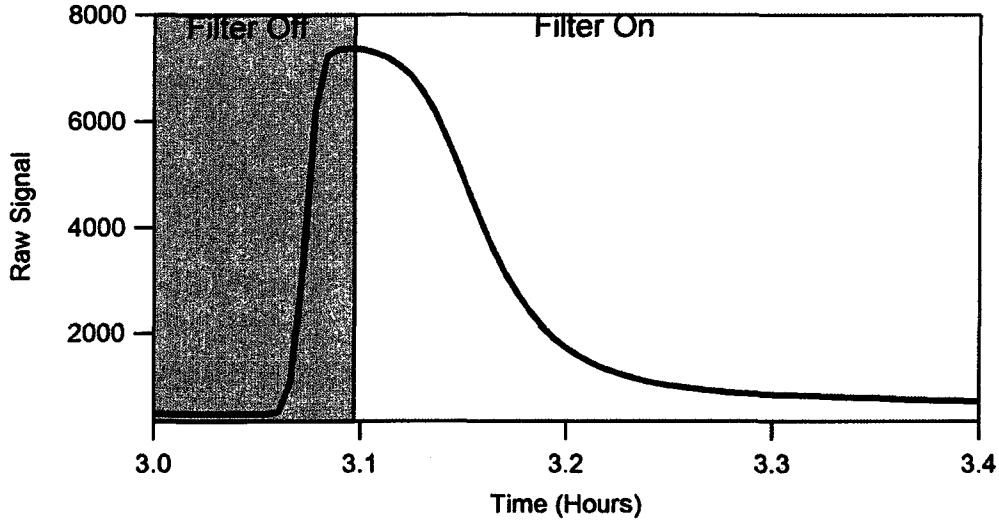

Figure 12: Time series of raw un-averaged signal as a result particle nitrite with and without a filter. The time required for the complete drop in signal is a result of the residence time of sampled nitrite in the LOPAP. The shaded area shows the LOPAP signal generated while sampling a $NaNO_2$ particle flow with no filter present. The area with the white background shows the LOPAP signal after a filter was placed in front the LOPAP's sampling coil.

When the filter was placed in front of the LOPAP's sampling coil, denoted by "filter on" in Figure 12, it was able to remove the $NaNO_2$ interference. These experiments were performed with $NaNO_2$ particle flow in zero air only. There was no NO_x present during these experiments.

Since it was apparent that the LOPAP could measure particle nitrite when there was no filter present, further experiments were undertaken using the York University smog chamber. The impetus for this was twofold, 1). To determine whether or not the signal due to particles and the signal due to HONO could be separated and 2) To potentially determine HONO uptake on a variety of particles. Initial experiments using only zero air in the dark chamber showed consistent background amounts of HONO in the 10's of pptv's. When the experiment shown in Figure 13 was

performed, the chamber had been flushed with zero air for more than a week prior. The concentration of NO_2 was below the detection limit of the NO_x chemiluminescence detector. When the chamber lights were turned on there was a dramatic increase in HONO signal. Nitrous acid was believed to be desorbing from the chamber walls as the temperature increased. Chamber walls have been shown to be a source of HONO in other studies as well [Rohrer et al., (2005)].

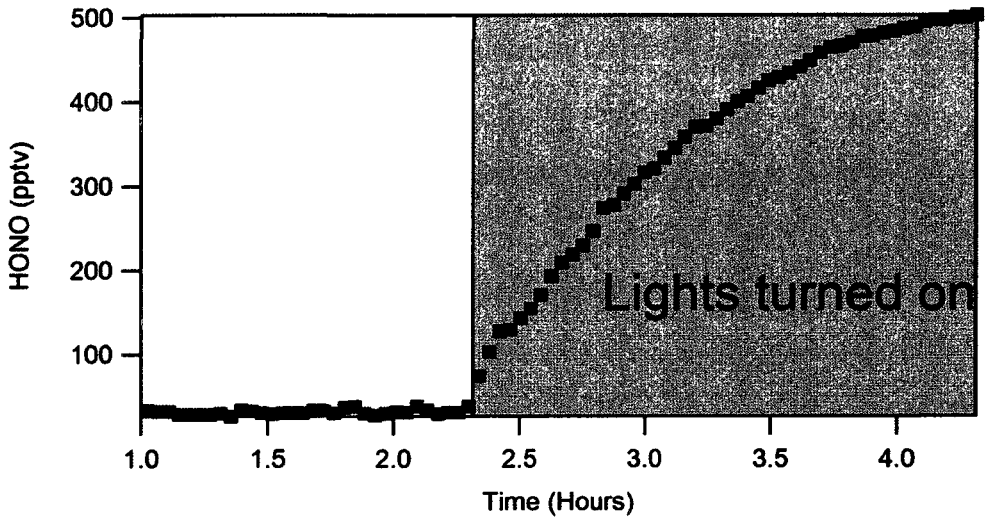

Figure 13: A time series of the LOPAP measurement of HONO from the York University Smog Chamber after flushing with zero air.

Experiments were then performed using the chamber to determine if filters would be effective for removing the nitrite signal in the presence of NO_2. .The chamber lights were also turned on which generated HONO as shown in Figure 13. Using a calibration tank of NO_2, 20 ppbv of NO_2 was put into the chamber to act as an additional source of HONO. A flow of $NaNO_2$ aerosol (>500 nm in diameter, size selected using a DMA) put into the chamber and the $NaNO_2$ particle NO_2/HONO mixture was sampled by the LOPAP with and without a 500 nm filter in front of the sampling coil. Figure 14 shows the signal with and without the filter

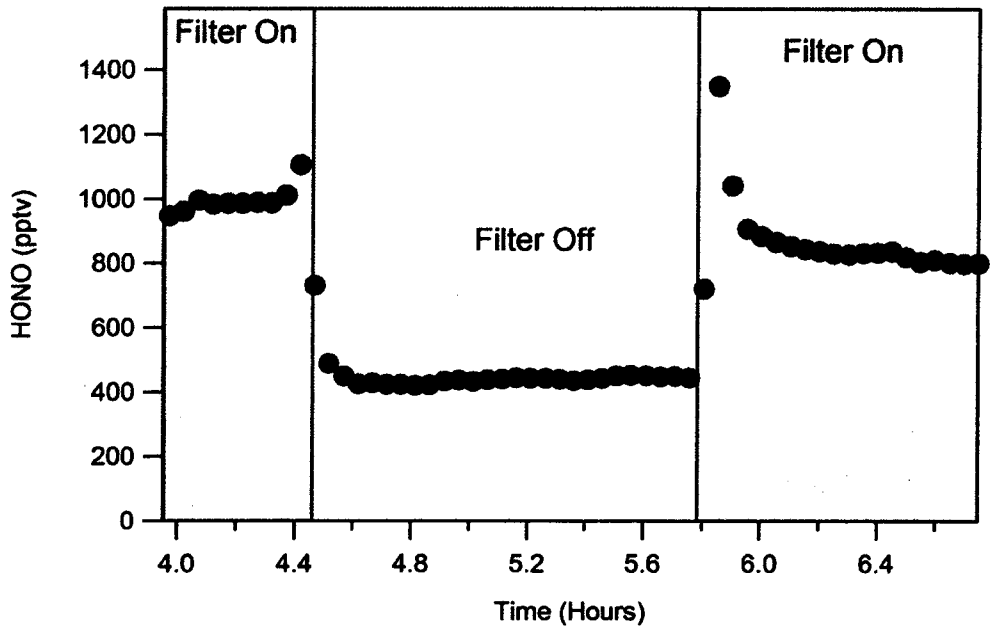

Figure 14: Time Series of HONO signal with and without a filter in the presence of particulate NO_2^- and NO_2.

The signal when the filter is off denoted by "Filter Off", is due to the sum particulate nitrite and gas phase HONO from the chamber. The signal when the filter is on denoted by "Filter On", in front of the LOPAP should only be due to the gas phase HONO; however, the signal is a factor of 2 larger than that without the filter. This indicates that artefact HONO is being formed on the filter, consistent with other studies [Gutzwiller et al., (2002); Zhou et al., (2002)); Kleffmann et al., (1998)] making it impossible to distinguish between particulate nitrite and gas phase HONO by this method. This interference generated by the filter made it impossible to perform further experiments to determine whether HONO would be taken up on particles using the existing LOPAP.

While the particulate NO_2^- sensitivity is clearly a problem in the laboratory setting it is unlikely to have a large effect on ambient measurements of HONO. The likelihood of finding a large fraction of the sum nitrite ($HONO+NO_2^-$) in the particle phase appears to be low [Lammel and Cape, (1996)]. The solubility of HONO is pH dependant, requiring an alkaline particle for quantitative uptake [Park and Lee, (1988); Gutzwiller et al., (2002); Lammel and Cape, (1996)]. The anthropogenically influenced atmosphere is generally more acidic [Lammel and Cape, (1996)] and HONO (pK_a=3.25) will not be taken up by an acidic particle. While the potential exists for uptake on neutral or alkaline ice or snow, it seems unlikely this would be a significant problem under most measurement conditions.

Comparisons of the LOPAP technique with a well established DOAS system, which is totally insensitive to particulate NO_2^-, have been performed by other groups [Kleffmann et al., (2006)] under heavily polluted conditions (daytime HONO mixing ratios of >200 pptv). The correlation between the LOPAP technique and DOAS was 0.987±0.015. The LOPAP technique has also been validated against the DOAS during two separate smog chamber experiments yielding correlations of 0.99877±0.0003 and 0.9787±0.013 [Kleffmann et al., (2006)].

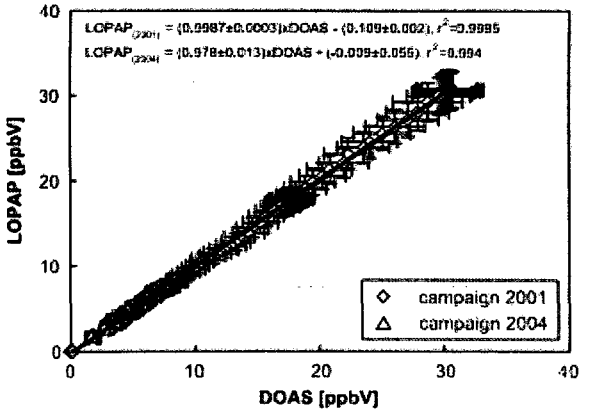

Figure 15: Correlation of LOPAP and DOAS data taken from smog chamber studies Kleffmann et al., (2006).

The effects of particulate nitrite are expected to be of minor importance in ambient measurements, although further comparisons with non chemical measurement (e.g. spectroscopic) methods would be valuable to further confirm this. Since filters were clearly shown to produce artefact HONO during chamber studies, no filters were used during ambient measurements.

3 Atmospheric Measurements

Ambient HONO concentrations were measured at three different types of sites: one urban, one forested, and one agricultural. All of the sites were located in Southern Ontario. It was expected that the urban site would be dominated by direct emissions of HONO from combustion sources, predominantly automobile engines, while the forest and agricultural sites would be dominated by secondary production. Figure 16 is a satellite image showing the locations of the sites. The urban sampling site was near Highway 401 in Toronto. The forested sampling site is a rural site located in a forested section of Canadian Forces Base Borden, and the agricultural site was located on the property Agriculture Canada' s Harrow research station in Harrow, Ontario.

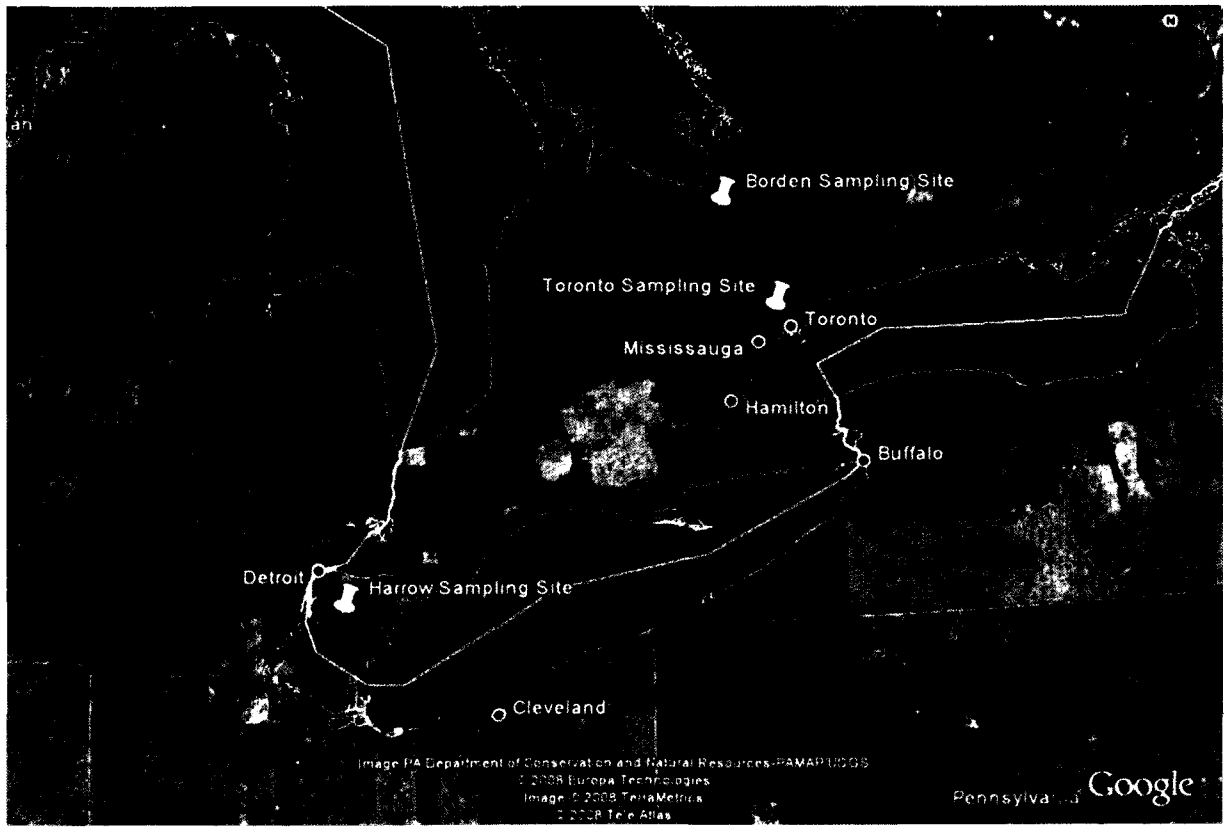

Figure 16: Map of locations of Southern Ontario sampling sites using Google Earth.

3.1 Urban Site - Toronto

Measurements at an urban site were performed at the Ontario Ministry of the Environment (OME) measurement station at 125 Resources Road Toronto, Ontario (43.709528°, -79.543324°). An overhead image of the site is shown in Figure 17.

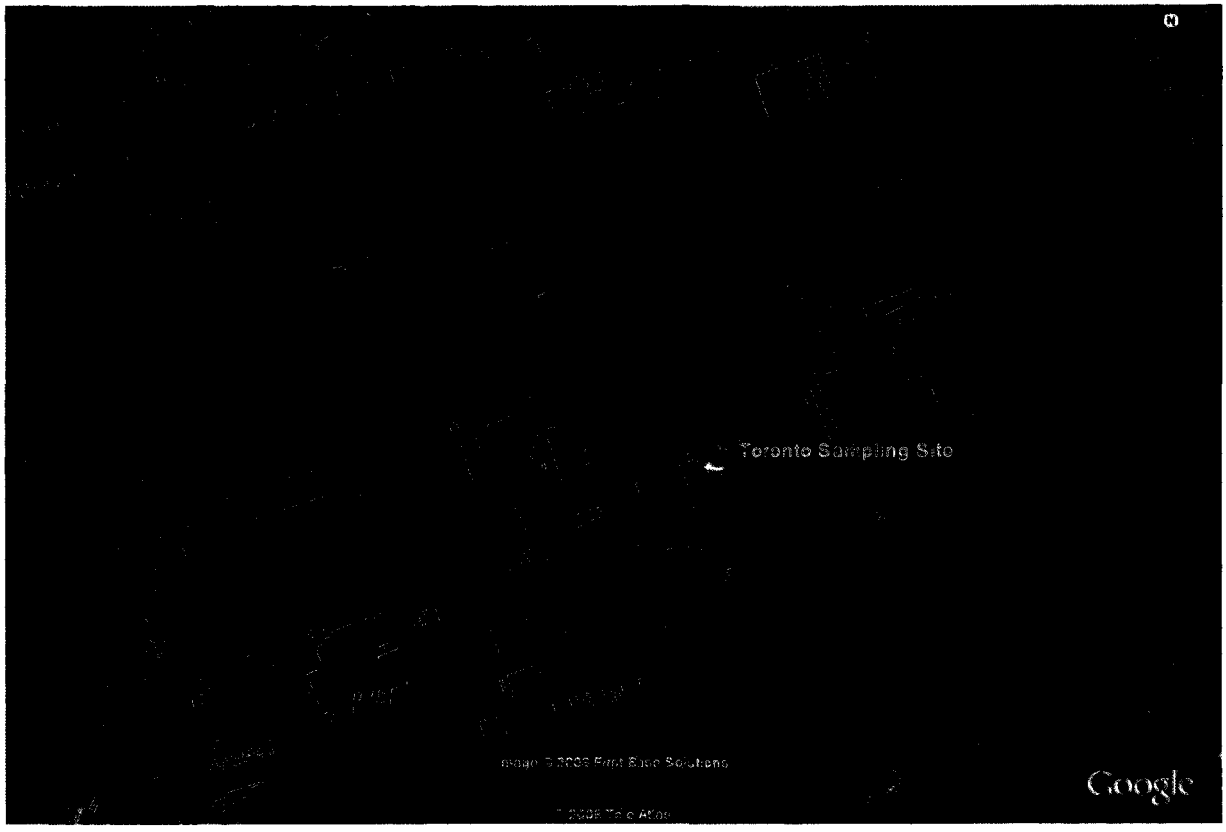

Figure 17: Overhead image of the Toronto sampling site using Google Earth.

Measurements were performed between February 15 and March 15, 2007. Directly north of the measurement site is highway 401. Highway 401 is one of the busiest highways in the world where 24 hour traffic volumes can exceed 370,000 automobiles on most days [Ontario Ministry of Transportation. (2009)]. It is 16 lanes wide in the section directly north of the measurement site,

thus it is a large pollution source. It is expected that the majority of the HONO measured would be a result of direct emission or of HONO formation directly after emission of exhaust from automobiles.

3.1.1 Instrumentation at the Urban Site

The LOPAP was located in the main garage of the OME building. The main garage is a North West to South East oriented building. The sampling coil of the LOPAP was mounted against the wall with a PFA tube 20 cm in length running through a hole in the East facing wall for air sampling. The LOPAP used a gas sampling rate of 1 L min^{-1} and liquid flows (both SA and NED) of 0.4 mL min^{-1}. The measured data was averaged for five minutes and the detection limit of the instrument was determined to be 5 pptv calculated as three times the standard deviation of the absorption of the starting materials. The Ontario Ministry of the Environment measures NO_x, O_3, PM 2.5, and standard meteorological data on regular basis at this site. Their data was used during this study. The NO_x and O_3 measurements were performed using air sampled through a glass manifold on the roof of the building. This manifold was not used for the measurement of HONO since it has been shown that HONO can be produced on the surface of these types of manifolds [Zhou et al., (2002)].

3.1.2 Urban HONO Measurements

A time series of the HONO mixing ratios measured by the LOPAP and of all of the measurements performed by the Ministry at the Toronto site is shown in Figures 18-22. They are broken into five periods of HONO measurement over the course of the study, a result of restricted site access. The uncertainties in the HONO measurements are calculated from the sum of uncertainties of the gas flow rate, the liquid flow rate, and the uncertainty of the slope of the calibration fit. The total uncertainty is ~10%. High concentrations of HONO were observed throughout the study. Mean values over the course of the study were 232 pptv. The maximum observed mixing ratio was 1.6 ppbv. Diurnal profiles were not often observed over the course of the campaign. The third period of the campaign (February 26th-March 3rd) was the only continuous period where night-time maxima were observed. The noontime maximum of J_{HONO} on sunny days during the campaign is estimated to be ~0.8×10^{-3} s^{-1} based on UV measurements made by Environment Canada several kilometres North East of the site. The maximum is 40% lower than expected during the summer months. Photolytic data was not available at the site throughout the campaign making it impossible to accurately assess any daytime production of HONO. The study periods were characterized by mostly gray cloudy skies during the daytime.

During all five time periods there was a rise in HONO, NO_x and PM 2.5 loading during the morning rush hour period (06:00-10:00). Evening rush hour peaks were not always discernable from the HONO data as concentrations would continue to rise from late afternoon into the night-time hours. The rush hour peaks were not always apparent in the NO data due to the rapid oxidation of NO to NO_2 in the presence of large amounts of O_3. A high variability in HONO data was observed during several periods of the campaign. While it is likely that this is a result of the proximity of the highway it is discussed further in the next section.

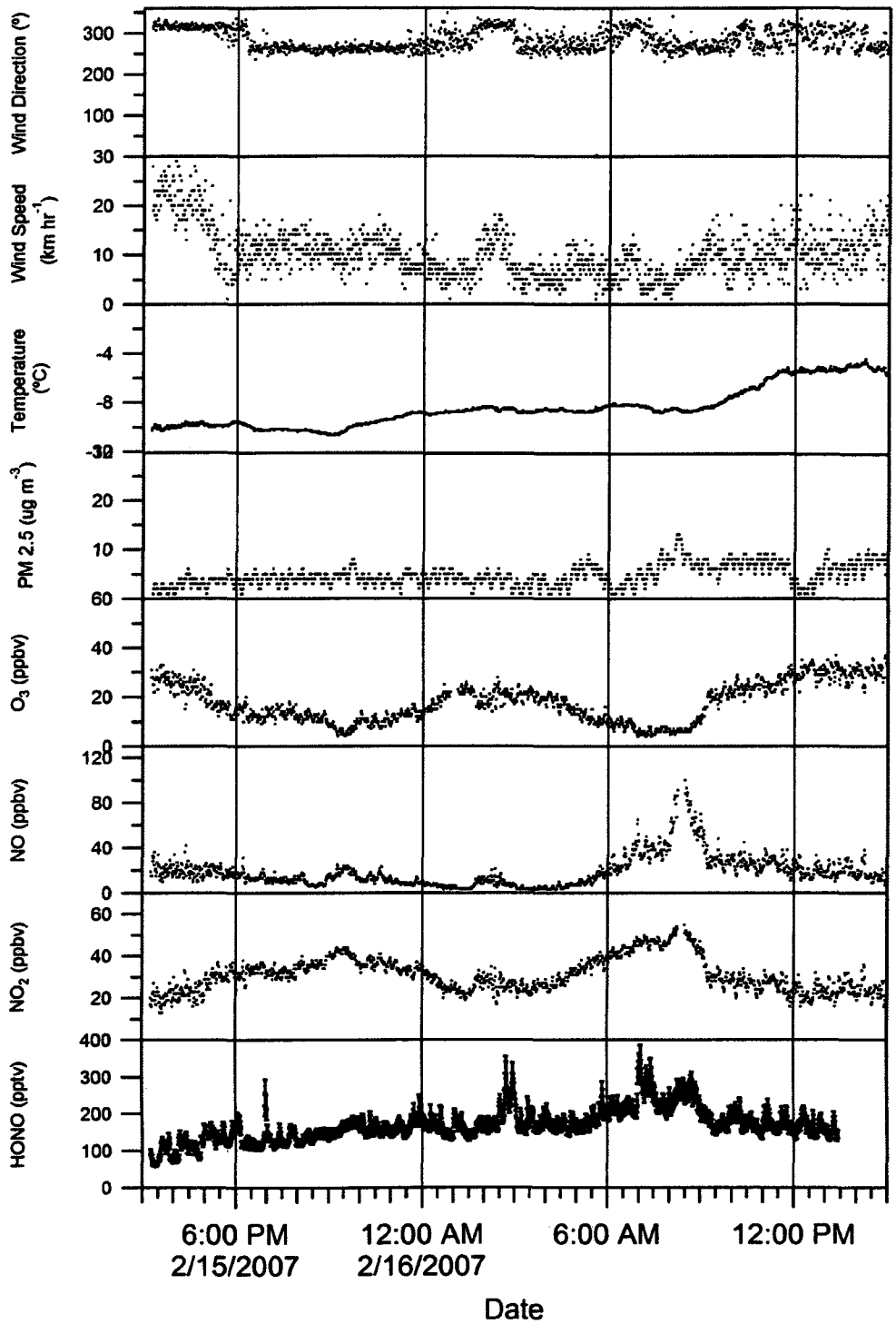

Figure 18: Measurements of HONO, NO, NO_2, O_3, PM 2.5, temperature, wind speed and wind direction between 15:00 on February 15 and 15:00 on February 16, 2007.

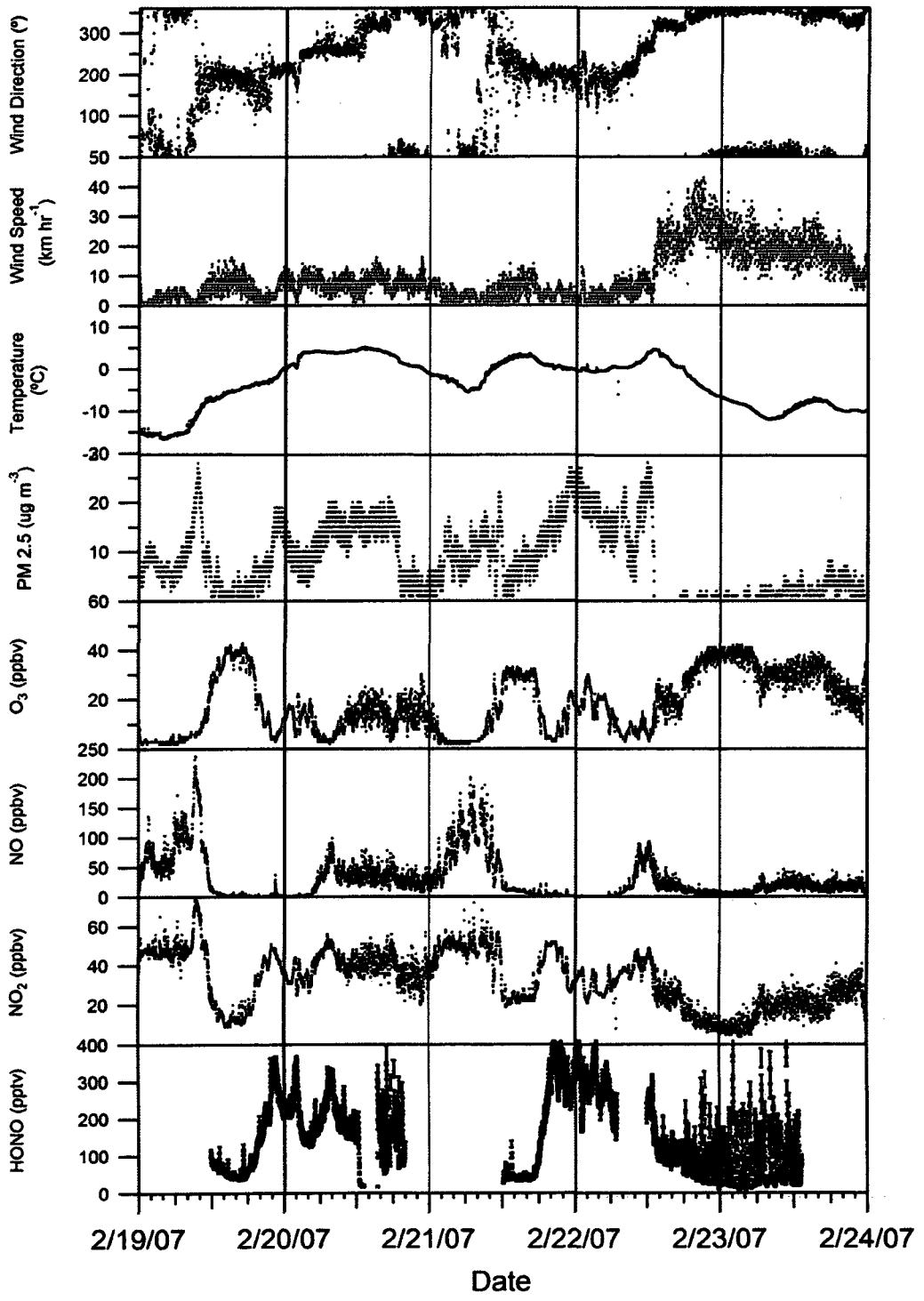

Figure 19: Measurements of HONO, NO, NO_2, O_3, PM 2.5, temperature, wind speed and wind direction between 12:00 on February 20 and 13:00 on February 23, 2007, (gridlines occur at midnight).

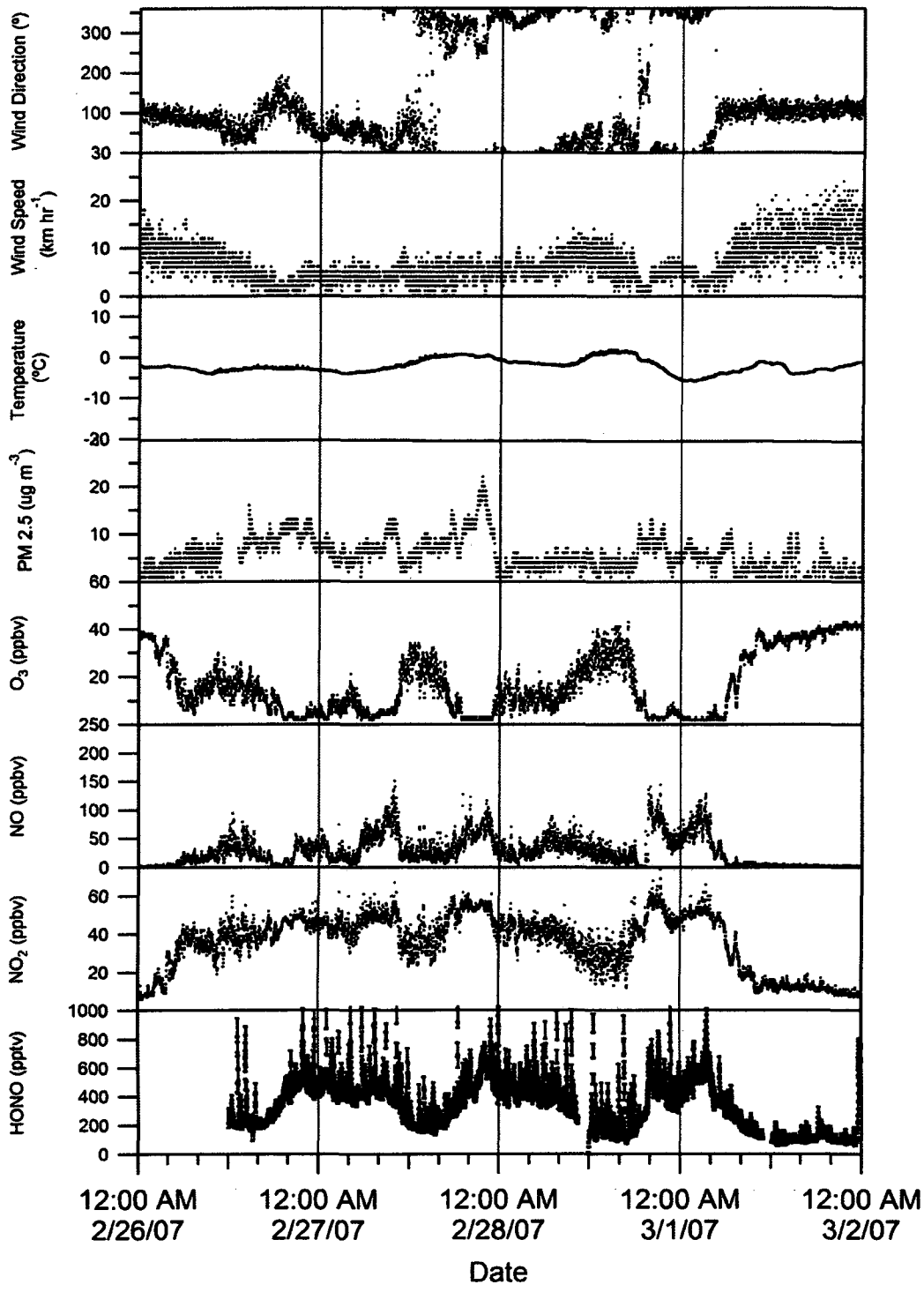

Figure 20: Measurements of HONO, NO, NO_2, O_3, PM 2.5, temperature, wind speed and wind direction between 12:00 on February 26 and 00:00 on March 2, 2007 (gridlines occur at midnight).

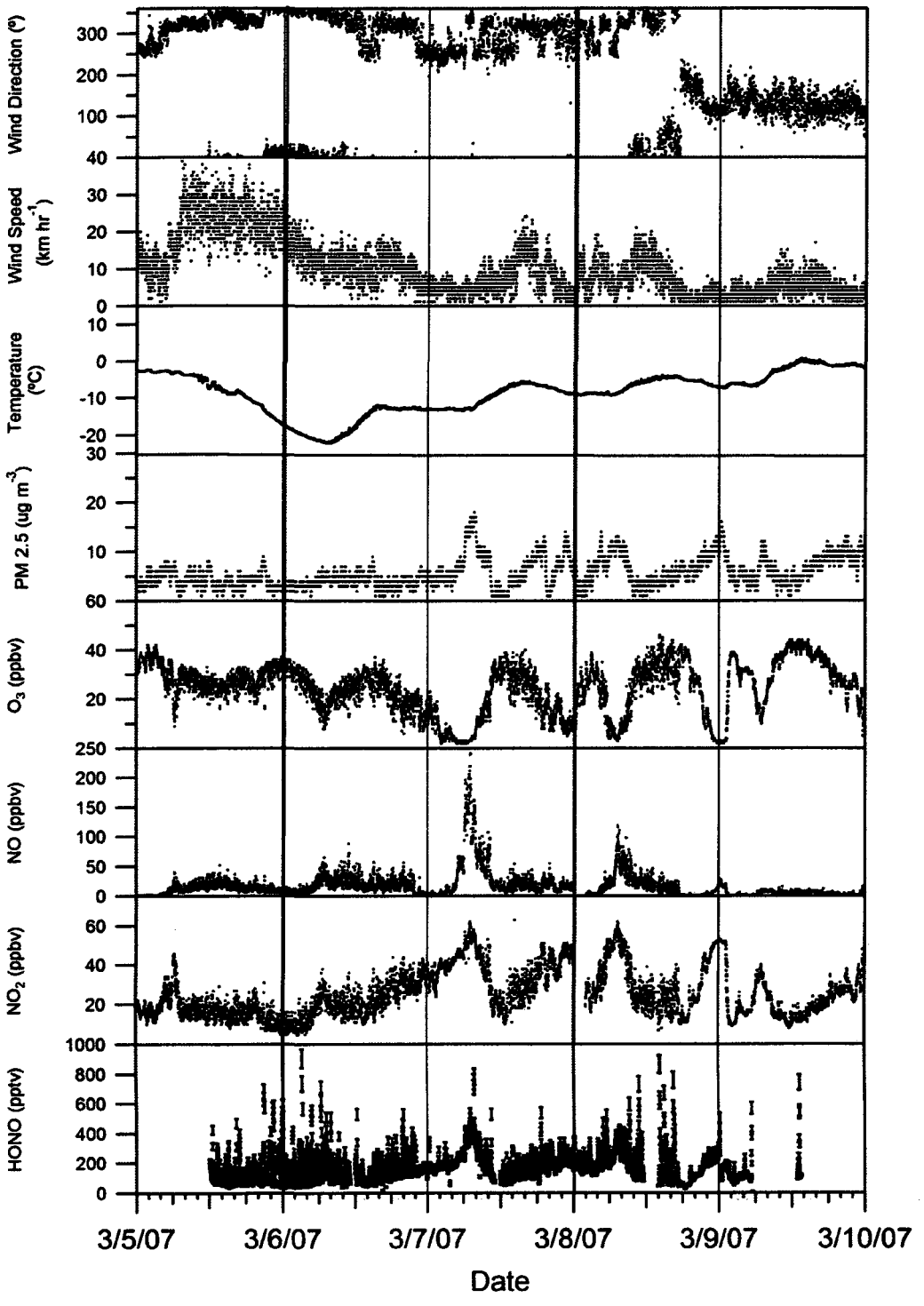

Figure 21: Measurements of HONO, NO, NO_2, O_3, PM 2.5, temperature, wind speed and wind direction between 12:00 on March 6 and 13:00 on March 9, 2007 (gridlines occur at midnight).

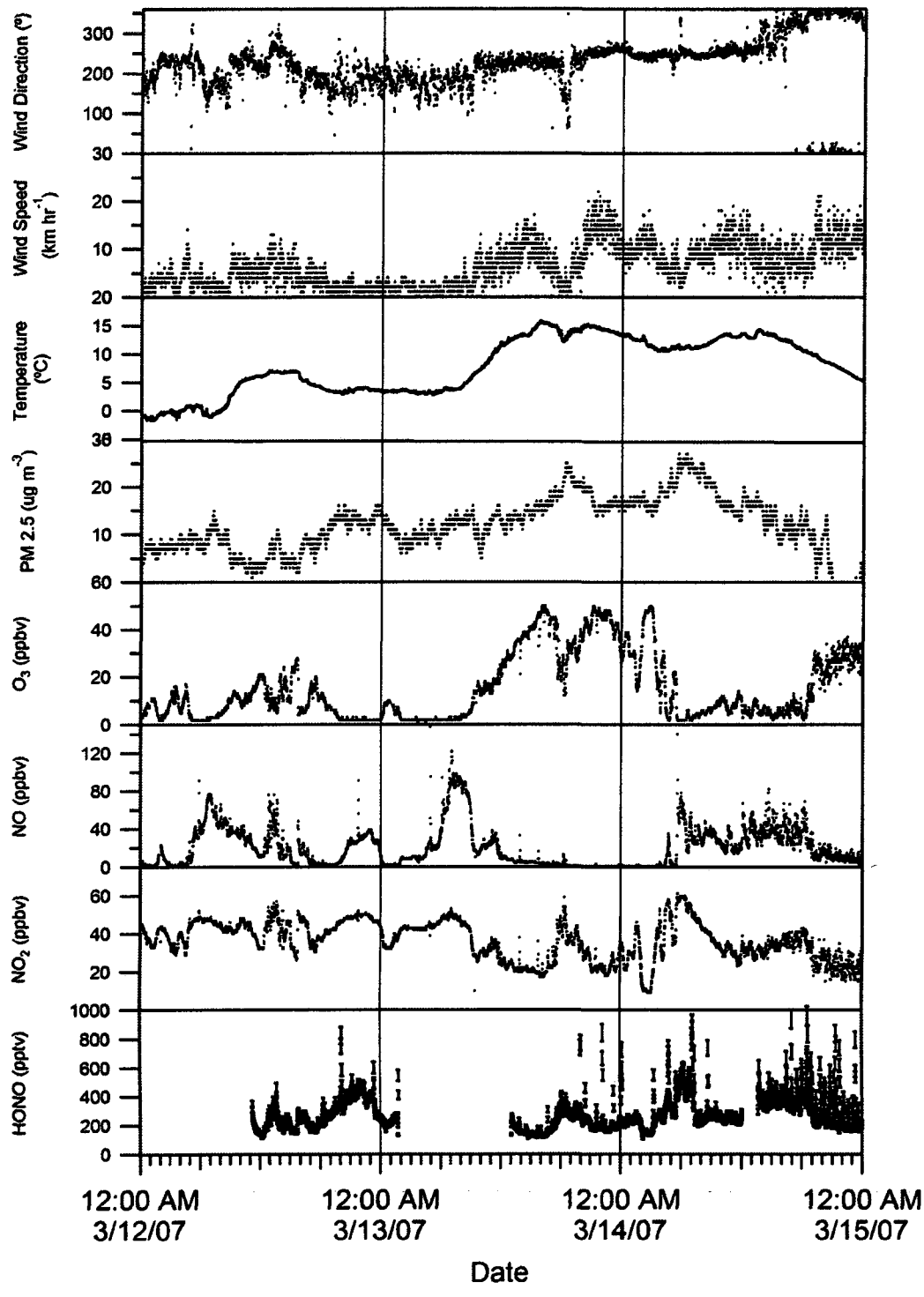

Figure 22: Measurements of HONO, NO, NO_2, O_3, PM 2.5, temperature, wind speed and wind direction between 12:00 on March 12 and 12:00 on March 15, 2007 (gridlines occur at midnight).

3.1.3 High Variability HONO Data

On the evening of February 20th and the night of the 22nd/ 23rd a large amount of variability in the HONO data set was observed. During the late afternoon and early evening of the 20th wind speeds were ~10 km hr^{-1} and a large variability in the NO, NO_2 and O_3 data was observed. There was an observed decrease in O_3 at 18:00 corresponding to oxidation of NO to NO_2. Concentrations of NO_2 began to decrease after O_3 concentrations rose, shortly after 18:00. There was only a very small increase in NO during this period. It appears to have been effectively titrated by O_3. Loadings of PM 2.5 which had been between 10 and 15 μg m^{-3} also decreased as ozone began to rise indicating the end of the rush hour period. Winds at this time were from the North. Since this occurred between 16:00 and 20:00 local time it's possible this variability was caused by poor mixing of rush hour emissions or a different source to the North of the highway.

The variability in the data from the 22nd/23rd was also significant. It began as wind speeds rose to over 40 km hr^{-1}. The increase in wind speed corresponds to a shift in wind direction from the South West to the North. Wind speeds varied between 15-30 km hr^{-1} for the rest of the night and morning. Over the course of the night and morning there were large variations in concentrations of other compounds as well, concentrations of NO_2 varied by as much as 20 ppbv and O_3 concentrations varied by roughly 10 ppbv. It is possible the measured HONO was simply not well mixed due to the gusting winds from the North of the site. The variation in HONO/NO_2 ratio during this period was between 0.5-6% which could be explained by point source emissions. While it is impossible to determine whether there was an increase in HONO concentration at rush hour, there was a small peak in concentrations of NO and NO_2 as well as a decrease in O_3 as it titrated NO to NO_2. There was no distinct increase in PM 2.5. The likely explanation for the lack of

increase in PM 2.5 loadings is the higher wind speeds which were not present during the other two rush hour periods.

During the remaining time periods there were again periods of rapid variability observed in the HONO data. This variability was also observed in the NO, NO_2 and O_3 data sets. The variation in the HONO/NO_2 ratio however was again only a few percent. The three day period (February 27^{th}- March 1^{st}) was dominated by low wind speeds (5-10 km hr^{-1}) while the night of March $5^{th}/6^{th}$ showed wind speeds 10-30 km hr^{-1} (winds were again from the North). The night of March 15^{th} also showed variability when winds were between 10-15 km hr^{-1}. The variations in the HONO and NO_x data regardless of varying wind speed in addition to the wind direction (predominantly from the North) indicate that the variability is likely caused by passing traffic emissions.

During the first time period at the site (Feb.15-16), there is an observable periodicity in the PM 2.5 data. While this cannot be confirmed it's probable that the instrument was not functioning properly at the time leading to this effect in the data and it must be treated with caution.

3.1.4 HONO/NO_x Direct Emission Ratios

The relationship between HONO and NO_x was examined for all morning rush hours (6:00-10:00) and evening rush hours (16:30-19:00) when HONO data was available during the campaign. Before examining these relationships further the HONO data was smoothed in order to remove the large unknown variability observed at times in the HONO data set which was discussed in the previous section. Individual points greater than 10% larger than data points before and after were removed for the analysis. The morning rush hour correlation parameters are shown in Table 4 and the evening rush hour parameters in Table 5.

Table 4: Correlation data between HONO and NO_x during morning rush hours (6:00-10:00) during the study. The table includes mean PM 2.5 values during the morning rush hour.

Date	R^2	Slope (HONO/NO_x) (%)	Intercept (HONO pptv)	PM 2.5 ($\mu g\ m^{-3}$)
Feb. 16, 2007	0.70	0.09	137	10
Feb. 20 2007	0.82	0.16	79	15
Feb. 27, 2007	0.28	-0.05	494	10
Feb. 28, 2007	0.29	0.07	287	5
Mar. 1, 2007	0.70	0.66	24	5
Mar.6, 2007	0.59	0.08	43	5
Mar.7, 2007	0.71	0.13	114	17
Mar.8, 2007	0.82	0.15	88	10
Mar.14, 2007	0.80	0.48	172	28

The quality of correlation was determined from the R^2 value. It is the ratio of the variation in Y which is dependant on X to the total variation in Y and denotes the strength of the linear association between X and Y. Values of R^2 greater than or equal to 0.64 (correlation coefficient R >= 0.80) are considered to be strong correlations, correlation coefficients (R) greater than 0.8 are generally described as strong, whereas coefficients less than 0.5 are generally described as weak. Strong correlations were observed between HONO and NO_x for several morning rush hour periods

(February 16 and 20, March 1, 6, 7, 8 and 14) with slopes ranging from 0.93-4.82 (HONO pptv)/(NO_x ppbv). Intercepts also varied 24-172 pptv of HONO. Poor correlations were observed between HONO and NO_x during the evening rush hour periods as can be seen in Table 5. The poorer correlations during the evening rush hour period can be attributed to the fact that there was often no distinct peak in HONO during the early evening period. Nitrous acid would rise in the early evening and continue to rise into the night due to lack of photolysis. Slopes similar to the morning rush hour values were observed (0.07-0.57 (HONO/NO_x %) on days when strong correlations were observed (R^2>0.64). Intercepts for evening rush hours varied between 26-136 pptv similar to that of the daytime values.

Table 5: Correlation data between HONO and NO_x during evening rush hours (16:30-20:00) during the study. The table includes mean PM 2.5 values during the evening rush hour.

Date	R^2	Slope (HONO/NO_x) (%)	Intercept (HONO pptv)	PM 2.5 ($\mu g\ m^{-3}$)
Feb. 15, 2007	0.21	0.06	90	5
Feb. 19, 2007	0.19	0.16	26	5
Feb. 20, 2007	0.19	0.09	59	15
Feb. 21, 2007	0.56	0.38	43	12
Feb. 22, 2007	0.52	0.15	26	3
Feb. 26, 2007	0.11	-0.16	333	10
Feb. 27, 2007	0.52	0.19	136	15
Feb. 28, 2007	0.21	0.14	88	12
Mar. 1, 2007	0.22	-0.34	157	10
Mar. 5, 2007	0.07	0.09	45	5
Mar. 6, 2007	0.003	0.01	97	5
Mar. 7, 2007	0.19	0.11	77	10
Mar. 8, 2007	0.67	0.07	39	5
Mar. 12, 2007	0.32	0.26	99	15
Mar. 13, 2007	0.66	0.57	43	22
Mar. 14, 2007	0.61	0.23	197	12

The slopes from the HONO versus NO_x correlations during morning and evening rush hours were plotted against PM 2.5 loadings, shown in Figure 23. The observed relationship indicates higher

HONO/NO_x ratios when larger amounts of PM 2.5 are present. It is possible that on the days when higher HONO/NO_x ratios were observed a larger fraction of the vehicles passing the site had diesel engines which are expected to produce more HONO and PM than gasoline engines [Kurtenbach et al., (2001)]. The effect is likely a combination of fleet composition and increased conversion of NO_x to HONO on increased aerosol surface, or conversion on fresh carbon [Gutzwiller et al., (2002)].

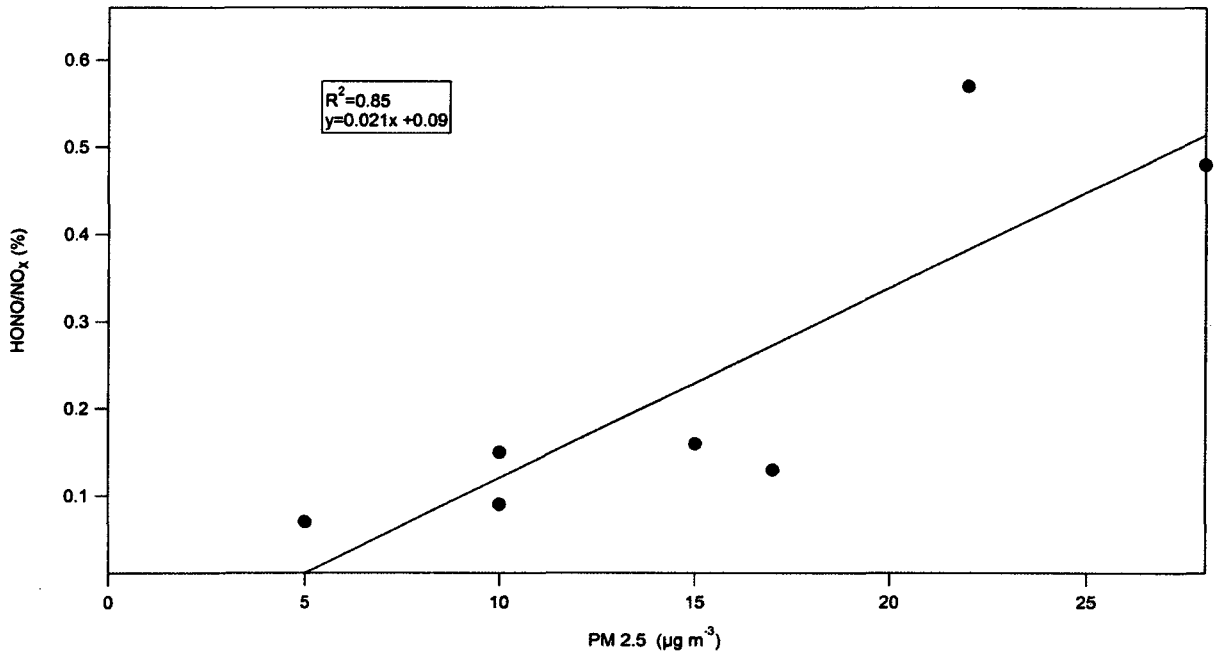

Figure 23: Plot of HONO/NO_x ratio (%) and PM 2.5 during morning and evening rush hours.

If this is representative of conversion of NO_x to HONO on aerosol or black carbon the intercept of the HONO vs. NO_x plots would represent measured HONO not produced through this pathway, such as HONO emitted from some other local point source.

The HONO/NO_x ratios from Tables 4 and 5 are an order of magnitude smaller than those observed on many nights when HONO/NO_x ratios were often between 0.5 and 1.5% around midnight, as shown in Figure 24. The largest observed ratio during rush hours was ~0.5% (the

evening of March 13th and morning of March 14th). The discrepancy between the rush hour $HONO/NO_x$ ratios and the often higher night-time $HONO/NO_x$ ratios indicates there is likely significant amounts of secondary HONO formation proceeding during the night-time hours.

3.1.5 Estimates of night-time HONO production

Production of HONO during the night-time hours at the urban sampling site was estimated using the ratio of $HONO/NO_2$ shown in Figure 24. During a few nights of the campaign (February 19th, 22nd and 28th) there is a clear increase in $HONO/NO_2$ ratio. This increase was used to estimate the amount of conversion of NO_2 to HONO. The ratio of $HONO/NO_2$ should be relatively constant if HONO concentrations are a direct result of emissions (and the diesel/non diesel fleet ratio is constant). The increases in $HONO/NO_2$ ratio occurred after rush hour when HONO concentrations may be strongly influenced by secondary formation. The mean increase in $HONO/NO_2$ on the three selected nights was 0.125% hr^{-1} (February 20th), 0.25% hr^{-1} (February 22th), and 0.075% hr^{-1} (February 28th). These may be expressed in the usual notation as $\frac{d\frac{HONO}{NO_2}}{dt} = \frac{0.00125}{3600\ s} = 3.4x10^{-7}\ s^{-1}$.

First order conversion rates of 3.4 x 10^{-7} s^{-1}, 6.9 x 10^{-7} s^{-1} and 2.1 x 10^{-7} s^{-1} are obtained for the three nights respectively. These are roughly an order of magnitude lower than conversion efficiencies observed during two urban campaigns in Berlin and Milan where values ranged from 3.3 x 10^{-6} s^{-1} (Berlin) and 5.8 x 10^{-6} s^{-1} (Milan), [Alicke et al., (2003); Alicke et al., (2002)]. Wind speeds on all three nights were below 10 km hr^{-1} making it unlikely that produced HONO was simply blowing away. On both the 20th and 22nd winds were from the South West, while on the 28th they were from the North West. It is plausible that HONO produced during the night-time is being taken up by snow, leading to a lower than expected night-time production from NO_2 or that the conditions (aerosol surface area and/or surface composition) were not favourable for conversion. Uptake of HONO has been observed on alkaline snow in other studies [Beine et al., (2005)]. The pH of the snow in the surrounding area of the Toronto measurement site is unknown.

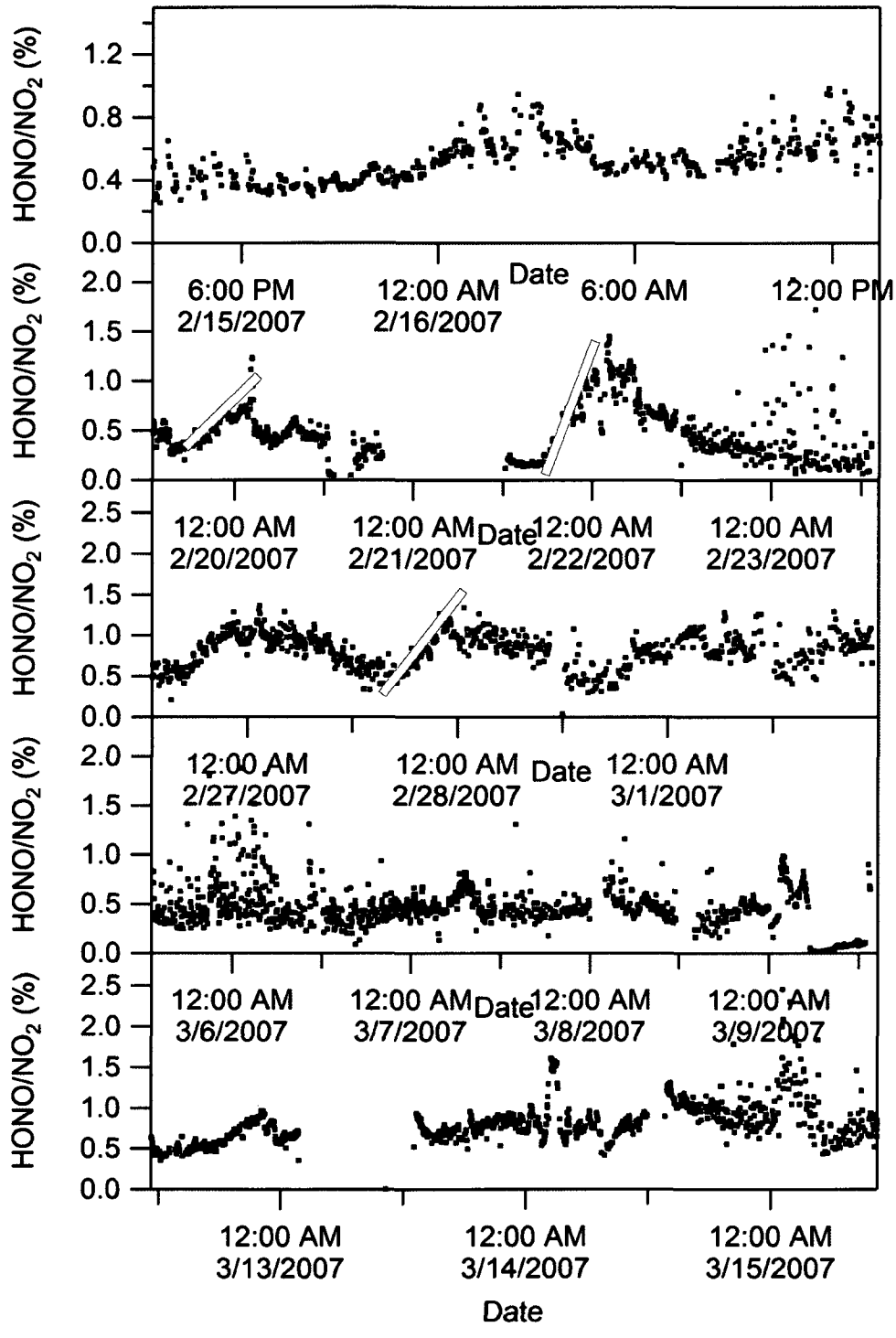

Figure 24: Plot the $HONO/NO_2$ time series over the 5 time periods of the Toronto study.

3.1.6 HONO NO_2 relationships during the urban campaign.

The relationships between HONO and NO_2 mixing ratios (day and night) were examined for each of the 5 time periods of the urban study. For each time period the HONO and NO_2 peaks due to rush hour were not included. The slopes, intercepts and R^2 values are found in Table 6.

Table 6: List of slopes, intercepts and correlation coefficients from HONO NO_2 correlations.

Time Period (2007)	R^2	Slope (HONO/NO_2) (%)	Intercept (pptv)
Feb. 15-16	0.55	0.25	**80**
Feb. 20-23	0.86	0.95	**-59**
Feb. 26-Mar. 2	0.83	0.92	**-34**
Mar. 5-9	0.81	0.50	**-8**
Mar. 12-15	0.75	0.58	**53**

It is apparent that even with rush hour emissions removed HONO and NO_2 are strongly correlated. While the correlations ranged from 0.545-0.857, there is a large variability in the slopes (and intercepts) of the five plots. There is believed to be no physical meaning to the intercepts. The third time period (Feb. 26-March 2) showed a strong correlation (R^2>0.64) and had low wind speeds (<10 km hr^{-1}) for the duration of the period. It appears HONO correlations with NO_2 were stronger during periods with lower wind speeds.

The HONO/NO_2 ratio is examined as a function of wind direction (Figure 25) with wind speeds less than 5 km hr^{-1} removed. During both the daytime and night-time a large fraction of the observed winds were from 225-45°. The only distinct difference between the day and night-time

periods is the higher HONO/NO_2 (>1%) ratios observed during the night when winds were from the North. It is likely that these higher ratios indicate an increased importance of secondary production of HONO in air coming from the North.

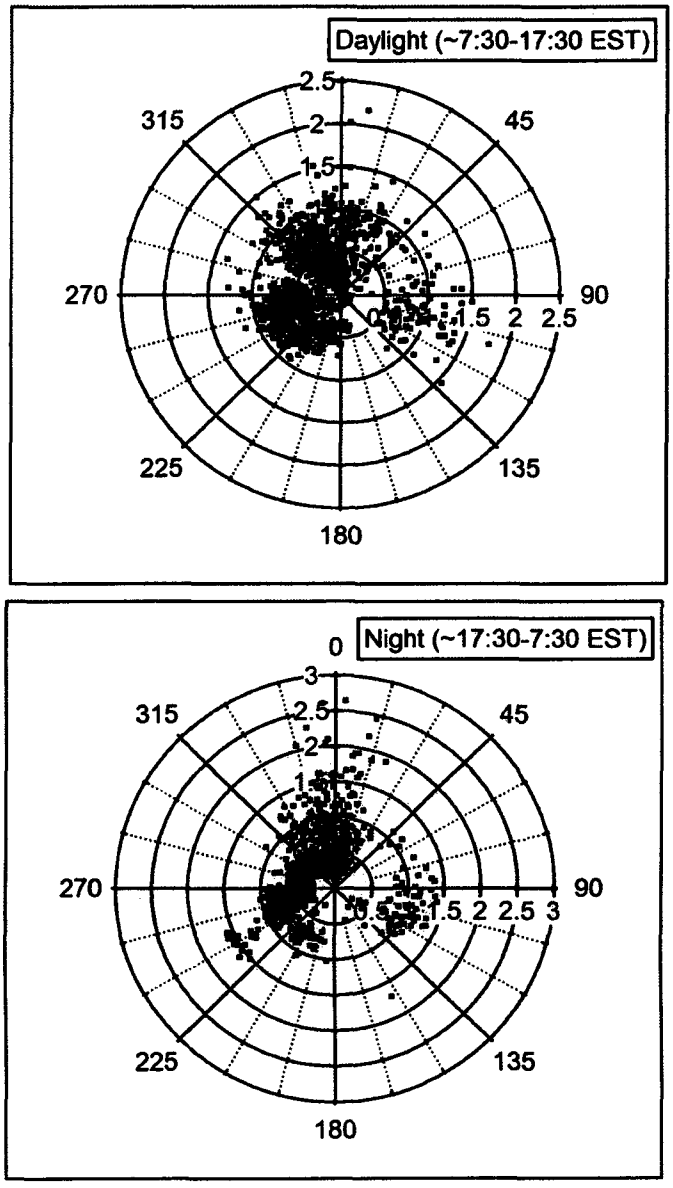

Figure 25: Polar plots of HONO/NO_2 ratio (%) as a function of wind direction. Points with wind speeds below 5 km hr^{-1} have been removed.

In summary at the Toronto site, fresh emissions of HONO from traffic and/or heterogeneous processes involving NO_2 can explain the major features in the HONO data. Increases in HONO and NO_x concentrations, often large increases, were observed during rush hour periods at the site. Periods of high variability in the HONO data appear to a result of variability in the NO_x concentrations resulting from poorly mixed emissions. Any daytime photoenhanced processes could not be discerned in the presence of the large direct emission sources in the area of the sampling site.

3.2 Forested Site - Borden

Environment Canada's Forest Flux [Environment Canada. (2008)] monitoring site is located on the north end of Canadian Forces Base Borden (44° 19' N, 79° 56' W) and was chosen as a rural site for HONO measurement. The site is in a mixed deciduous forest, the dominant species present are red maple, trembling aspen, large-tooth aspen, white ash, black cherry and white pine. It is 120 m above sea level. The site has been used for many other studies over the years [Fuentes et al., (1992); Fuentes et al., (1995); Makar et al., (1999); Gu et al., (1999)]. An image of the location can be seen in Figure 26.

Figure 26: Overview of Borden sampling site.

The site is located under a forest canopy (22 m in height) which shields it from direct sunlight for large portions of the day. While the area surrounding the site is forested, there are also agricultural crops and pastures within a kilometre of the site to the North. While the site can be affected by pollution from the Greater Toronto Area (approximately 70 km South East of the site), it is usually quite clean, with NO_x levels generally below a few ppbv.

3.2.1 Instrumentation

The LOPAP was located in a trailer at the base of the meteorological tower installed by Environment Canada. The LOPAP sampling coil was located outside of the trailer in a heated box keeping the temperature of the sampling coil at or above 298K to ensure a consistent sampling efficiency of HONO and reducing the possibility of condensation in the lines. Measurements were performed during the months of July and August 2006. Other gas phase species measured at the site included NO_x, O_3, SO_2, and NH_3 as well as several VOC's. These measurements were performed by Environment Canada. Meteorological parameters that were measured included temperature, wind speed, relative humidity and short wave and long wave solar radiation, these measurements were also performed by Environment Canada.

The LOPAP was set up as described earlier and had a detection limit of 5 pptv. Measurements of NO_2 at the site were performed by a standard NO_x chemiluminescence instrument with a photolytic converter to convert NO_2 to NO. The temperature measurement was performed below the canopy while wind speed and wind direction measurements were made above the forest canopy. J_{HONO} was estimated Wall et al., (2006) from measurements using an Eppley total UV radiometer in the canopy. Measurements of NO_x, temperature and UV were performed by Environment Canada. Wall et al., (2006) used a chemical actinometer to measure J_{HONO} values. A Heraeus Amersil Electrically Fused quartz cell was used as their photolysis cell on the roof of a building in Toronto Ontario. The actinometer was set up so that known amounts of HONO could be sent through the cell to the HPLC detection unit or diverted directly to the HPLC detection unit. The measured difference was used to calculate values of J_{HONO}. Their estimated error in J_{HONO} values under clear sky conditions was 11% at sunrise and 4% at solar noon during the summer months. The chemically measured HONO photolysis frequency was correlated with the

output of an Eppley total UV radiometer. This relationship was used in order to estimate the values of J_{HONO} at the Borden site. Based on the error in the original J_{HONO} measurement (from clear sky conditions) and the unknown filtering properties of the canopy, J_{HONO} values are estimated to be accurate within 20%.

3.2.2 Measurements of HONO beneath a Forest Canopy

Time series of HONO, NO_2, NO, O_3, J_{HONO}, relative humidity, temperature, wind direction and wind speed at Borden are shown in Figure 27 and 28. No data prior to 8th of August is shown due to power problems and precipitation at the site. Meteorological data is also missing between the 16th and 18th of August due to power problems.

The majority of the study was characterized by rural background air. Winds were from the North West and North East for the majority of the campaign carrying clean air from Northern Ontario instead of more polluted air from the GTA. The mean wind speed was 2.5 km hr^{-1} above the canopy. The temperature inside the canopy varied between 9-36 °C (mean=22.1 °C), with high night-time relative humidity (typically greater the 70%).

Nitric oxide followed a diurnal cycle (with a night-time maximum and a daytime minimum) over the course of the study. Soil emissions and low night-time O_3 concentrations must be responsible for the higher night-time concentrations as there were no combustion sources nearby. Based on the anti correlation of the NO and O_3 data sets it appears NO was rapidly oxidized by O_3 in the morning hours after the breakup of the boundary layer. Nitrogen dioxide concentrations followed a diurnal cycle (night-time maxima, daytime minima) during several periods of the study (August 8-10, August 18). Concentrations of NO_2 also rose on the night of the 19th and remained between 1 and 2 ppbv until the morning of the 20th.

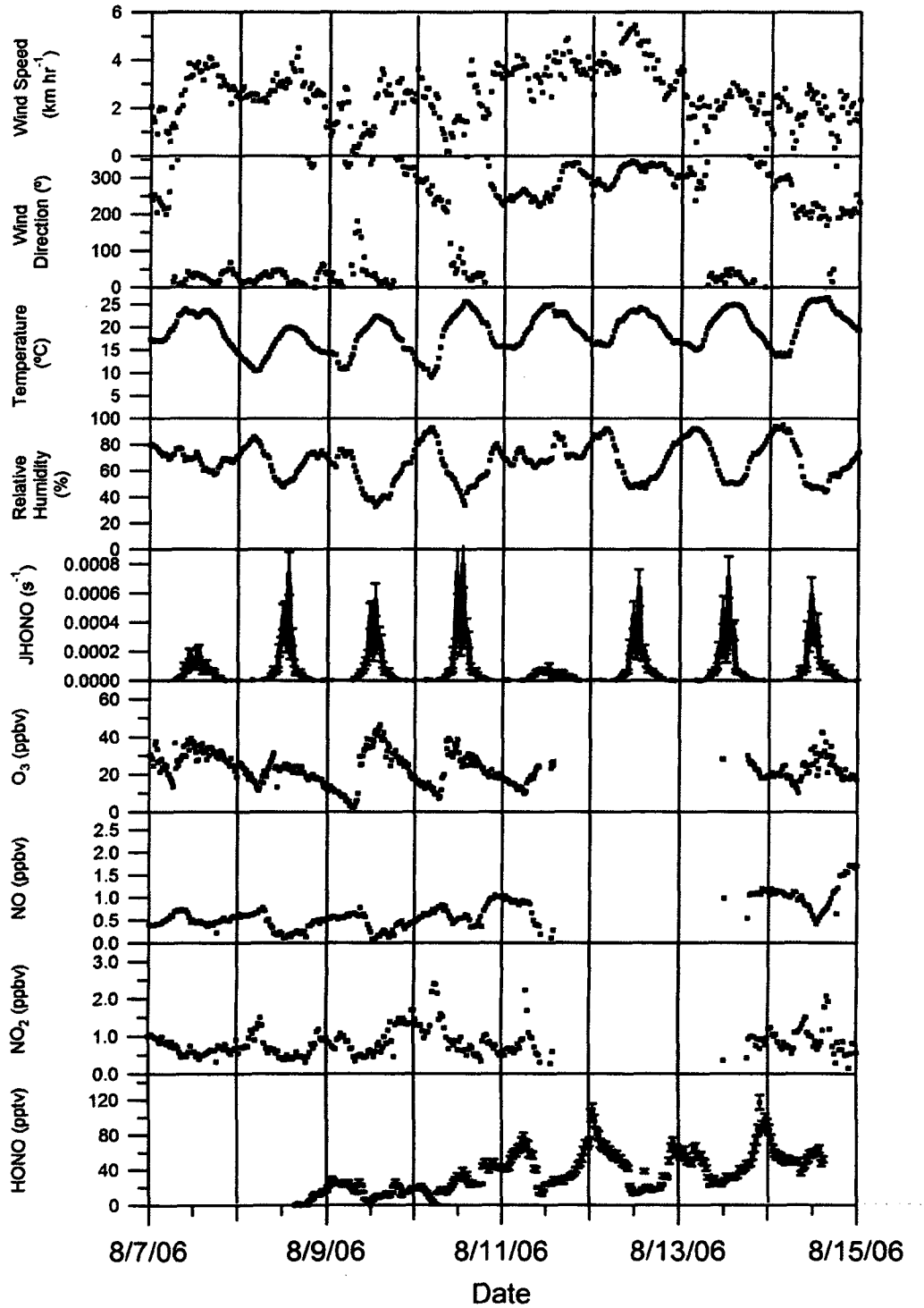

Figure 27: Plot of time series for chemical and meteorological measurements at Borden sampling site from August 8-14, 2006 local time.

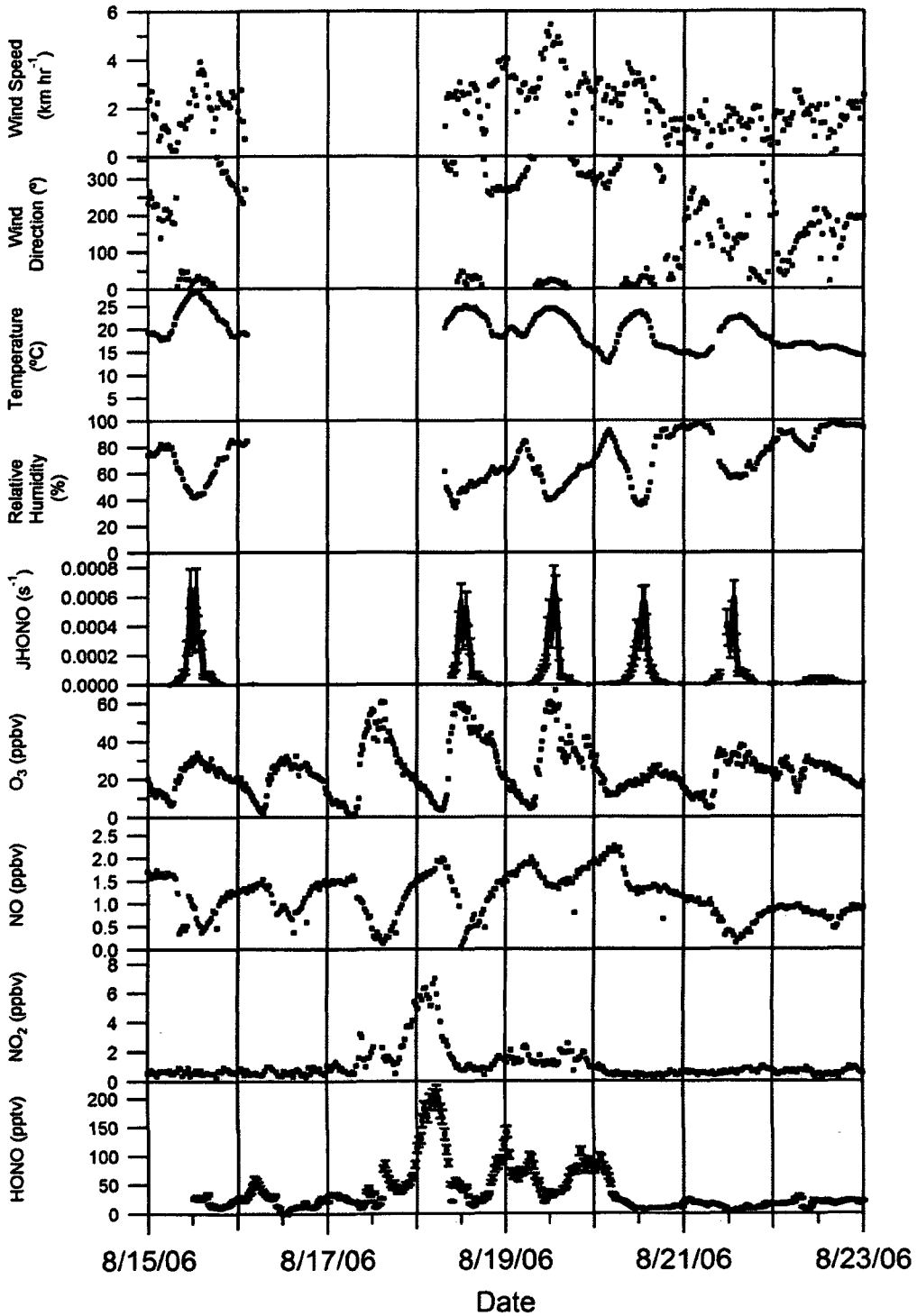

Figure 28: Plot of time series for chemical and meteorological measurements at Borden sampling site from August 15-23, 2006 local time.

3.2.3 Night-time Production of HONO

Nitrous acid mixing ratios followed a diurnal cycle on several days of the study. Night-time maxima were observed on the 9^{th}, 11^{th}-14^{th} and 18^{th}-20^{th}. Mixing ratios increased each evening, with a mean HONO production rate of ~8 pptv/hr, and dropped in the morning. The largest peak in HONO concentration occurred shortly -midnight on August 18^{th} when concentrations reached 237 pptv. This peak coincided with the largest NO_2 concentrations observed, (~6 ppbv). Since meteorological data was not available for that night, back-trajectories were determined from HYSPLIT. HYbrid Single-Particle Lagrangian Integrated Trajectory, HYSPLIT [ARL and NOAA. 2005] is a complete system for computing simple air parcel trajectories to complex dispersion and deposition simulations. The trajectories are allowed vertical motion. The method of vertical motion used was model vertical velocity, which uses the meteorological models vertical velocity fields. Using HYSPLIT, back trajectories were calculated and are shown in Figure 29.

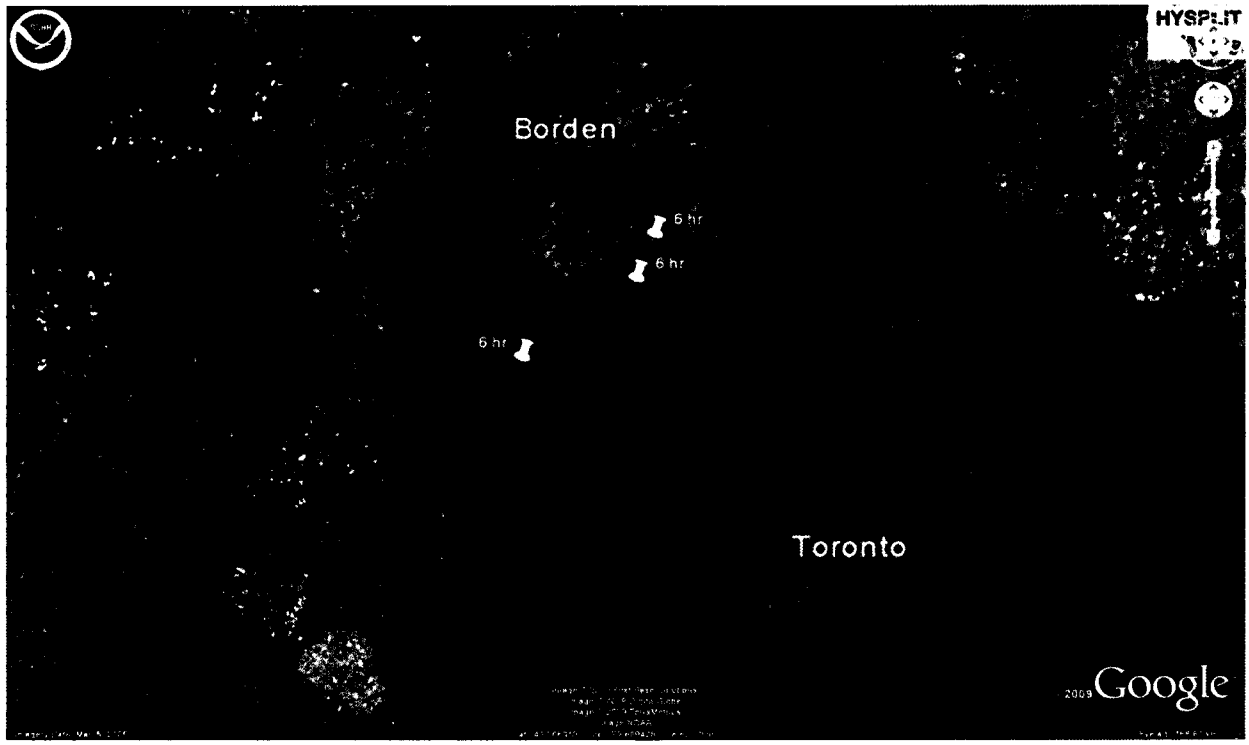

Figure 29: Back trajectory analysis using HYSPLIT showing the origin of the air mass (12 hr prior) observed on the night of August 17th/18th 2006. The different colours represent different end heights of the trajectories (green=50 m, red=100 m, blue =200 m). The yellow pins indicate the location of the air mass 6 hours prior to arriving at the Borden site.

The back trajectories show the air mass observed on the night of the $17^{th}/18^{th}$ passed over the GTA 12 hours earlier. This may explain where the relatively large observed HONO and NO_2 concentrations originated from.

There were peaks in HONO concentration the following two nights as well (~100pptv each night) with observed concentrations of NO_2 higher than the typical background NO_2 levels (~2 ppbv). While the winds were from the North and North West, wind speeds were quite low (~2 km hr^{-1}), resulting in the air below the canopy being likely quite stagnant and with the measured HONO expected to be produced from NO_2 hydrolysis. On both nights HONO is produced at a rate of roughly 15 pptv hr^{-1}.

During most days of the campaign HONO mixing ratios did not decrease to the detection limit of the LOPAP. Mixing ratios on the afternoons of August 11^{th}-14^{th}, and 18^{th}-20^{th} were between 20-50 pptv. The mean daytime mixing ratio during the study was 27 pptv. This is unexpected based on "classical" chemistry as HONO photolysis rates were as high as $0.7 X10^{-3} s^{-1}$, equivalent to a photolytic half life of ~30 minutes, (Maxima of J_{HONO} occurred sharply at midday when the sun was highest and least obscured by the canopy). In order to assess HONO production from NO_2, $HONO/NO_2$ ratios were examined. The ratio $HONO/NO_2$ is considered to characterise HONO formation [Kleffmann et al., (2003)] since HONO is formed from the heterogeneous reaction of NO_2 on damp surfaces [Lammel and Cape, (1996); Reisinger, (2000)]. A time series of the ratio is shown in Figure 31. Assuming that HONO formation is first order in NO_2 on surfaces [Harrison and Kitto, (1994)] the increase in $HONO/NO_2$ ratio over the course of the night is used to obtain a conversion rate of NO_2 to HONO. Using the increase in $HONO/NO_2$ ratio between 20:00 and 00:00 local time in the same manner as the urban data set, a mean conversion efficiency of $1.4 \times 10^{-6} s^{-1}$ (range between $1.1\text{-}1.7 \times 10^{-6} s^{-1}$) is obtained in agreement with other studies ($2\text{-}3 \times 10^{-6} s^{-1}$,Alicke et al., (2003); Alicke et al., (2002)).

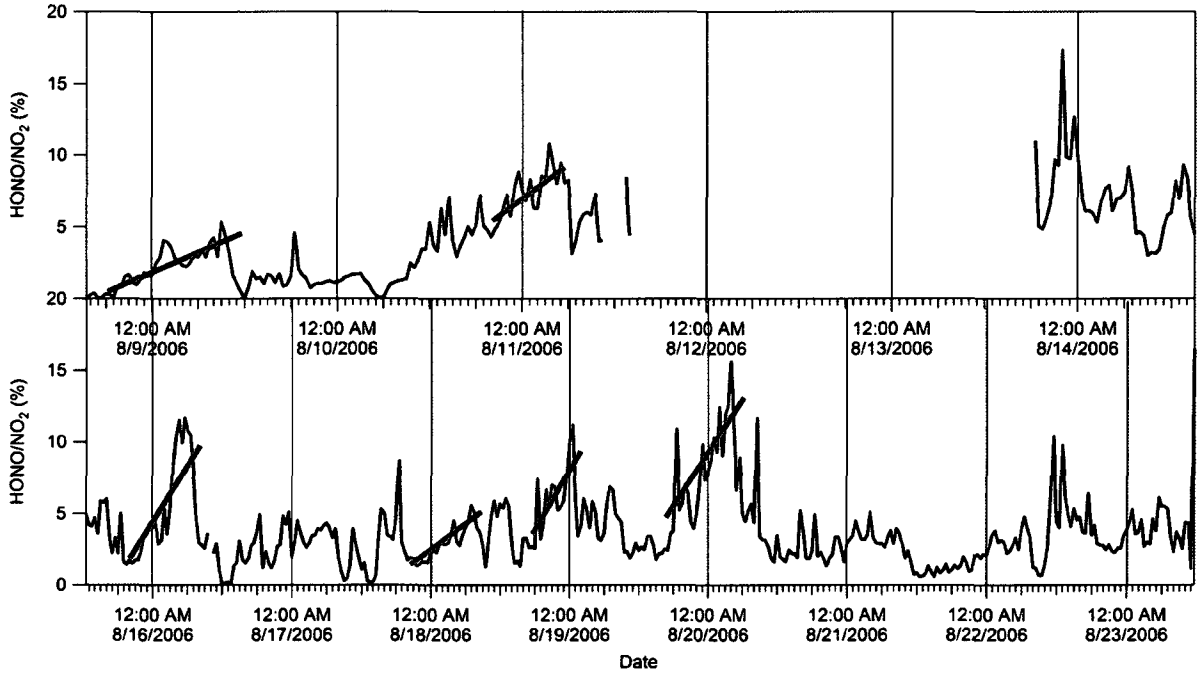

Figure 30: Plot of $HONO/NO_2$ ratio from August 8-23 during the Borden campaign. Tick marks indicate midnight on that day. Red lines indicate rise in $HONO/NO_2$ ratio per hour.

Assuming this night-time conversion of NO_2 to HONO occurs at the same rate during the daytime hours, the observed daytime HONO during the afternoons of August 11^{th}-14^{th}, and 18^{th}-20^{th} cannot be explained since the loss rate from photolysis is roughly two orders of magnitude larger than that for production. There are clearly other daytime HONO production processes occurring which are competitive with loss from photolysis. It appears possible that the mechanism involves NO_2 being converted to HONO through a different mechanism since there are peaks in the $HONO/NO_2$ ratio during the midday period of days such as the 17^{th} and the 19^{th}. Since the production process during the day does not occur during the night, it is apparent that solar radiation may be implicated either directly or by producing reactants that require solar radiation, as has been suggested in other studies [Kleffmann et al., (2005); Staffelbach et al., (1997b); Kleffmann et al., (2003); Kleffmann et al., (2002); Huang et al., (2002); Zhou et al., (2002); Neftel et al., (1996)]. This will be examined in more detail in Chapter 3.2.4.

3.2.4 HONO relationships with NO_x, NO and NO_2

Nitrous acid mixing ratios showed some dependence on NO_x and NO_2 mixing ratios if all data are used, (R^2=0.75, Figure 31, R^2=0.71, Figure 32). However, the relationship between HONO and NO_2 was examined with the August 17th/18th peak removed (Figure 33). Concentrations of HONO and NO_2 were significantly higher on that night than other nights during the study which strongly affected their correlation. As the back trajectory showed (Figure 29), the air reaching the site had been affected by emissions in air brought from the GTA region, bringing higher levels of NO_2 and HONO than were observed on any other night. Exclusion of the night of the 17th/18th resulted in very little correlation between NO_2 and HONO (R^2=0.41) indicating that the one night was driving the correlation.

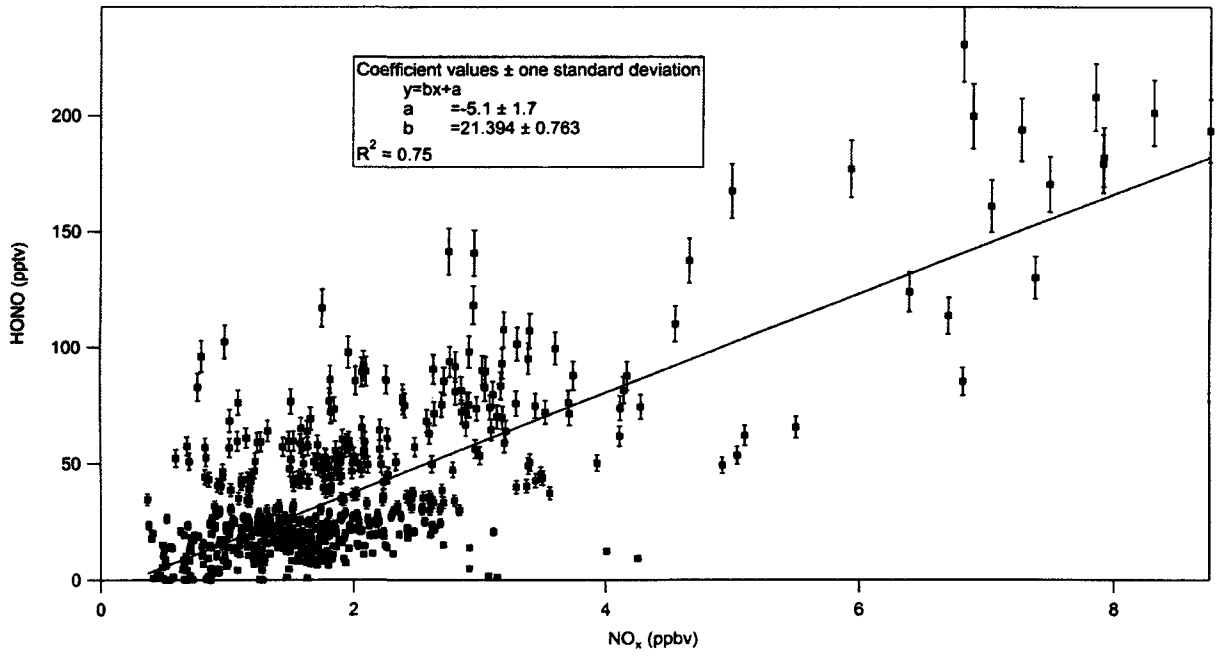

Figure 31: Plot of HONO mixing ratio as a function of and NO_x mixing ratio for all data at the Borden measurement site.

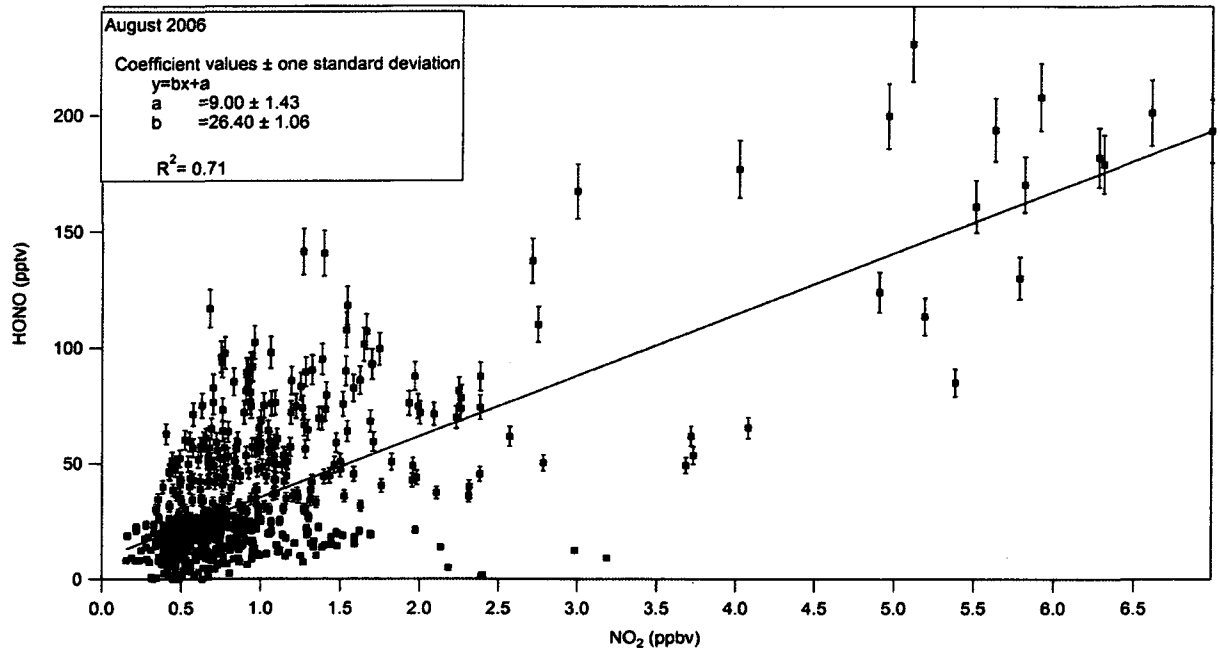

Figure 32 Plot of HONO mixing ratio as a function of NO_2 mixing ratio at the Borden measurement site.

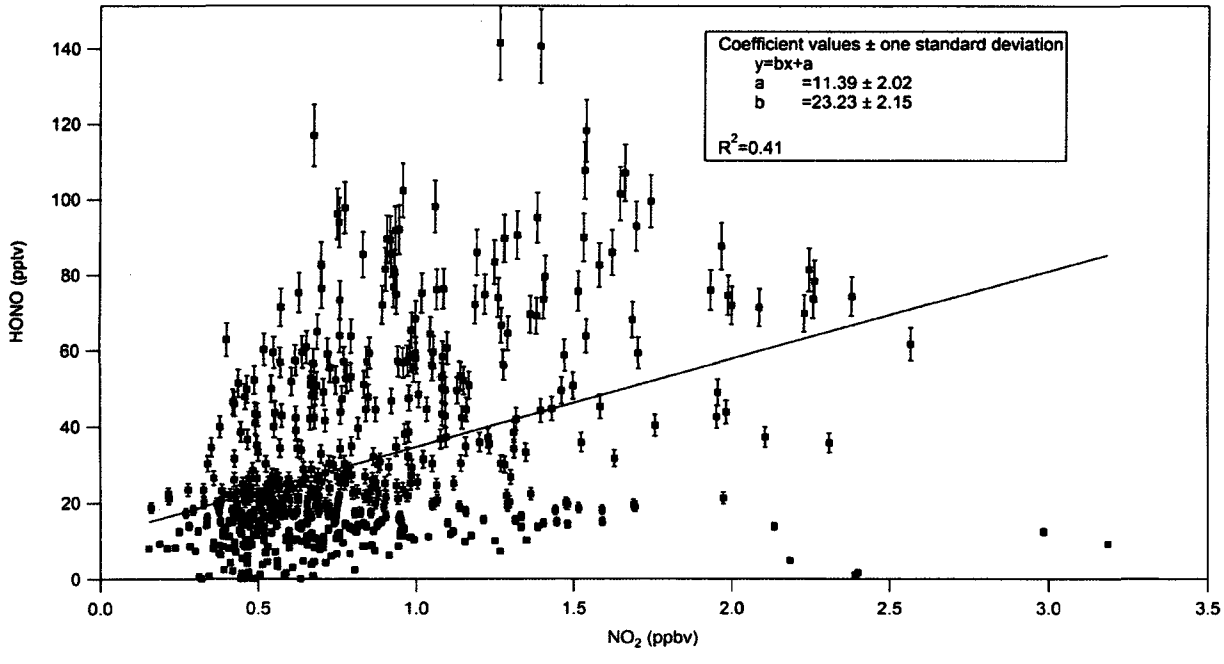

Figure 33: Plot of HONO mixing ratio as a function of NO_2 mixing ratio between August 8-23 with the night-time peak on August 18 removed.

Similar low correlations were observed with NO vs. HONO when all data are used (Figure 34). Correlations of HONO with NO have been observed in other studies where there are high NO_x emissions from combustion [Kurtenbach et al., (2001); Kleffmann et al., (2003)]. Correlations between HONO and NO at the Toronto site were observed during rush hour (R^2~0.80).

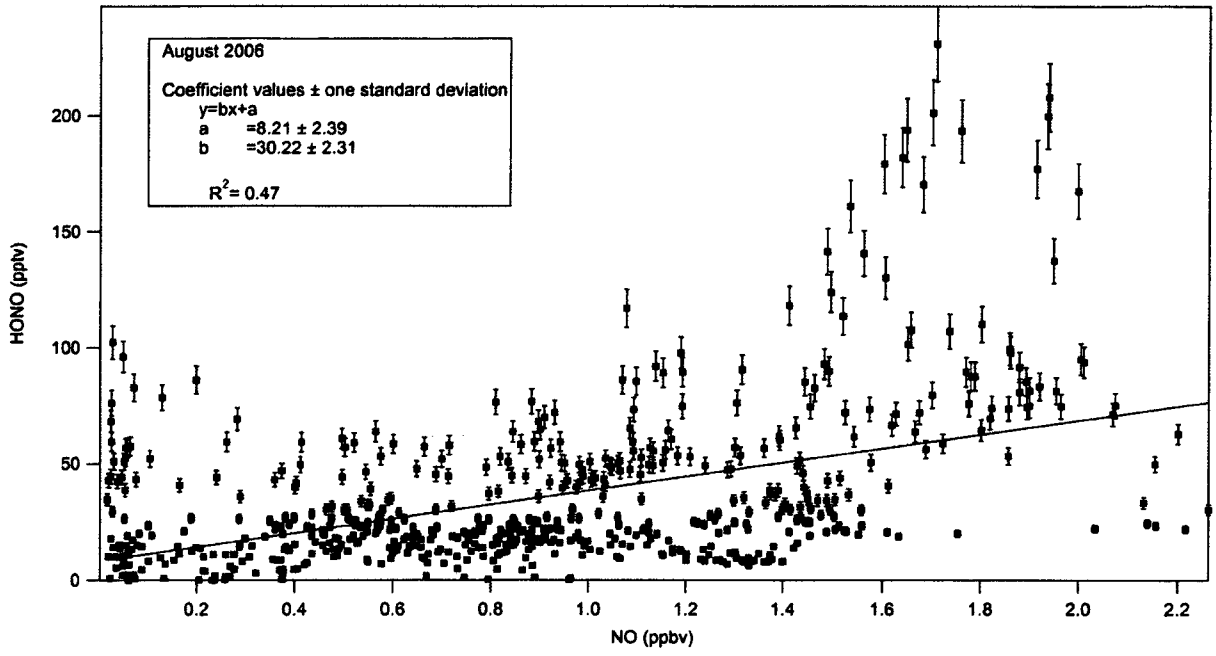

Figure 34: Plot of HONO mixing ratio as a function of NO mixing ratio August 8-23, 2006.

The night of August 17th/18th was the only night where strong correlations with NO_2 were observed, shown in Figure 35, R^2=0.91. While it would be expected that HONO and NO_2 concentrations would correlate when emission levels from combustion are high, (e.g. at the Toronto site), this is not necessarily true in rural locations. Acker et al., (2005) observed varying correlations between HONO and NO_2 during the ESCOMPTE 2001 experiment. Positive correlations were only observed during pollution events when winds speeds were low (0-4 m s^{-1}).

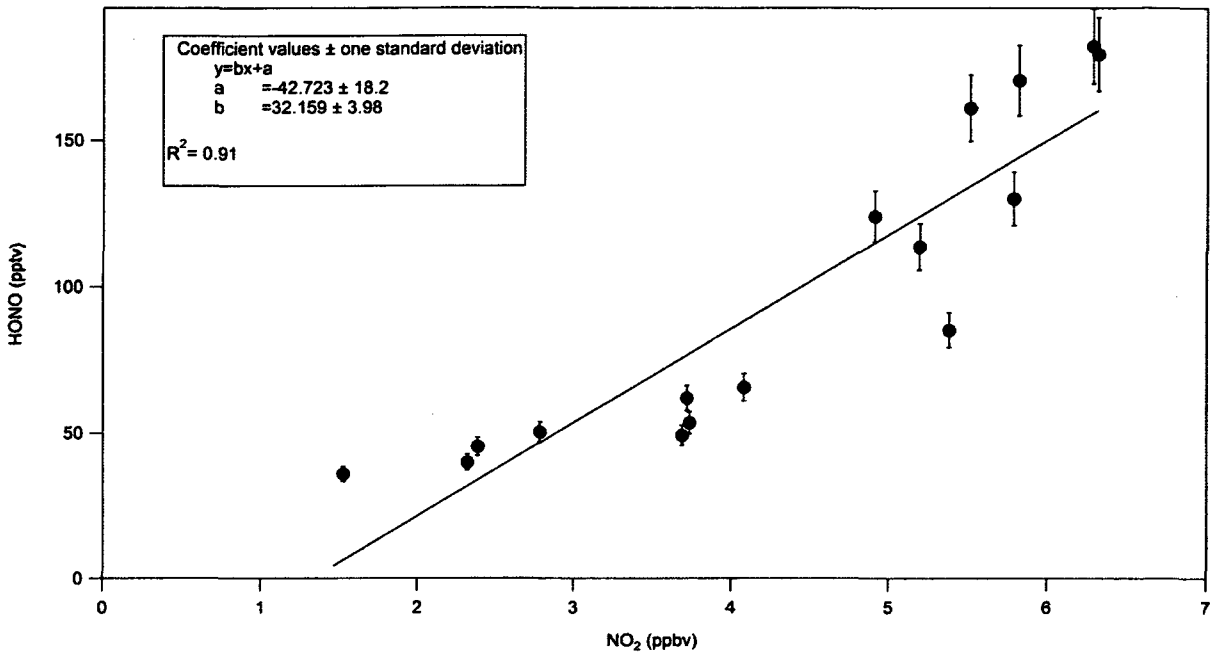

Figure 35: Plot of HONO mixing ratio as a function of NO_2 mixing ratio on the night of August 17th/18th 2006.

When HONO and NO_2 concentrations are separated by day and night (and the night of $17^{th}/18^{th}$ is not considered) the correlation observed for daytime HONO and NO_2 mixing ratios improves over that of the overall data set (daytime R^2=0.51 vs R^2=0.41 for day and night). The night-time only correlation decreases (R^2=0.35). The absence of a correlation in the night-time data could be plausibly explained by the increasing HONO/NO_2 ratio observed on many nights, as NO_2 is converted into HONO. During the daytime it is possible that measured HONO concentrations are not dominated by NO_2 alone. It is apparent from the calculated night-time HONO production rate that conversion of NO_2 alone cannot explain the measured daytime HONO.

3.2.5 Photolytic HONO Production

As discussed earlier, higher than expected daytime concentrations of HONO were observed on several occasions during the study. The night-time formation of HONO from NO_2, previously estimated to be on average 8 pptv/hr would not be able explain these observed daytime values as it is not competitive with photolysis, thus an additional pathway must be considered.

Recently suggested formation mechanisms for daytime HONO require solar radiation and NO_2 in order to produce HONO [George et al., (2005); Stemmler et al., (2006); Ndour et al., (2008)]. The solar radiation excites either an organic or inorganic surface (either ground or aerosol) which is able to reduce NO_2 to HONO. Since HONO photolyzes in the region between 300 and 400 nm our J_{HONO} values were taken as a proxy for solar radiation.

The 19th was chosen as a test case since minimum daytime concentrations were high, ~50 pptv at noon. A gas phase photo stationary state (PSS) of HONO was assumed, in order to calculate a background of HONO. The PSS is calculated from J_{HONO}, R 3, and a second HONO sink (R 11), and the mean heterogeneous formation rate to give:

$$[HONO]_{PSS} = \frac{(k_3[NO][OH] + 5.5 \times 10^4)\ molec\ cm^{-3}\ s^{-1}}{J_{(HONO)} + k_{11}[OH]} \qquad \text{(Eq. 4)}$$

A noontime OH value of 1x10^6 molec cm^{-3} was taken from Makar et al., (1999) and mixing ratios were estimated by using a diurnal variation (noontime maximum, zero at sunrise and sunset) given by a cos^3 (SZA) function (where SZA is the solar zenith angle). A cos^3 function was chosen since its shape closely matches the profile of O^1D production from O_3 photolysis. Using these estimated OH values in addition to measured NO and derived J_{HONO} values, a HONO PSS was

calculated. The calculated $[HONO]_{PSS}$ values were found to be only a part per trillion indicating that virtually all of the actually observed daytime HONO present was formed through unknown sources.

Using the HONO sinks (photolysis and reaction with OH) and the measured HONO amounts, a daytime production rate for the unknown source could be calculated by replacing $(k_3[NO][OH] + 5.5x10^4)$molec cm^{-3} s^{-1} with the unknown HONO source and rearranging equation 4 . In previous modelling studies unexplained daytime HONO sources have been found to be dependent on J_{NO2} and NO_2 [Vogel et al., (2003)], thus a correlation of the production rate of HONO with the product of NO_2 and J_{HONO} was examined. The values of J_{HONO} were used in lieu J_{NO2} since J_{HONO} and J_{NO2} show a constant ratio of about 2.5 [Kraus and Hofzumahaus, (1998)] J_{HONO} suffices when looking at the quality (R^2) of correlations. The scatter plot of HONO production as a function of the product of J_{HONO} and NO_2 for August 19th is shown in Figure 36. The error bars represent the estimated uncertainty in the HONO production rate and J_{HONO} NO_2 product, based on the uncertainty in J_{HONO} estimated to be 20%, the estimate of the uncertainty in NO_x (NO and NO_2, 15%) and the uncertainty in excess HONO (20%). Uncertainties in OH are not considered as the data used was modelled.

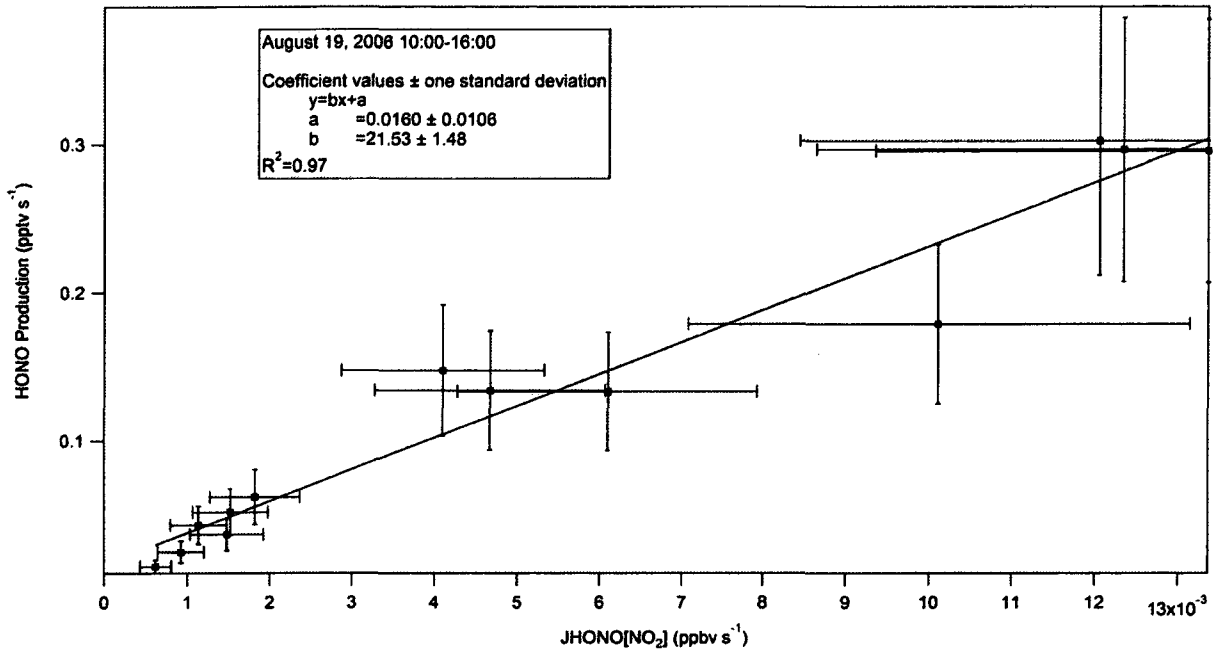

Figure 36: Plot of correlation of HONO production rate vs the product of HONO photolysis rate and NO_2 mixing ratio between the hours of 10:00 and 16:00 August 19, 2006. The slope is denoted by b, the intercept is denoted by a.

The hours of 10:00-16:00 EST were used in Figure 36 as these were the hours where maximum light was penetrating the canopy. The maximum solar radiation penetrating the canopy did not occur until roughly 13:00 local time. A strong correlation between the HONO production rate and the product of J_{HONO} and NO_2 was exhibited (R^2=0.97). A correlation between HONO production rate and J_{HONO} alone would not be surprising as both have a dependence on J_{HONO}. However the improved quality of the correlation with the addition of NO_2 is interesting.

A second day (August 20th) was examined and showed a similarly strong relationship between measured HONO production and the product of J_{HONO} and NO_2 mixing ratio as was observed on August 19th (R^2=0.97). The meteorological conditions during the afternoons of both days were similar. The relative humidity was approximately 60% with temperatures near 20 °C.

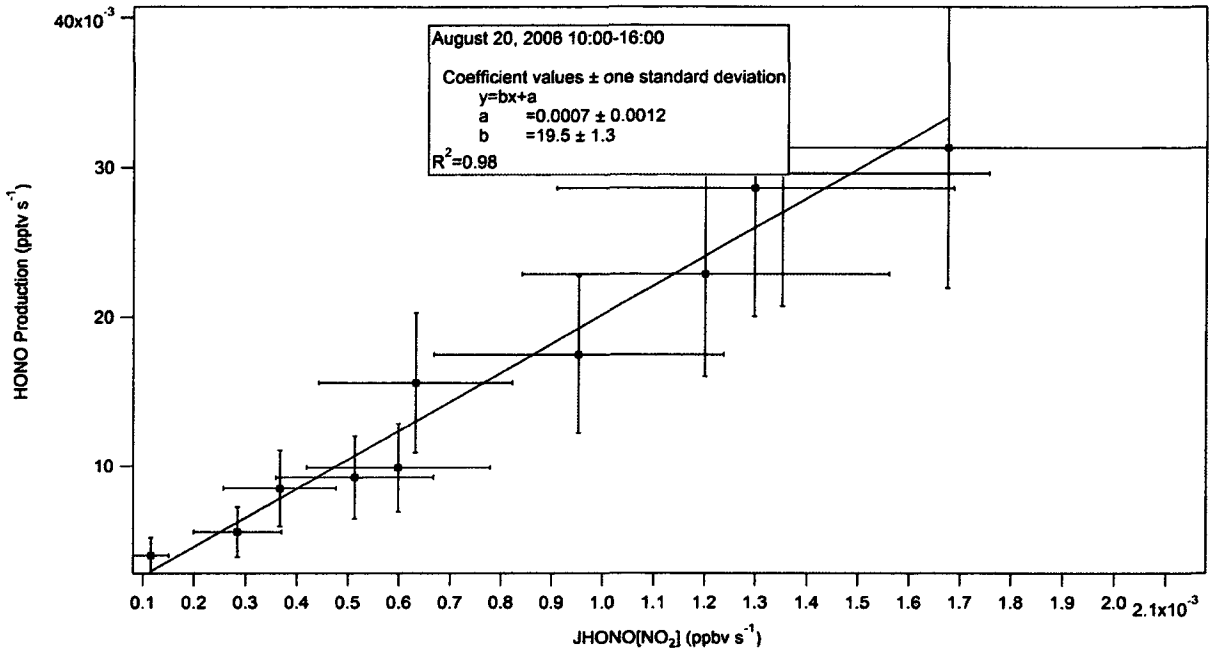

Figure 37: Plot of correlation of HONO production rate with the product of HONO photolysis rate and NO_2 mixing ratio between the hours of 10:00 and 16:00 August 20, 2006. The slope is denoted by b, the intercept is denoted by a.

Daytime HONO production and the product of J_{HONO} and NO_2 mixing ratio were then examined for all afternoons during the study period and is shown in Figure 38.

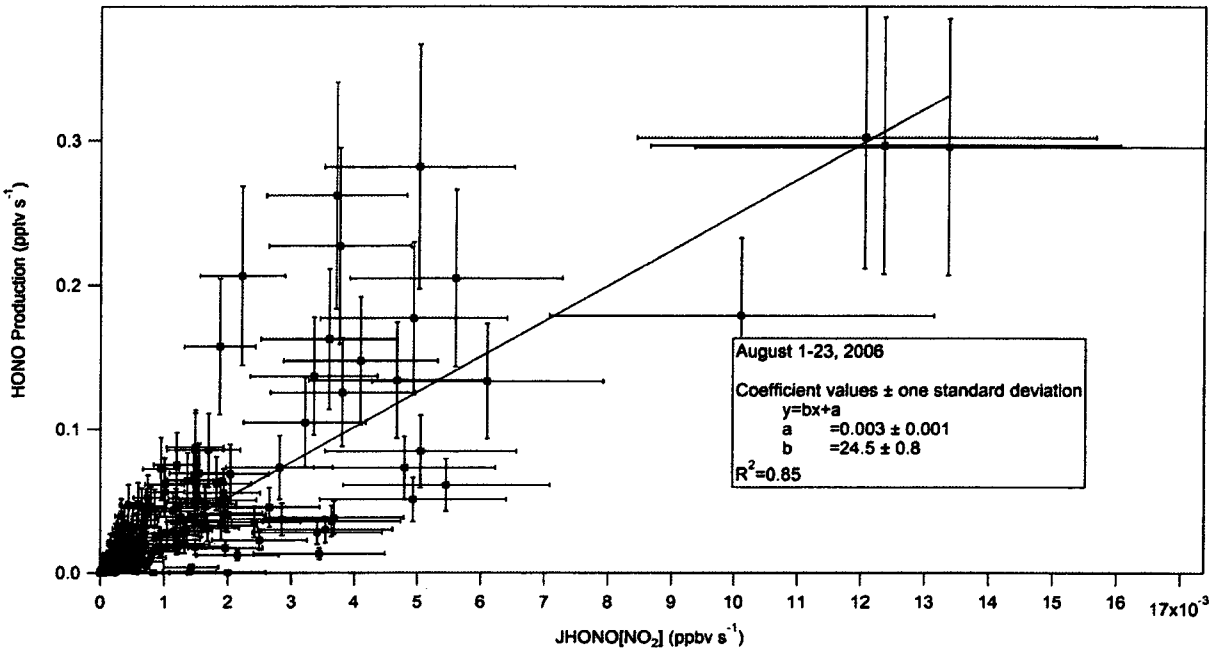

Figure 38: Plot of correlation of HONO production rate with the product of HONO photolysis rate and NO_2 mixing ratio for all afternoons where data was available from August 8-23. The slope is denoted by b, the intercept is denoted by a.

While the correlation was not as strong as the 19th alone it still produced an R^2=0.85. The slopes of these plots and calculation of apparent HONO production rate constants for a gas phase process will be discussed in Chapter 4.2.

The relationship between HONO production and a variety of other parameters from the Borden site was examined. The data used were from the midday period (10:00 to 16:00 EST) of August 8-23 (when data was available) and the results are summarised in Table 7.

Table 7: Summary of correlations of daytime HONO production.

Measurement	R^2
NO_x	0.12
NO	0.08
NO_2	0.11
J_{HONO}	0.78
J_{HONO}*NO_2	0.85
J_{HONO}*NO_2*H_2O	0.88
J_{HONO}*NO_2*NO	0.75
J_{HONO}*NO_2*Relative Humidity	0.69
Wind Speed	0.01
Temperature	0.26
Relative Humidity	-0.30

There was no clear correlation with NO_x, (NO or NO_2) and while there was an expected correlation with J_{HONO}, it was improved by roughly 10% by the inclusion of NO_2. The inclusion of absolute humidity increased the correlation coefficient yet again (R^2=0.88). Correlations between HONO production and the product of J_{HONO}, NO_2 mixing ratio and absolute H_2O mixing ratio are examined further in Chapter 4.2. Including NO mixing ratios or the relative humidity with the correlated product of J_{HONO} and NO_2 mixing ratio only decreased the R^2 values. No relationship was found between HONO production and any other meteorological parameters. The short lifetime of HONO above the canopy (10-15 minutes) makes transport over any significant distance during the daytime unlikely; the mean wind speed during the study was 2.5 km hr^{-1} making it unlikely that the site was affected by emissions greater than 1 km away at noontime. Since there were no known

combustion sources of HONO near the site it seemed likely that most or all of the HONO observed during the day must have been produced in or under the canopy. It is unclear whether or not the daytime HONO production process is a heterogeneous or gas phase process since both have been suggested in various laboratory studies.

3.2.6 Potential OH Production from HONO Photolysis

The higher than expected daytime HONO concentrations are important as they represent a possibly significant increase in OH production below the canopy. Based on measured HONO mixing ratio and estimated J_{HONO} values, HONO photolysis below the canopy represents a maximum noontime OH production rate of 7 x 10^6 molec. $cm^{-3}s^{-1}$ during the afternoon hours of August 8-23, 2006. Based on previously known chemistry it would have been expected that the HONO contribution should be negligible to the OH budget. During the ECHO study the typical noontime production of OH from HONO was 3.1 x 10^6 molec $cm^{-3}s^{-1}$, it was determined that HONO (mean=147 pptv) contributed 33% of the OH budget with total production rates varying from 8-11 x 10^6 molec. $cm^{-3}s^{-1}$. Ozone (mean~30 ppbv), and formaldehyde (mean~5.5 ppbv) photolysis contributed 28% and 31% respectively during the ECHO study with the ozonolysis of VOC's accounting for the rest. Under the VOC rich canopy the lifetime of OH is expected to be less than a second. Unfortunately photolysis data for O_3 and formaldehyde (or measurement data) are not available at Borden so it is not possible to quantify the overall contribution of HONO photolysis to the OH budget at Borden for the study.

Before further investigating the issue of homogeneous vs. heterogeneous mechanisms for the production of HONO and hence OH at Borden, the results of the third campaign at Harrow Ontario, during the summer of 2007 are presented.

3.3 BAQS-Met

During the summer of 2007 the LOPAP was deployed as part of the Border Air Quality and Meteorological Study (BAQS-Met) at the Harrow Ontario supersite (42.03418, -82.9174). BAQS-Met was a major collaborative study to help understand the effects of the transborder flow of pollutants, lake effects and gas/particle processing that often occur in Southern Ontario. There were three Supersite locations during the study; Harrow Ontario, Ridgetown Ontario and Bear Creek (southwest of Wallaceburg Ontario).Measurements were also performed at two smaller sites, one on Pelee Island, the other in Windsor Ontario. A map is shown in Figure 39.

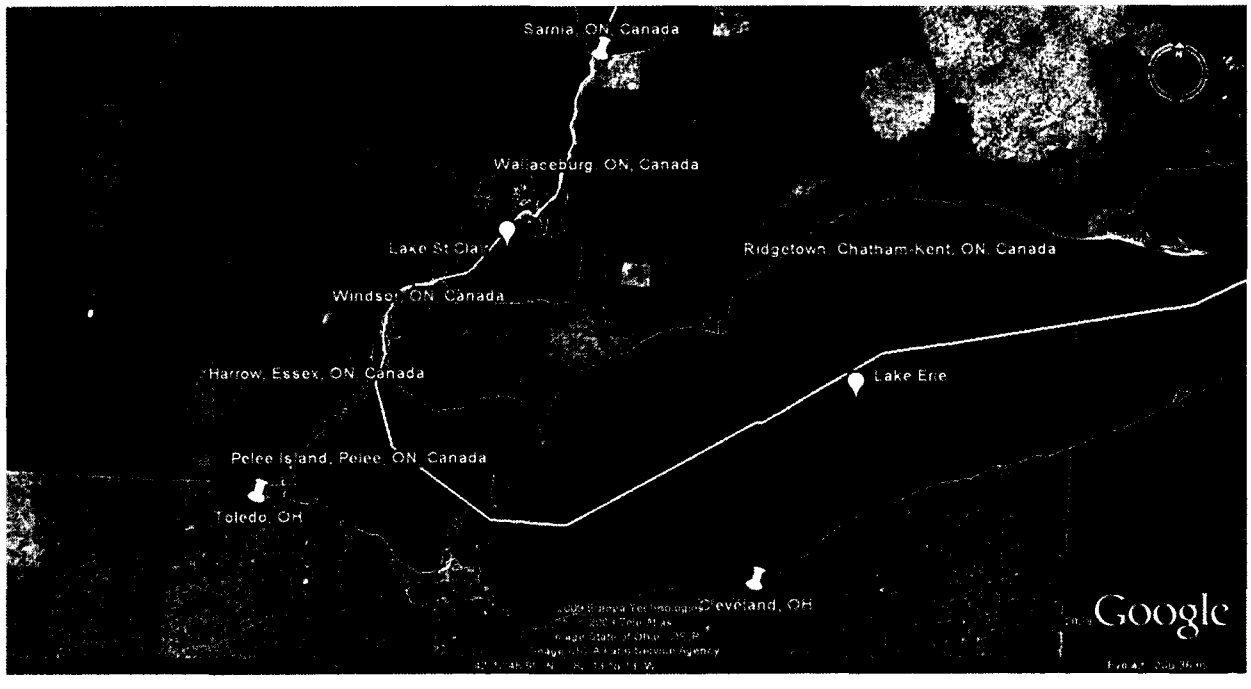

Figure 39: Map South Western Ontario showing BAQS-Met measurement sites in green and industrial towns in the Lake Erie area (in yellow)..

Harrow is in close proximity to the metropolitan Detroit and Windsor areas. It is a semi rural location which is frequently affected by emissions from Detroit/Windsor as well the Ohio Valley and Sarnia, figures 41 and 42 show point source emissions from Canada (Canada's National Pollutant Release Inventory) and United States (US EPA Emissions Inventory).

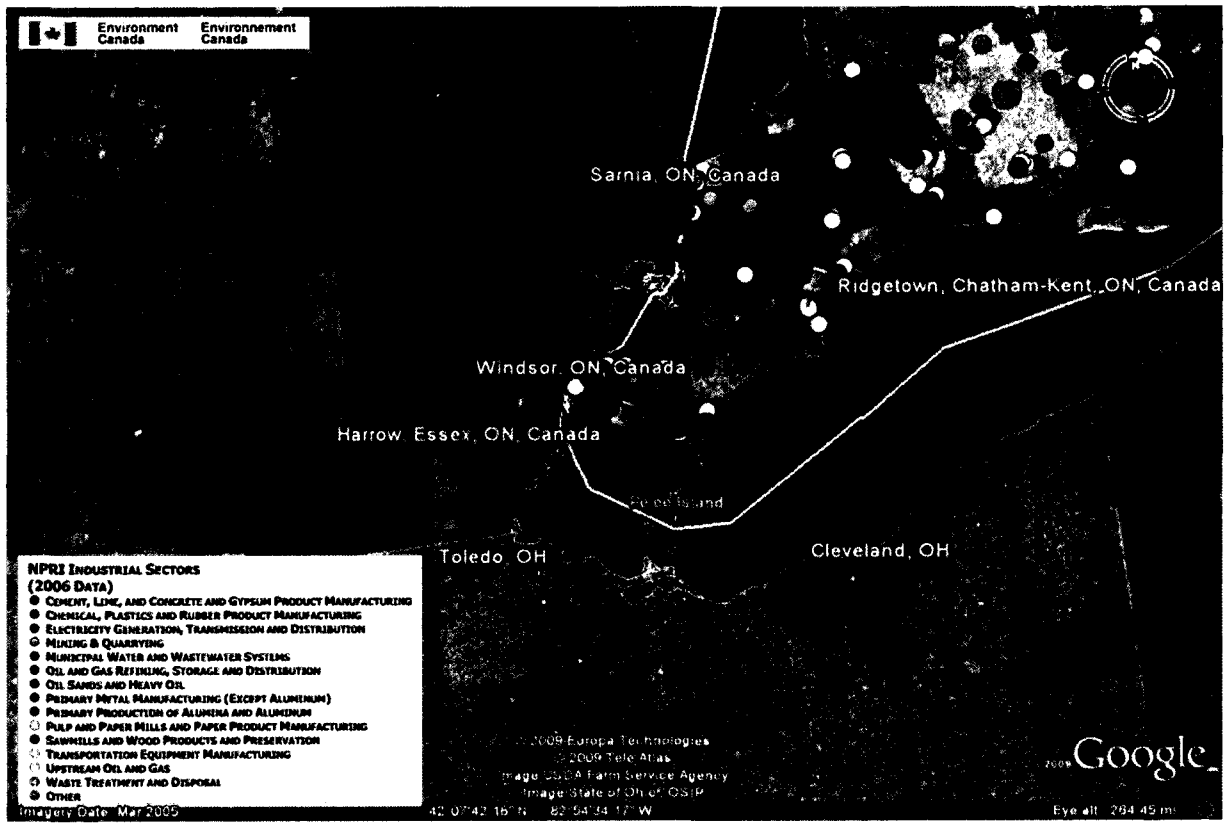

Figure 40: Map of emissions inventory from Canada's National Pollutant Release Inventory showing industrial pollution in South Western Ontario.

As can be seen from Figure 40 there are a large number of chemical, plastics and rubber production faciliities in the Sarnia area. Closer to the Harrow site, there are also cement manufacturing, chemical manufacturing and power plants in the Windsor area which can directly affect the air quality in nearby Harrow.

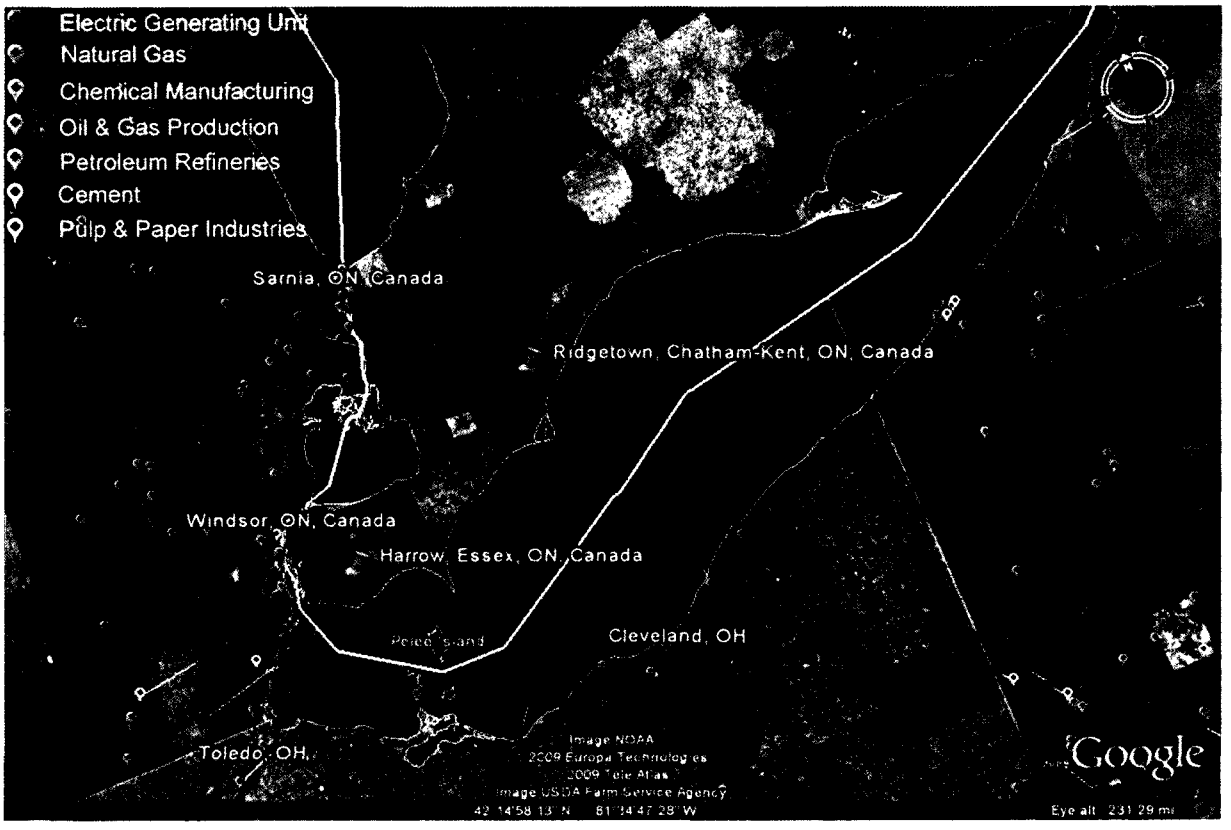

Figure 41: Map of the South Western Ontario region showing industrial pollution sites on the United State's side of the border (US EPA Emissions 2005).

Figure 41 shows that the Harrow area may be impacted by transborder pollution. There are a number of electric generating units, chemical manufacturing plants and petroleum refineries on both the Southern and Western sides of Lake Erie. Pollution from all of these sites affects the air quality in Harrow and Essex County when winds bring pollution from the the South East to the North West.

3.3.1 Site Instrumentation

At the Harrow site the LOPAP was installed in a trailer that contained other instruments for measuring gas and aerosol concentrations. The sampling coil was mounted through a window of the trailer, which was located in the middle of a field on the grounds of Agriculture and Agri-Foods Canada's Greenhouse and Processing Crops Research Centre. An overhead image of the site is shown in Figure 42. Also located at the site was the Southern Ontario Centre for Atmospheric Aerosol Research's (SOCAAR), Mobile Analysis of ParticuLate in the Environment (MAPLE) mobile laboratory (Principle Investigator Professor Greg Evans, University of Toronto).

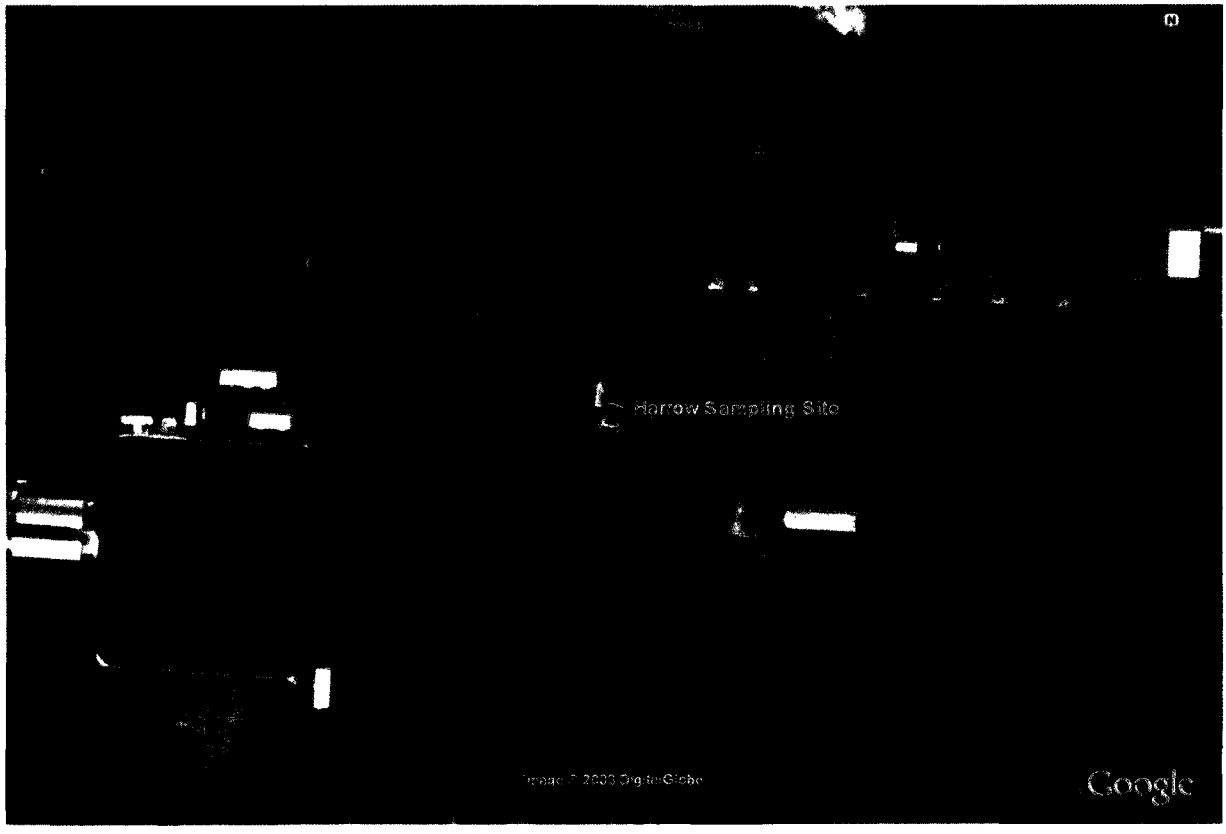

Figure 42: Overhead image of Harrow sampling site. Courtesy of maps.google.ca.

In addition to the LOPAP there were a number of other instruments located at the Harrow site. The instruments found at the Harrow site are summarized in Table 8.

Table 8: List of chemical and aerosol measurements at Harrow measurement site as part of BAQS-Met.

Species	Instrument	Principle Investigator	Affiliation
HONO	LOPAP	Prof. G.W. Harris	York University
NO_x	NO_x analyser (Thermo-Scientific)	Ontario Ministry of the Environment	Ontario Ministry of the Environment
O_3	O_3 monitor (Thermo-Scientific)	Ontario Ministry of the Environment	Ontario Ministry of the Environment
NH_3	NH_3 Quantum Cascade Laser Trace Gas Detector (Aerodyne)	Prof. J.G. Murphy	University of Toronto
Acids/Bases and +/- ions in Aerosols	Ambient Ion Monitor Ion Chromatograph (URG 9000)	Prof. J.G. Murphy	University of Toronto
VOC's	Proton Transfer Mass Spectrometer (Ionicon Analytik)	Prof. J.P.D. Abbatt	University of Toronto
J_{HONO} (estimate)	Total UV Radiometer (Eppley)	Prof. G.W. Harris	York University
Aerosol Hygroscopic Properties	Hygroscopic Tandem Differential Mobility Analyser	Prof. M. Mozurkewich	York University
Particle Speciation	Aerosol Mass Spectrometer (TSI)	Prof. Greg Evans	University of Toronto
Particle Size Distribution	FMPS (TSI)	Prof. Greg Evans	University of Toronto

3.3.2 HONO Measurements during BAQS-Met

Nitrous acid measurements were made between June 21st and July 6th 2007. Mixing ratios of HONO followed a typical diurnal cycle over many nights during the study with a daytime minimum and night-time maximum. A time series of the measurements of HONO, NO_2, NO, J_{HONO}, O_3, relative humidity, temperature, wind speed, wind direction and barometric pressure at the Harrow measurement site is shown in Figures 44 and 45.

During many nights of the campaign HONO concentrations would build up over the course of the night and begin to decrease in the morning when wind speeds increased and photolysis would begin. Minimum HONO concentrations were not reached until the late afternoon and rarely decreased below detection limits (5 pptv). The mean daytime mixing of HONO was 61 pptv (maximum=473 pptv), while the mean night-time value was 102 pptv, (maximum=376 pptv). The maximum daytime mixing ratio was observed at roughly 10:00 EST on the morning of June 25, 2007.

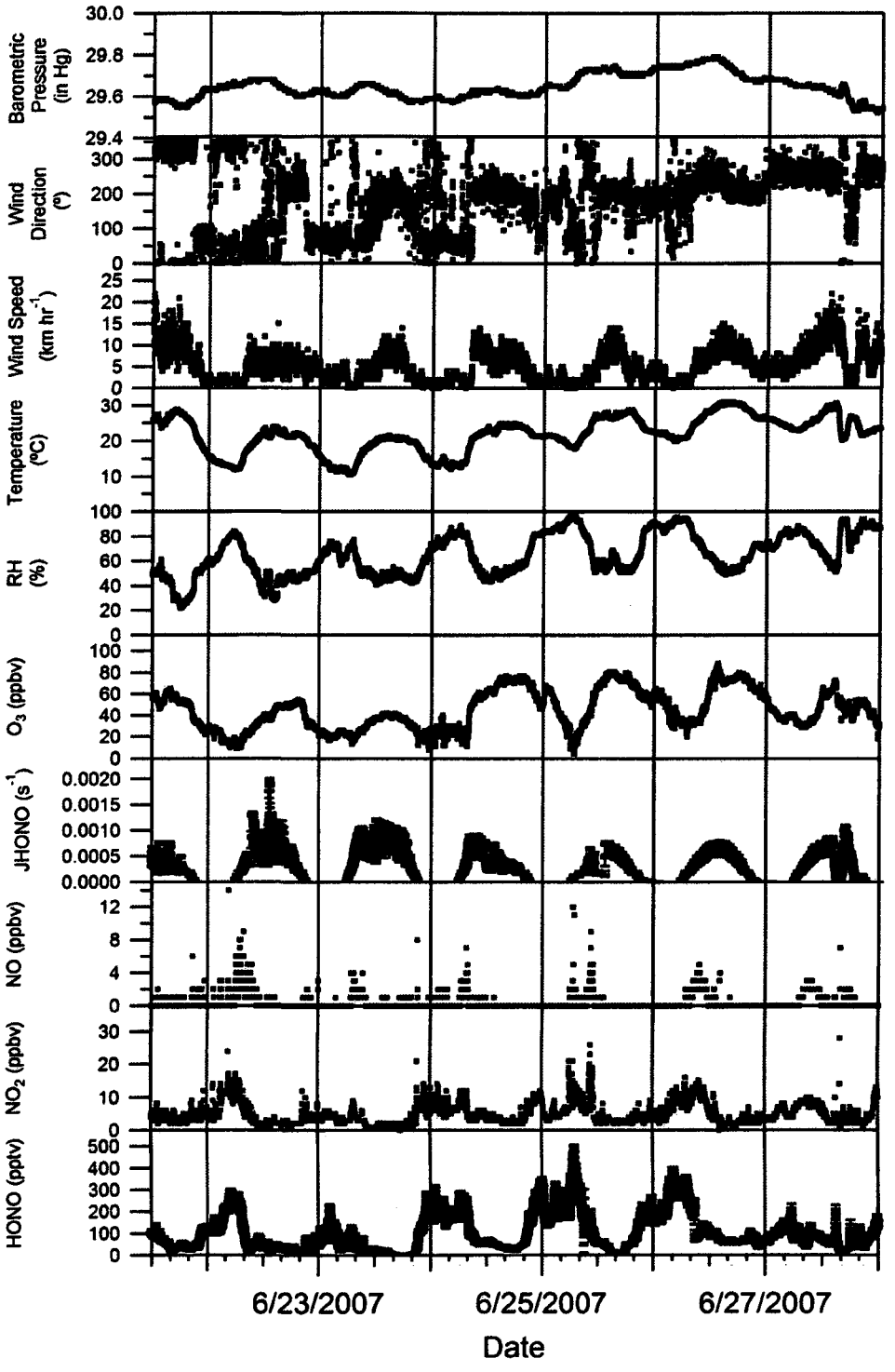

Figure 43: Time series of the measurements of HONO, NO_2, NO, J_{HONO}, O_3, relative humidity, temperature, wind speed, wind direction and barometric pressure at the Harrow measurement site from June 21-June 27, 2007.

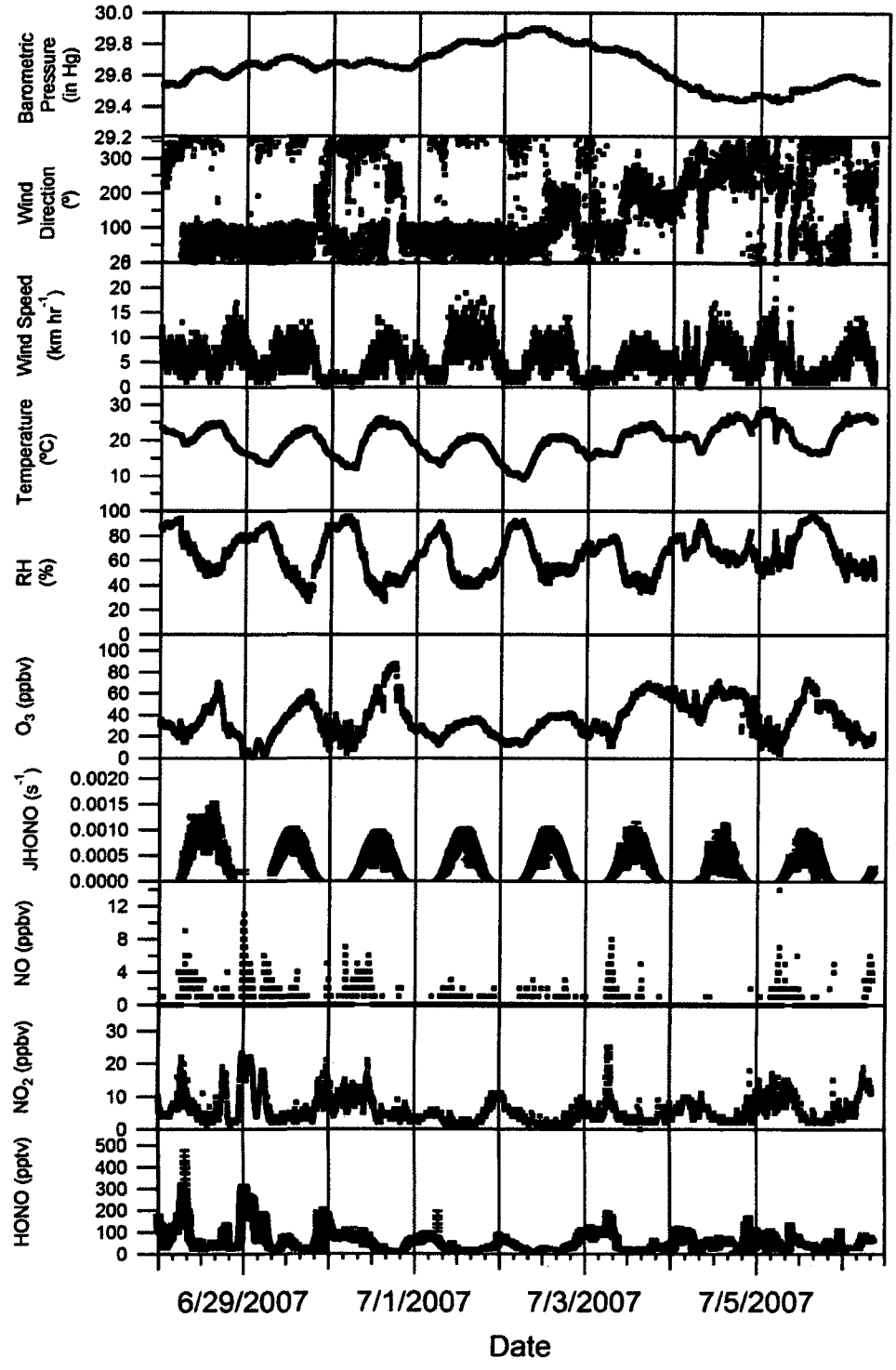

Figure 44: Time series of the measurements of HONO, NO_2, NO, J_{HONO}, O_3, relative humidity, temperature, wind speed, wind direction and barometric pressure at the Harrow measurement site from June 28-July 6, 2007.

The majority of the NO_x observed was in the form of NO_2 (~95%). The fraction of NO_x resulting from NO_2 is likely artificially high, as a result of the 1 ppbv detection limit for NO of the NO_x monitor. The results in all values less than 1 ppbv appearing to be zero when in fact they could potentially have been in the range of several hundred pptv. Significant amounts of O_3 may have helped suppress NO concentrations during the study, but there was not enough present to result in 95% of the mean NO_x value be due to NO_2. The NO data should therefore be treated with caution.

During the period from June 21st to June 27th (Figure 43), the HONO mixing ratios consistently reached 300 pptv or more during the night-time. Winds during this time were generally from between 150-250°. The increases in HONO during this period were matched by increases in NO_2 mixing ratio. As the sun rose concentrations would show an initial sharp decrease in the early morning which would continue more slowly throughout the day until minimum mixing ratios were reached generally late in the afternoon. As the sun set (typically not until ~21:00 EST), and wind speeds decreased, HONO and NO_2 mixing ratio would increase. Mixing ratios of HONO would rise as quickly as 81 pptv hr^{-1} when winds were calm as was the case on the nights of the 24th-26th of June.

Nitrous acid mixing ratios were consistently lower between June 28th and July 6th. Winds during this time were typically from the North East bringing pollution from the Sarnia area (the location of many chemical, plastics and rubber making facilities). The peaks and valleys in the HONO data showed a similar pattern to that of NO_2 and NO. The relationship between HONO and NO_2 will be examined in the following section.

3.3.3 HONO-NO_2 relationship during BAQS-Met

Concentrations of HONO and NO_2 correlated when all data points from each half of the study are included (Figure 45 and Figure 46).

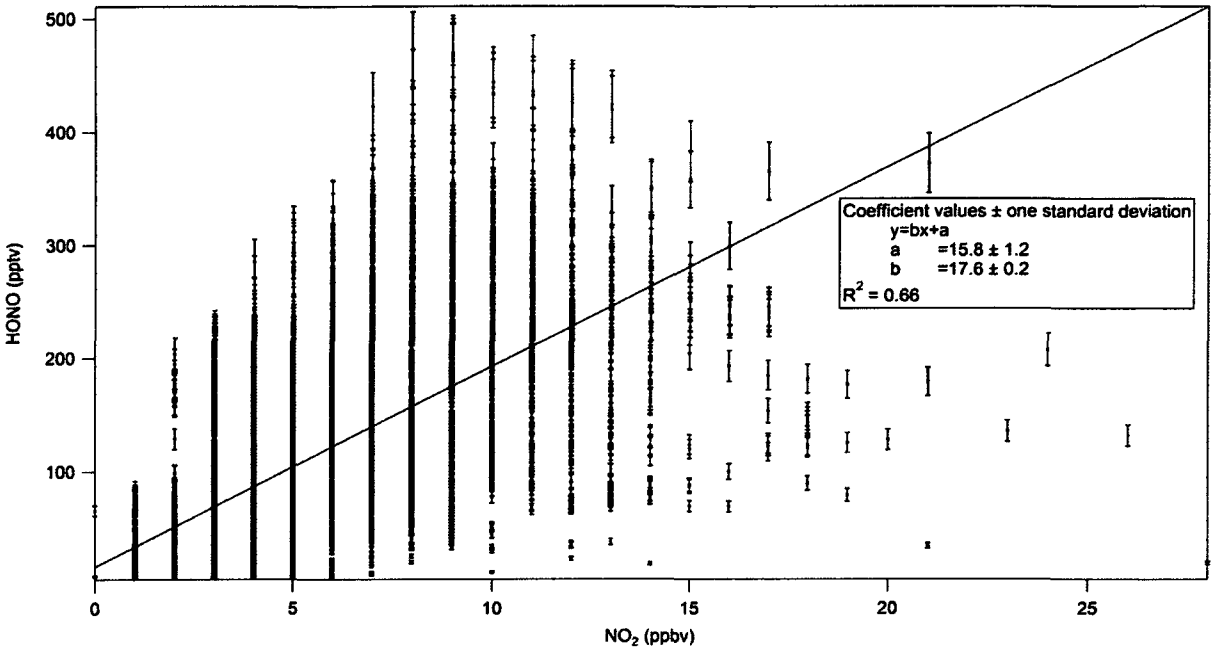

Figure 45: Plot of HONO mixing ratios as a function of NO_2 mixing ratios from June 21-June27, 2007, during BAQS-Met Study.

Mixing ratios of HONO and NO_2 showed a slightly better correlation during the second half of the study (R^2=0.71) when winds were from the North East than during the first half (R^2=0.66) when winds were from the South West. Further sectioning the data into periods of consistent meteorological conditions showed an ever clearer relationship between HONO and NO_2.

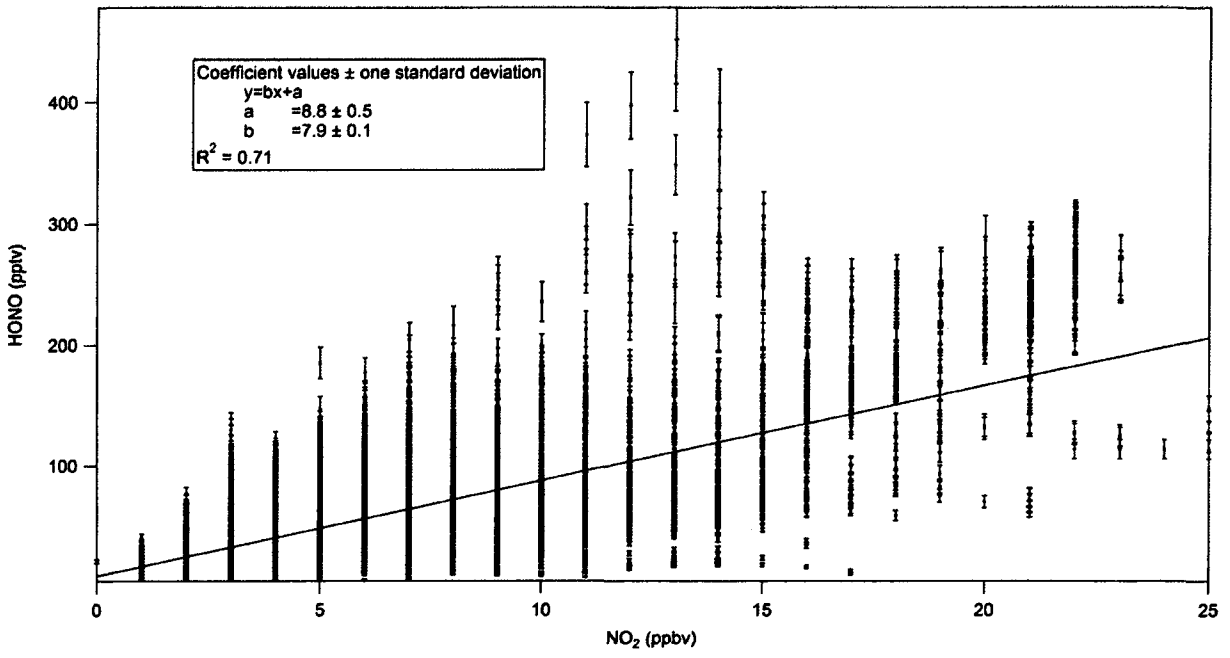

Figure 46: Plot of HONO mixing ratios as a function of NO_2 mixing ratios from June 28-July 6, 2007, during BAQS-Met Study.

The HONO and other parameters are plotted as a time series for the period of June 22nd to midday of the 24th (Figure 47). The night-time HONO and NO_2 mixing ratios during this time were highly correlated with an R^2 of 0.81, (Figure 48). Each night the wind speeds were low and the relative humidity reached ~80%. Mixing ratios of HONO and NO_2 decreased in the morning hours as wind speeds increased and the boundary layer broke up.

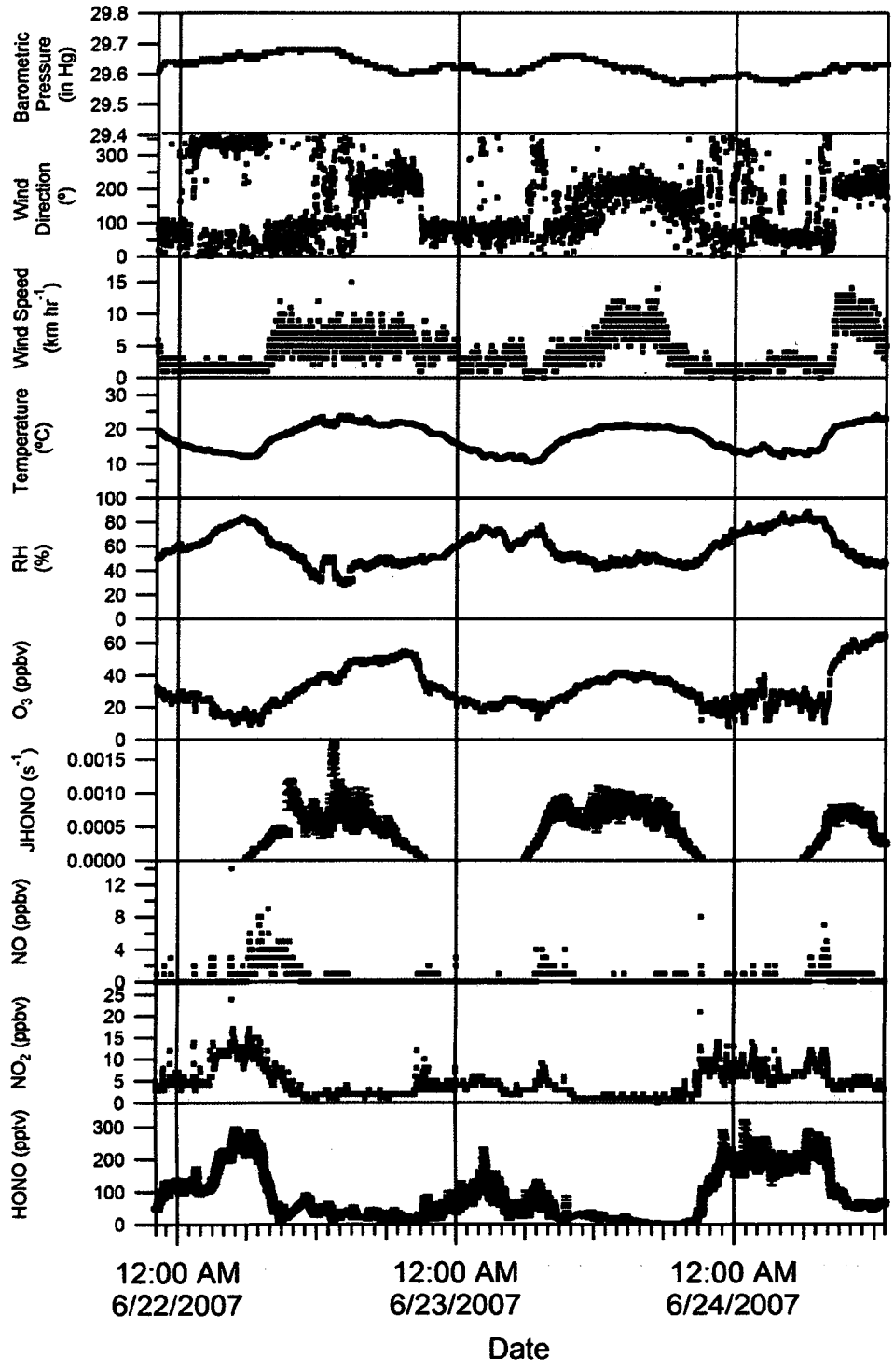

Figure 47: Time series of the measurements of HONO, NO_2, NO, J_{HONO}, O_3, relative humidity, temperature, wind speed, wind direction and barometric pressure at the Harrow measurement site from June 22nd through June 24th 2007.

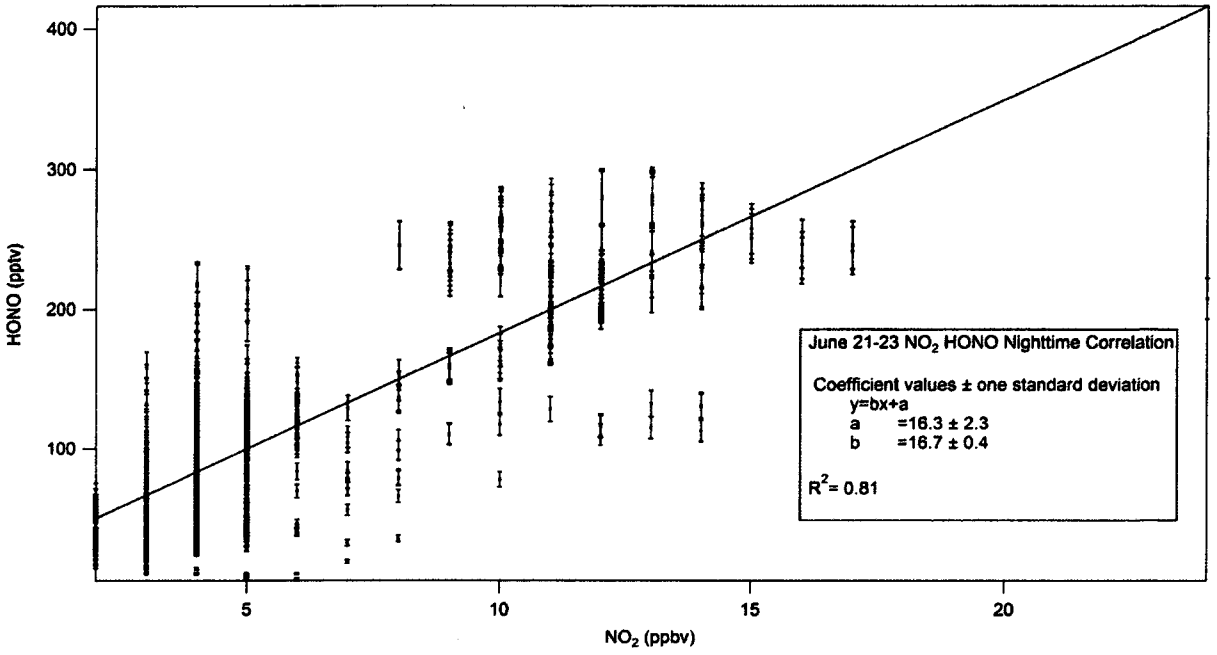

Figure 48: Night-time correlation between HONO and NO_2 mixing ratios between June 21st and June 23rd 2007.

The night of June 23rd/24th was interesting as HONO concentrations reached 200 pptv and remained roughly constant for the duration of the night. Since wind speeds were low that night it is not obvious why HONO concentrations would not rise for the duration of the night until the breakup of the boundary and onset of photolysis in the morning hours. This phenomenon has been observed before by Stutz et. al. (2002). Stutz et. al. (2002) showed that NO_2 concentrations greater than 10 ppbv lead to HONO formation (positive HONO gradients) over grass in Milan. They determined a compensation point in the HONO/NO_2 ratio of 3% where HONO would begin to deposit on the grass surface under stable meteorological conditions. It was believed that NO_2 was hydrolyzing on the damp grass to produce the measured HONO. This is consistent with the HONO/NO_2 ratios (Figure 52) observed on the night of the 23rd/24th when HONO/NO_2 ratios were between 2-4%. While NO_2 concentrations were not consistently greater than 10 ppbv on this night it appears plausible that deposition was the cause of the relatively constant HONO concentrations

observed that night, with production matched by deposition. During the night of June 28th/29th (Figure 50) HONO and NO_2 were highly correlated, as can be seen in Figure 49. Winds were consistently from the North East and decreased from 10 to <5 km hr^{-1} in the early part of the evening. Two decreases in concentration of HONO, NO_2 and NO were observed, the first minima occurred at 01:00 and the second occurred at 04:00 (both local time), correspond with increases in O_3 concentration. Ratios of HONO/NO_2 varied between 0.5-2 percent (Figure 51) on this night, below the compensation point for HONO gradients suggested by Stutz et. al. (2002). This makes it less likely that the decreases in HONO were due to deposition. The increase in O_3 concentration during both minima in HONO and NO_x is likely due to entrainment of fresh air from above the boundary diluting the HONO and NO_x rich air below the boundary layer and decreasing concentrations of both. It's also possible that small changes in wind direction caused the decreases in NO_x and HONO as there are small changes in wind direction shown in Figure 50. Mixing ratios of HONO and NO_2 began to decrease on the morning of the 29th (~06:00 local time) as O_3 concentrations increased, prior to the onset of photolysis.

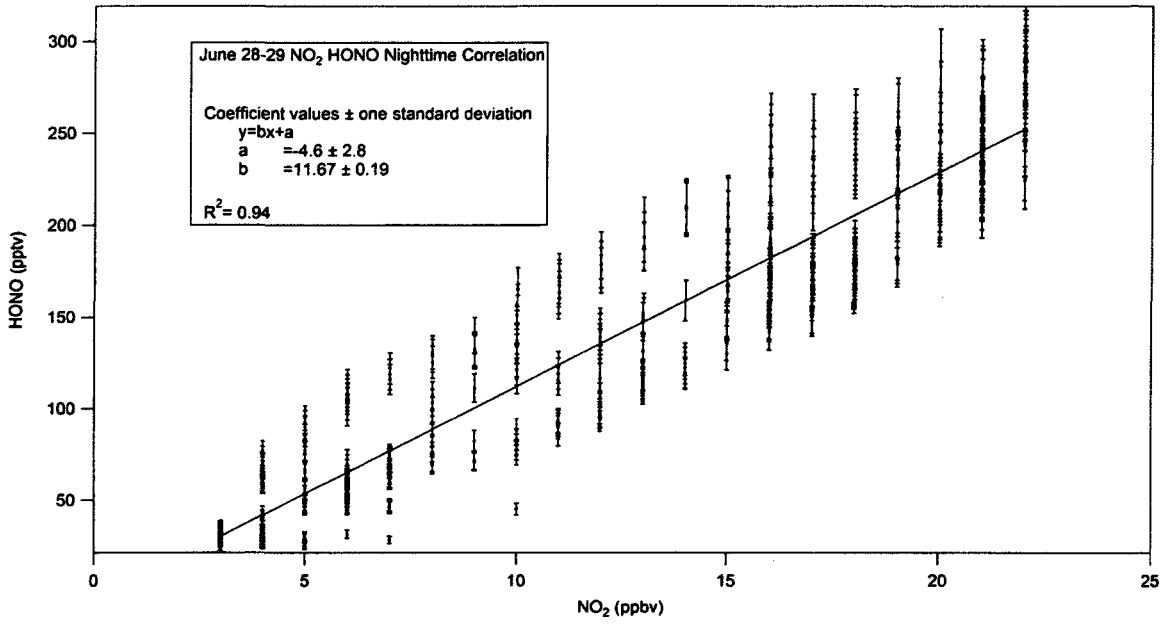

Figure 49: Night-time correlation between HONO and NO_2 mixing ratios between June 28th and 29th 2007.

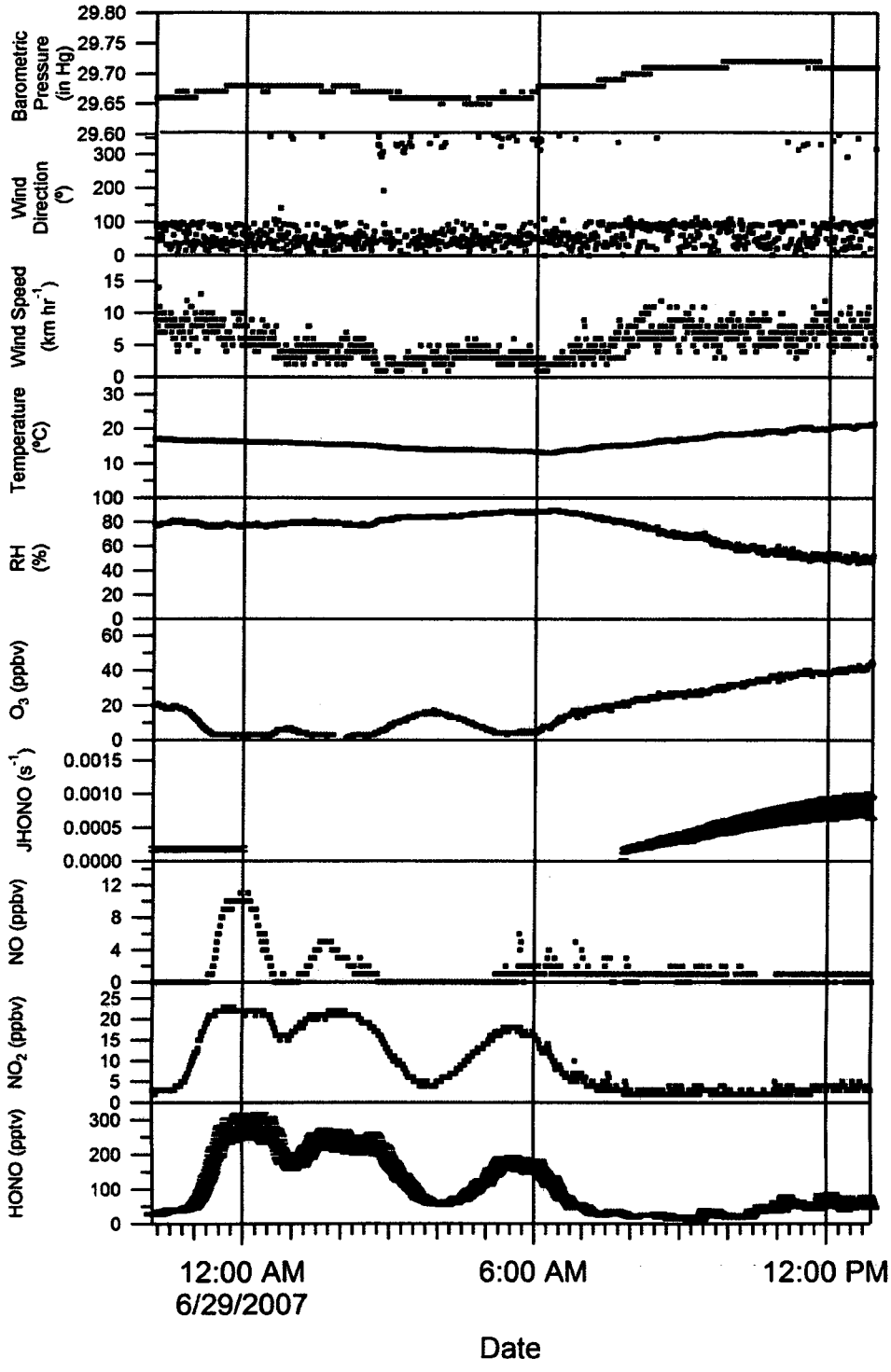

Figure 50: Time series of the measurements of HONO, NO_2, NO, J_{HONO}, O_3, relative humidity, temperature, wind speed, wind direction and barometric pressure at the Harrow measurement site for the night of June 28th/29th 2007.

Back-trajectory analysis using HYSPLIT, ARL and NOAA. (Figure 52) indicated that that the pollution observed on the night of the 28th/29th had passed through the Sarnia area less than six hours prior to the air mass arriving at the Harrow site. As with the previous back trajectory used with the forested measurements the method of vertical motion used was model vertical velocity, which uses the meteorological models vertical velocity fields and the heights represent the end height of the air mass.

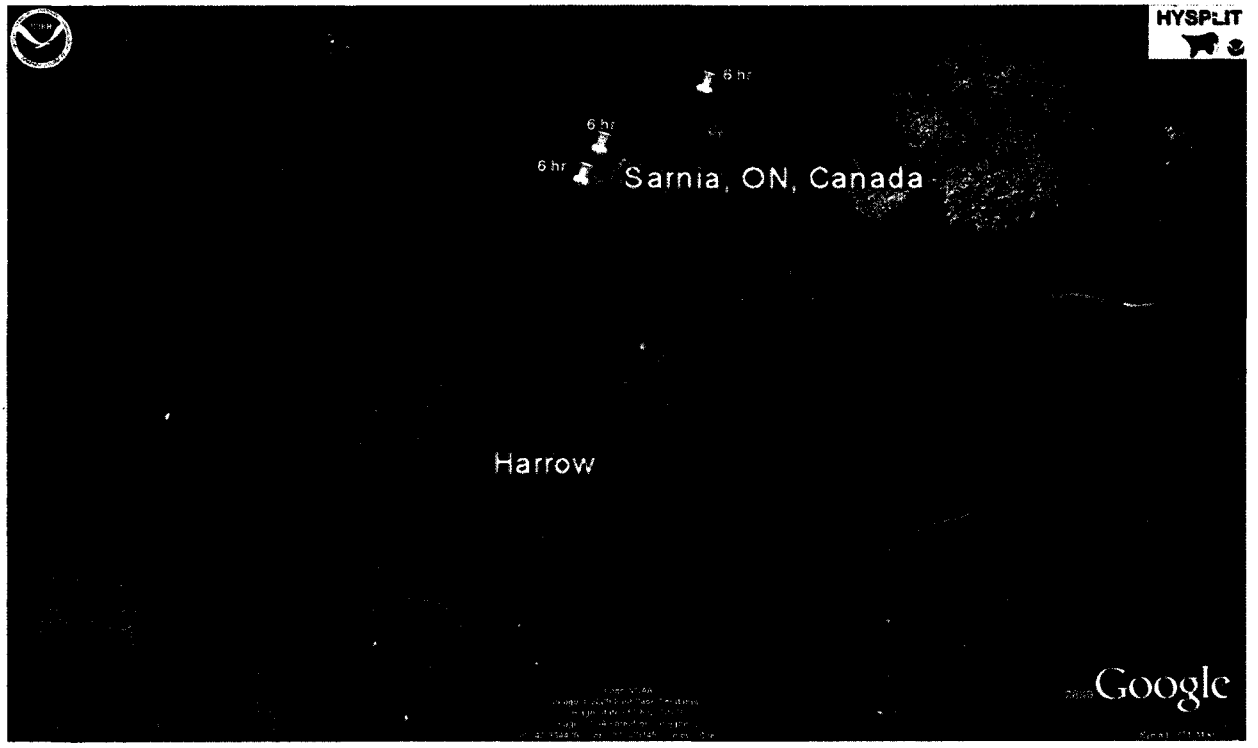

Figure 51: Back-trajectory analysis from HYSPLIT of the air mass observed on the night of June 28th/29th 2007. The trajectory at 50 m=red, 100 m=blue 500 m= green.

3.3.4 Variations in HONO/NO_2 ratio during the BAQS-Met study

The ratios of HONO/NO_x and HONO/NO_2 over the course of the study were also examined and are shown in Figure 52. The ratios of HONO/NO_x ranged from 0.05-12% (mean=1.6%) while those from HONO/NO_2 were between 0.06-10.1% (mean=1.5%). The variation in the two ratios is similar over the course of the campaign since NO_2 was the dominant component of NO_x present (NO_2/NO_x=95) as previously discussed.

The HONO/NO_2 ratio can be used as before as an indicator of the extent of HONO production from NO_2 [Kleffmann et al., (2003)]. Using the HONO/NO_2 ratio on a night when meteorological conditions were stable, a conversion efficiency of NO_2 to HONO could be calculated. On the night of the 23rd/24th the HONO/NO_2 ratio increased from 0.5-4% over the course of a four hour period (20:00-00:00 local time). This gives a first order conversion of 2.43×10^{-6} s^{-1}. The value of the first order rate constant is roughly a factor of two larger than that calculated from the data at the forested site in Borden Ontario. It is also comparable to values calculated from data in polluted urban sites such as Berlin (3.3×10^{-6} s^{-1}) and Milan (5.8×10^{-6} s^{-1}) [Alicke et al., 2002, 2003].

On average the ratio of HONO/NO_2 did not vary greatly from the day (mean=1.5%) to the night (mean=1.7%) again implying that a daytime source converting NO_2 to HONO would have to be significantly more rapid than the night-time hydrolysis of NO_2 since the photolytic lifetime of HONO at midday is only 10-15 minutes.

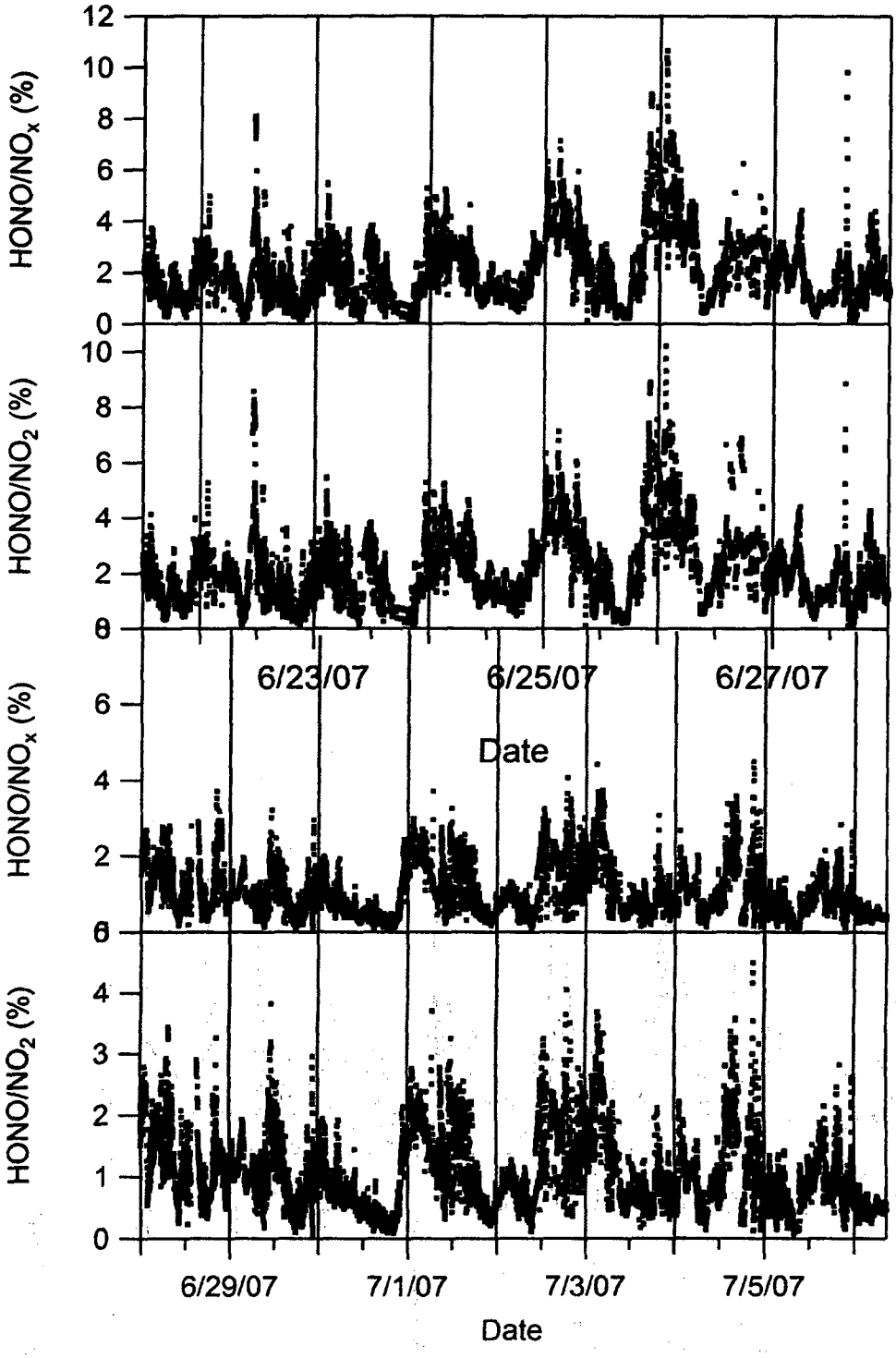

Figure 52: Time series of the $HONO/NO_x$ and $HONO/NO_2$ ratio during the BAQS-Met campaign. Vertical lines occur at midnight of each day.

To determine if the $HONO/NO_2$ ratio was a function of the direction of wind impacting the site the ratios of $HONO/NO_2$ were examined as function of wind direction during the day and night. Polar plots showing $HONO/NO_2$ ratios as a function of wind direction for both days and nights are shown in Figure 53, with wind speeds less than 5 km hr^{-1} were removed due to unclear wind direction during low wind conditions. Shown on these plots is the approximate direction of the nearest, major industrial centres. During the daytime period the highest ratios are observed when winds are from between 180-270°. In both cases air masses would have to travel over Lake Erie in order to reach the Harrow site. Ratios during the daytime when winds were from either the North East or South East are also lower than during the night-time hours.The night-time ratio plot shows $HONO/NO_2$ ratios >5% coming from the South and South-west. This is not observed in the daytime data. Ratios greater than 3% are not often observed when winds are from 270-90°during either the day or the night. It may be that increased humidity from air travelling over the lake may increase the conversion of NO_2-HONO.

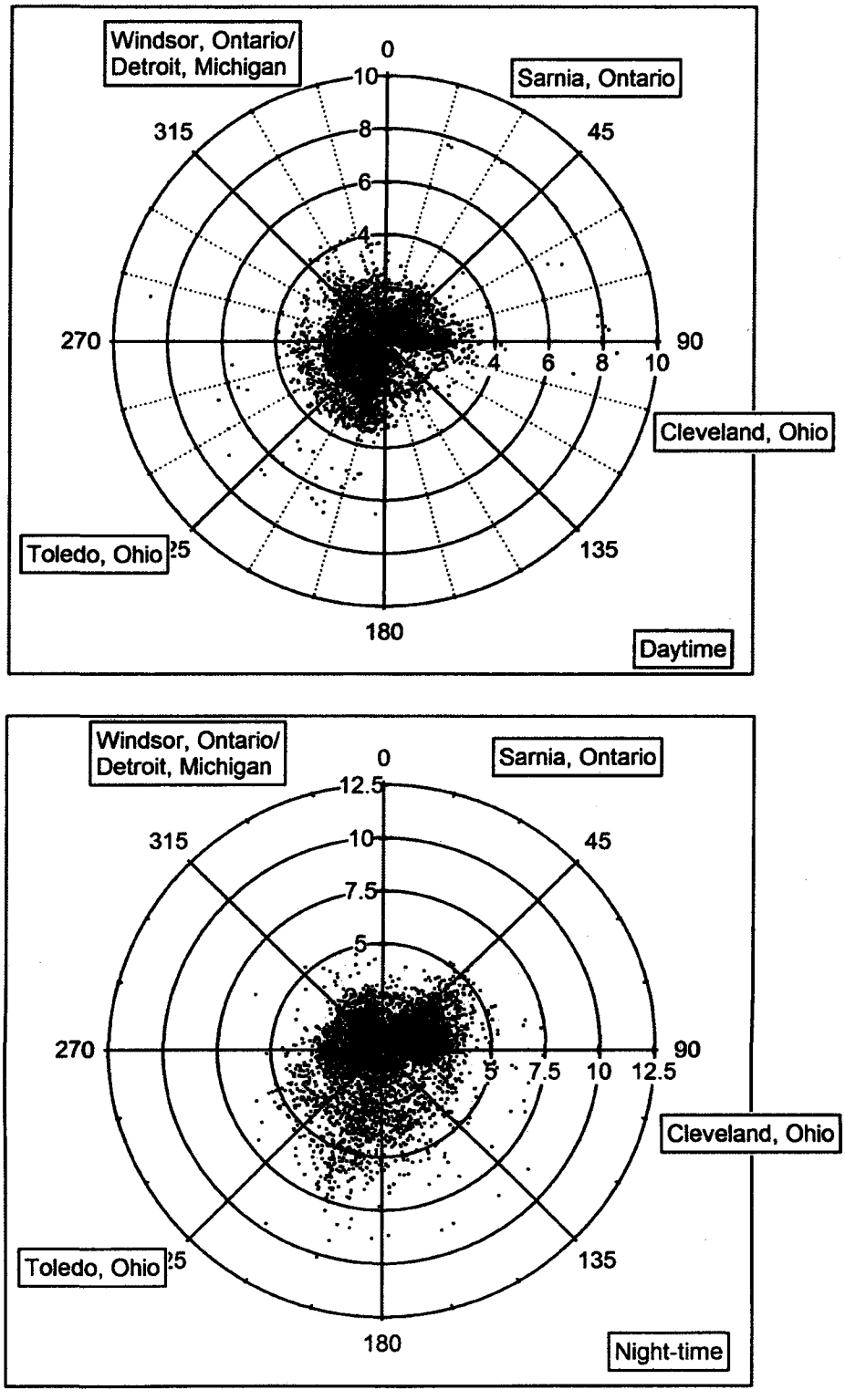

Figure 53: Polar plots of HONO/NO2 (%) as a function of wind direction. The daytime ratios are in the top plot, the night-time ratios are in the bottom plot Points where wind speeds are below 5 km/hr have been removed.

3.3.5 Daytime Production of HONO

Daytime production of HONO was examined more closely since HONO mixing ratios remained well above zero during the daytime for the duration of the study (mean=61pptv). This cannot be explained by the first order conversion rate determined in the previous section ($2.43x10^{-6}s^{-1}$), as that is roughly two orders of magnitude smaller than HONO photolysis at midday. It is not believed that there any large emission sources of HONO in the area of the Harrow site which could account for the high daytime concentrations.

A HONO production rate was calculated for measured HONO in excess of "classical" PSS chemistry in the same manner as the Borden data set. Correlations between HONO production rates and various gas, aerosol and meteorological parameters were examined. The R^2 values are shown in Table 9.

Table 9: Tabulated R^2 values for HONO production correlations.

Correlation Parameter	R^2
NO_x	0.12
NO_2	0.04
NO	0.32
J_{HONO}	0.62
$J_{HONO}[NO_2]$	0.70
$J_{HONO}[NO_2][H_2O]$	0.76
O_3	0.16
Particle Surface area Density	0.31
$J_{HONO}[NO_2]$(Particle Surface Area Density)	0.61
Relative Humidity	0.14
Wind Speed	0.21
Temperature	0.25

The strongest correlations found were with J_{HONO}, the product of the J_{HONO} and the NO_2 mixing ratio, and the product of J_{HONO}, the NO_2 mixing ratio and the H_2O mixing ratio. As before it was

expected that a correlation with J_{HONO} would be present however it is strengthened by the inclusion of NO_2 and H_2O mixing ratios. There was no strong correlation present between HONO production and particle surface area density alone (R^2=0.31). Surface area density was determined from the particle size distribution measured with a fast mobility particle sizer using the assumption of a spherical particle shape. Particles measured by the instrument were in the range of 5.5 to 560 nm. Thus it is unlikely that HONO production occurred predominantly on aerosols and it is more likely that the majority of production occurred on the ground (e.g. grass or soil), or that production is simply occurring homogeneously in the gas phase. The correlation plot of HONO production rate with product of J_{HONO} and NO_2 is shown in Figure 54.

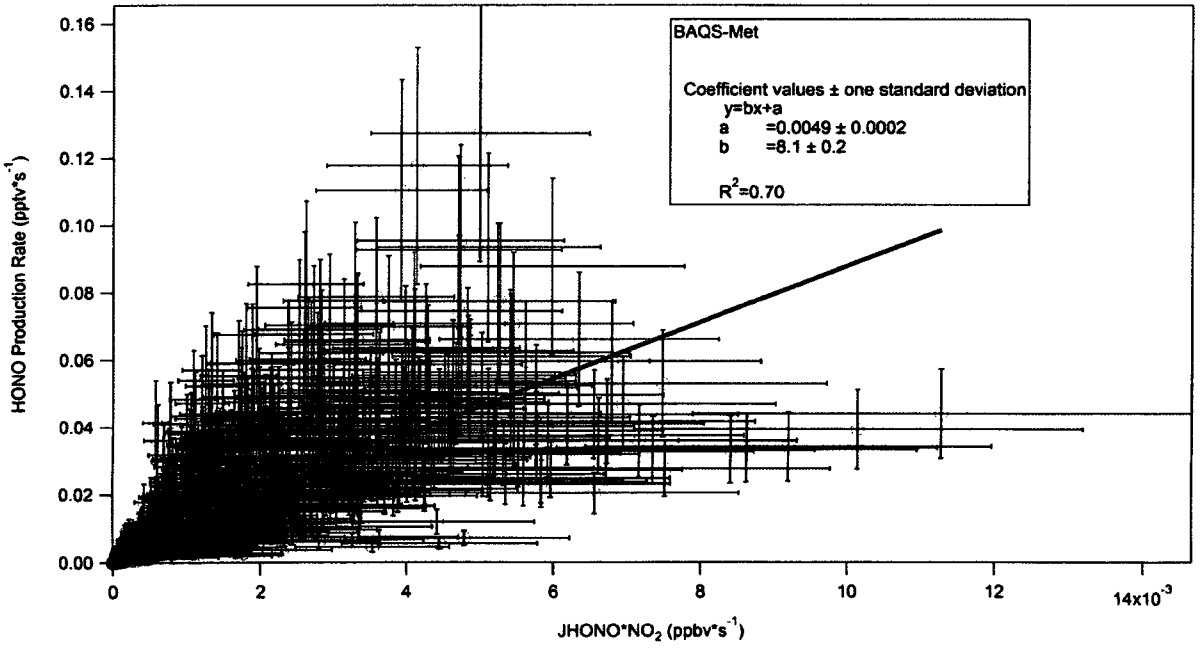

Figure 54: HONO Production Correlation with J_{HONO} and NO_2 for all daytime values during the study

The error bars represent the estimated uncertainty in the HONO production rate and J_{HONO} NO_2 product, based on the uncertainty in J_{HONO} estimated to be 20%, the estimate of the uncertainty in

NO_x (NO and NO_2, 15%) and the uncertainty in excess HONO (20%). Uncertainties in OH are not considered since a model value was used. The results of BAQS-Met are consistent with the data from the Borden site where strong correlations were also observed between HONO production and the product of J_{HONO}, NO_2 mixing ratio and H_2O mixing ratio. It is not yet known however whether this is simply a gas phase mechanism or a reaction occurring on the bulk ground surface. The calculation and discussion of apparent rate constant for the production of HONO as a function of radiation NO_2 and H_2O on various days during different time periods is found in Chapter 4.1.

3.3.6 OH Production from HONO during BAQS-Met

The large quantities of daytime HONO (mean=61 pptv) present would contribute significantly to the overall OH budget. Photolysis of HONO would lead to a maximum OH production rate of > 1.5 x 10^6 molec $cm^{-3}s^{-1}$ at midday during the study. The time series of OH production rate (estimated as d[OH]/dt) from HONO photolysis is shown in Figure 55.

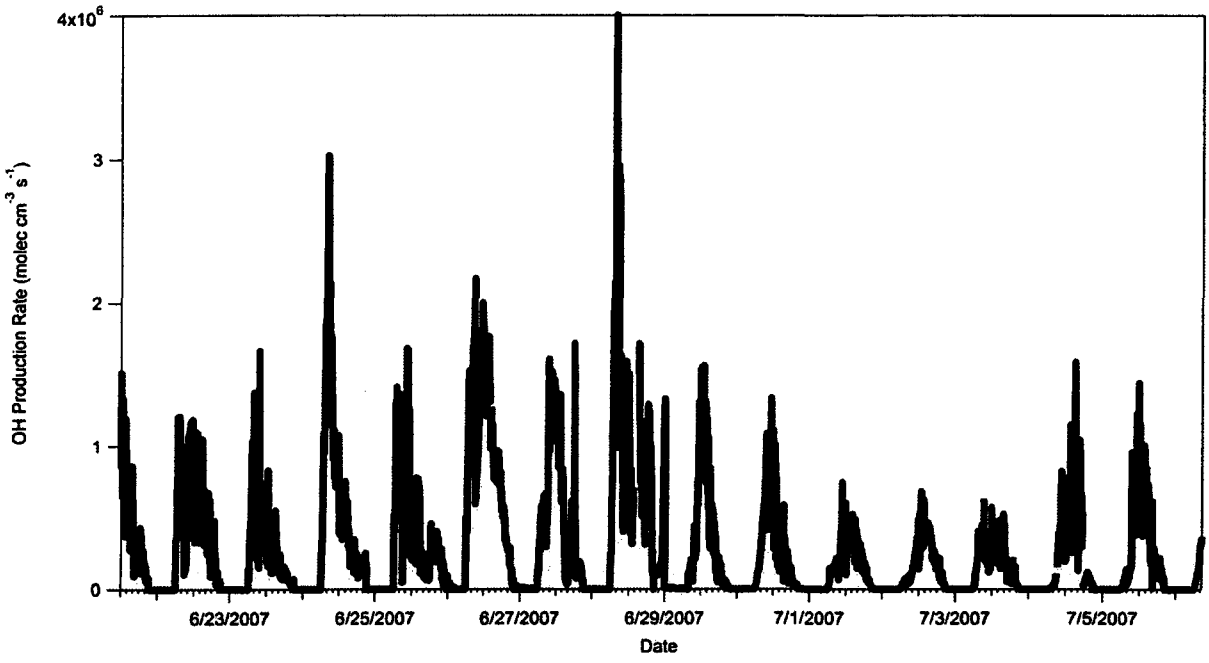

Figure 55: Time series of OH production rate from HONO as a function of HONO photolysis.

It is difficult to apportion the contributions of the various OH production pathways (shown in Table 1) at Harrow since no formaldehyde data is available. However it is likely dominated by the large amounts of O_3 present during the daytime (upwards of 80 ppbv). If one assumes a noontime maxmum in J_{O3} to be 2 x 10^{-5} s^{-1} (taken to be 15% of the maximum noontime J_{HONO} value,

Kraus & Hofzumahaus, 1998) the maximum midday production rate of OH from O_3 would be 7.87 x 10^7 molec cm^{-3} s^{-1}. While the contribution to OH production from HONO is roughly 50 times smaller than that of O_3 at midday, production of OH from HONO is not insignificant and would be relatively more important during the early morning hours when O_3 concentrations and photolysis rates are much lower.

In summary measurements of HONO at the Harrow site during BAQS-Met show high concentrations of daytime HONO present, mean=61 pptv. The daytime source appears to be consistent with that observed at the forested site in Borden Ontario and implies that HONO plays a larger role in the midday OH budget than originally thought. A night-time compensation point for heterogenous production and deposition of HONO consistent with the work of Stutz et. al. (2002) was also observed during the night-time when stable meterological conditions were present.

4 Comparison of Photolytic Production With Laboratory Measurements of k(NO_2*+H_2O)

As mentioned previously there have been conflicting reports as to the significance of photo enhanced reaction R 5 [Crowley and Carl, (1997); Li et al., (2008)].

$$NO_2^* + H_2O \rightarrow HONO + OH \qquad \text{R 5}$$

In the study by Crowley and Carl, (1997), NO_2 was excited using radiation between 430-450 nm. Radiation was obtained by pumping a dye laser (Lambda Physik Scanmate-2) with either a Nd:YAG laser (Quantel Brilliant B, pulse width = 5 ns), or an excimer laser (Lambda Physik Lextra 50). After passing through a series of irises the dye laser beam would enter a Teflon coated stainless steel reactor through a quartz window at the Brewster angle. The reactor was kept at a pressure of 20-24 Torr. Experiments were also carried out at 532 nm by coupling the second harmonic of the Nd:YAG laser directly into the reaction vessel through a series of irises. OH generated by the reaction of NO_2^* with H_2O were excited using an OH resonance lamp to promote the OH ($^2\Sigma^+$) ← OH($^2\Pi$) transition at 309 nm. An upper limit for the rate constant of 1.2×10^{-14} cm^3 $molec^{-1}$ s^{-1} was determined.

Li et al., (2008) studied the photo-enhancement using radiation at longer wavelengths, 565, 590 and 612.5 nm and determined a rate constant for R 5 of 1.2×10^{-13} cm^3 $molec^{-1}$ s^{-1}. The wavelengths for exciting NO_2 were generated by an optical parametric oscillator (Spectra Physics: MOPO-730), which was pumped by the third-harmonic of an injection seeded Nd: YAG laser (Spectra Physics: GCR-270). The OH generated from R 5 was monitored using the (0<-0) A-X transitions at ~308 nm using laser induced fluorescence (LIF). The 308 nm laser radiation is

generated by frequency doubling the output of a second Nd:YAG laser (Continuum: NY81-20) pumped dye laser (Continuum: ND60).

Carr et al., (2009) attempted to replicate the results of Li et al., (2008) using only unfocused laser light, as used by Crowley and Carl, (1997) and failed to observe any OH. They assigned an upper limit of R 5 that was a factor of 17 smaller than that of Li et al., (2008) and in agreement with Crowley and Carl, (1997). They suggested the reason for the discrepancies in rate constant values was due to R5 being a two photon process. Li et al., (2009) replied to this comment and noted that since OH production did not go as the square of NO_2 concentration that this could not be a two photon process. The difference in the measured rate constants is as yet unresolved. This reaction was however examined as a potential source of HONO for the Borden and Harrow studies.

At ground level the quenching of NO_2^* (a mix of the B^2B_1 and A^2B_2 excited electronic states and the X^2A_1 ground electronic state) is almost entirely due to collisional quenching (R 14).

$$NO_2^* + M \rightarrow NO_2 + M \qquad \text{R 14}$$

The rate of the quenching with water (R 15) is 1.7×10^{-10} cm^3 mol^{-1} s^{-1} [Thornton et al., (2000); Donnelly et al., (1979)].

$$NO_2^* + H_2O \rightarrow NO_2 + H_2O \qquad \text{R 15}$$

The overall rate of quenching in air at 1 atm is equal to 7.1×10^8 s^{-1} [Crowley and Carl, (1997)], giving a lifetime of 1.4 ns. In order for a comparison with our chemical HONO production rate to be performed, our estimates of J_{HONO} need to be converted estimates of J_{NO2}^*. This is a two step process. J_{NO2} can be derived from J_{HONO} using the following relationship,

$$J_{(HONO)} = 0.189 \times J_{(NO_2)} + 8.483 \times 10^{-2} J_{(NO_2)}^{2} \quad \text{(Eq. 5)}$$

given by Kraus and Hofzumahaus, (1998). J_{NO2} then needs to be converted to J_{NO2}* which is taken to be 5 times the rate of NO_2 photolysis based on the overall NO_2 cross section and the UV/VIS spectrum of sunlight Crowley and Carl, (1997) and is shown in Figure 56. While J_{NO2}* is not a true photolysis rate, it the rate constant of the excitation of $NO_2 \rightarrow NO_2$*, the J_{NO2}* nomenclature is used to remain consistent with the literature.

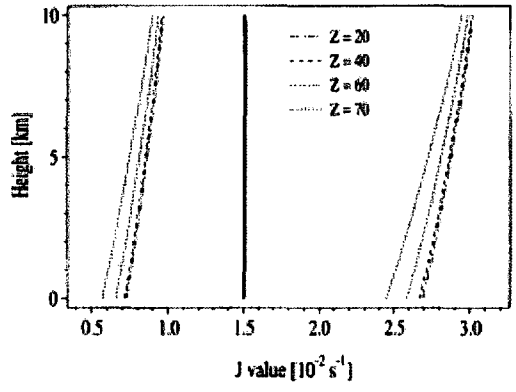

Figure 56: J values for photodissociation (left of solid vertical line) and for photoexcitation (right of solid vertical line) of NO_2 at Zenith angles (Z) between 20 and 70°, taken from Crowley and Carl, (1997).

Using J_{NO2}*, R 14 (the rate of which is taken to be 7.1×10^8 s^{-1}) and R 15 a HONO production rate is derived as

$$\frac{dHONO}{dt} = k_5 \frac{J_{NO_2^*}}{7.1 \times 10^8 s^{-1} + k_{15}[H_2O]} [NO_2][H_2O] \quad \text{(Eq.6)}$$

This calculated HONO production rate from the possible reaction R5 can be compared with the HONO production rates for the Borden and Harrow data sets which are estimated based on the measured daytime HONO concentrations and the known daytime losses (photolysis and reaction with OH).

4.1 Apparent k values during BAQS-Met

The plot of the measured daytime HONO production plotted against the calculated HONO production (Eq.6) from the daytime only Harrow data set is shown in Figure 57.

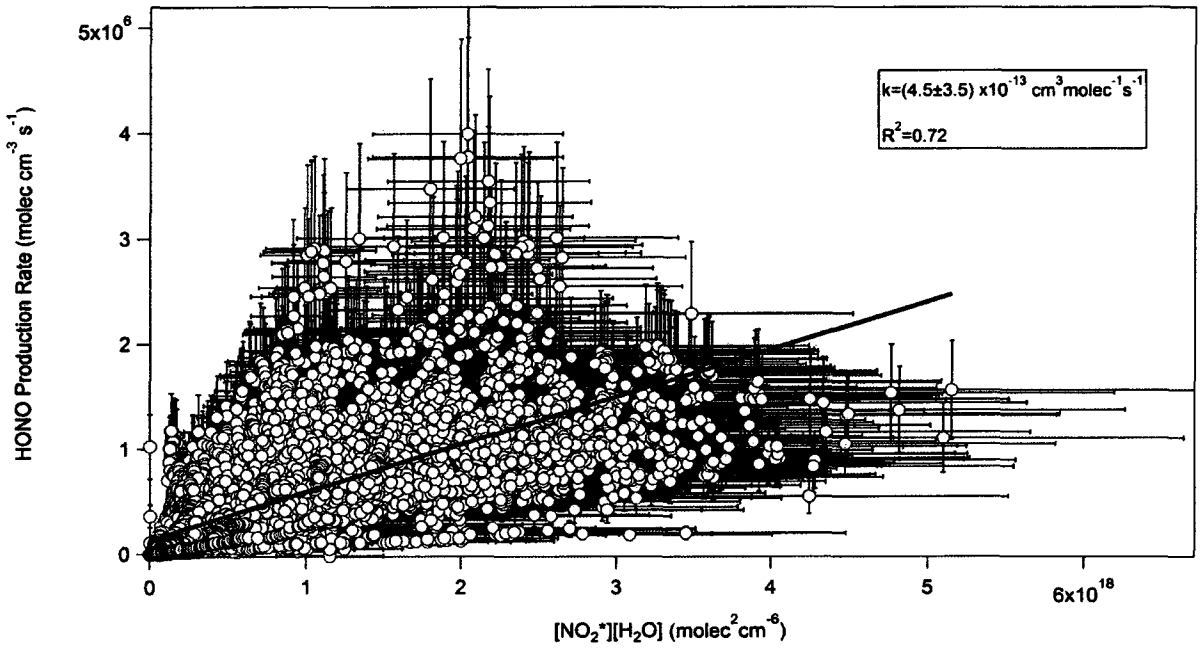

Figure 57: Plot of calculated chemical HONO production from measured HONO values and known HONO loss rates versus calculated HONO production from Equation 6.

The error bars represent the estimated uncertainty in the HONO production rate and the NO_2^* H_2O product, based on the uncertainty in J_{NO2}* estimated to be 20%, the estimate of the uncertainty in NO_x (NO and NO_2, 15%) and the uncertainty in excess HONO (20%). Uncertainties in OH are not considered as model data was used.

The data in Figure 57 yielded an R^2 of 0.72 but the slope yields an apparent rate constant of (4.5±3.5)x10^{-13} $cm^3molec^{-1}s^{-1}$, nearly 4 times that reported by Li et al., (2008) for the

homogeneous process. There is however a large amount of scatter in the data. To further examine this relationship specific time periods were chosen. Figure 58, Figure 59, Figure 60 and Figure 61 show correlations for the afternoons of June 21st, June 24th, the morning of June 30th and the morning of July 4th respectively.

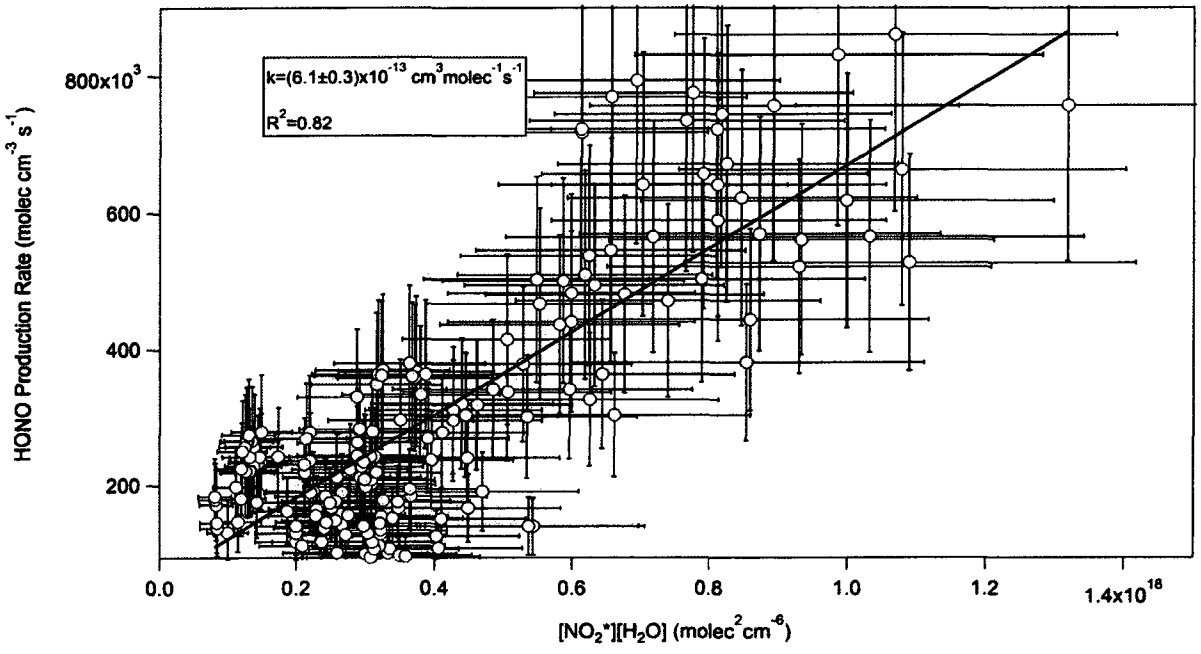

Figure 58: Plot of measured HONO production rate with the calculated HONO production rate for the afternoon of June 21, 2007.

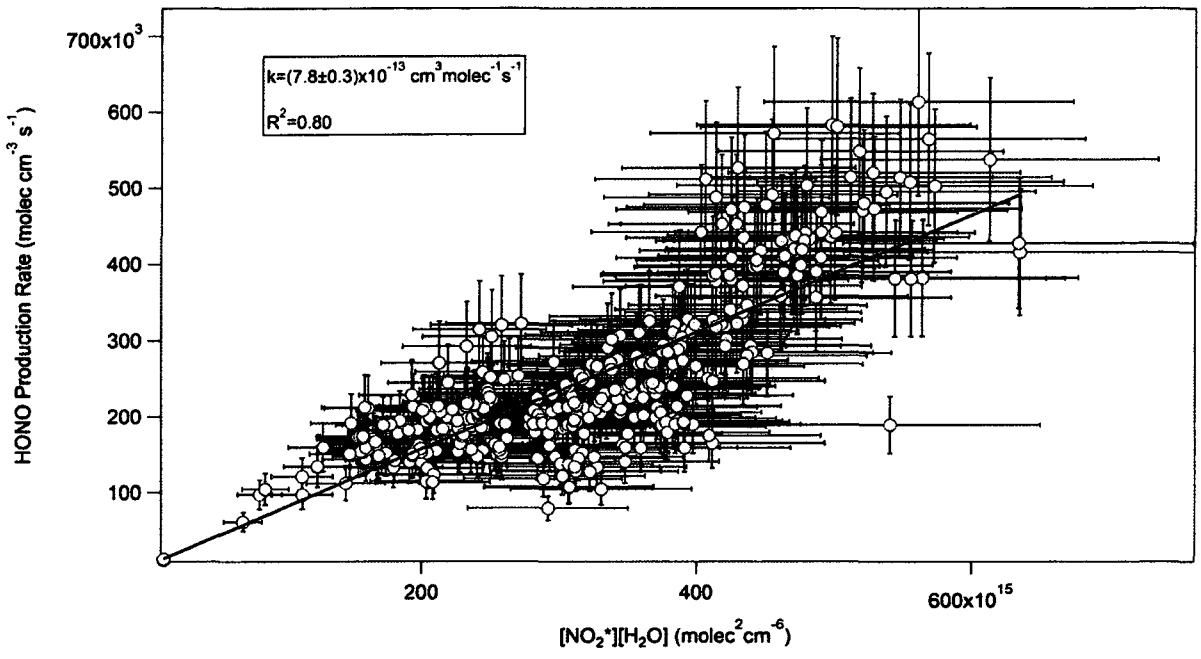

Figure 59: Plot of measured HONO production rate with the calculated HONO production rate for the afternoon of June 24, 2007.

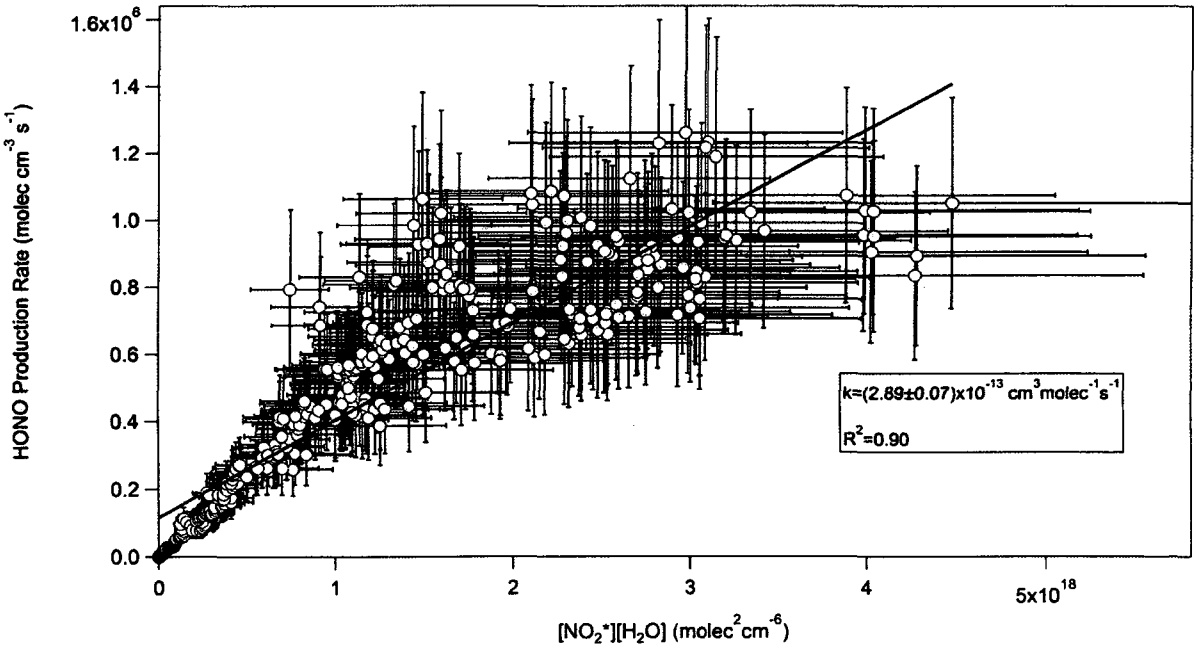

Figure 60: Plot of measured HONO production rate with calculated HONO production rate for the morning June 30, 2007.

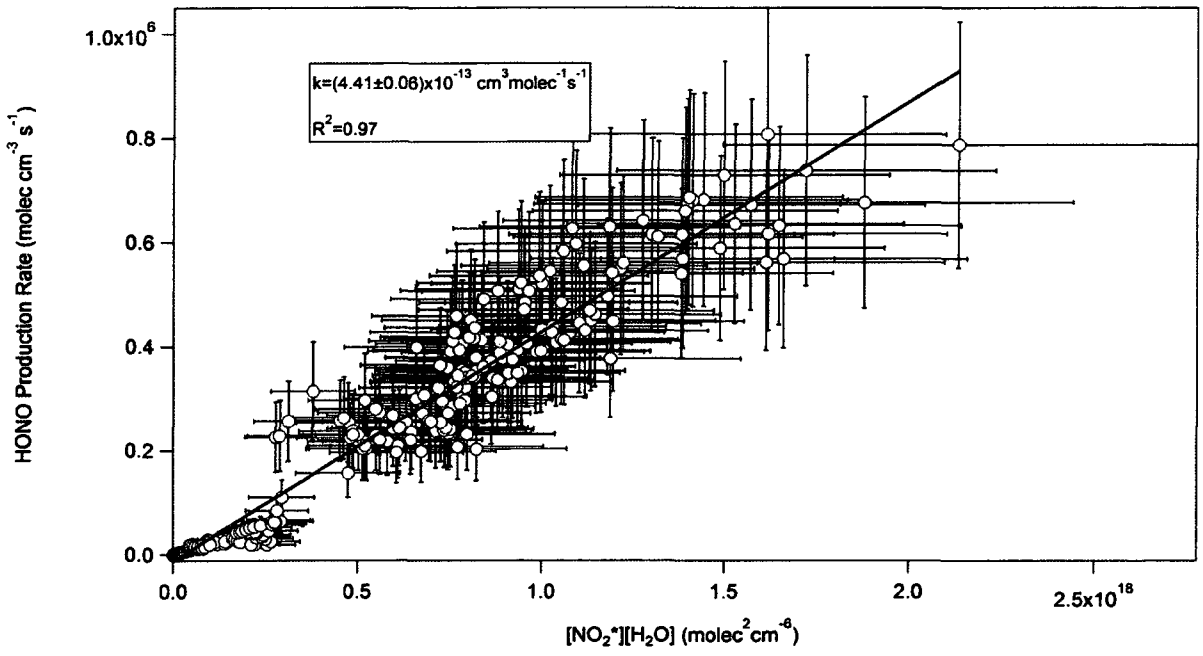

Figure 61: Plot of measured HONO production rate with the calculated HONO production rate for July 4, 2007.

The apparent rate constants for the chosen periods are shown in Table 10. The error value associated with the rate constant represents 1 standard deviation of the apparent rate constant value. In each case the yielded k value is different with only that of the morning of July 4, 2007 being near to the average for the entire study. The dominant wind directions were different each day (Table 10), meaning that the sources of NO_2 were also different each day and that the surfaces that the air mass travelled over prior to arriving at the measurement site were different. During the afternoon of June 21 winds were from the North West, the direction of Detroit/Windsor and several electricity generating and chemical manufacturing plants. A larger apparent k value was calculated for the afternoon of June 24th when winds from the South West brought air from the general direction of Toledo, Ohio. There are several electricity generating units on the United States side of the border ranging from the South West to North West presumably producing large amounts of NO_x. The afternoon of June 24th yielded the largest apparent k value.

Table 10: List of apparent rate constants and dominant wind directions during 4 selected periods of the Harrow study.

Time Period	k (cm^3 $molec^{-1}s^{-1}$)	R^2	Dominant Wind Direction
All daytime data	$(4.5\pm3.5)x10^{-13}$	0.75	–
July 21, 2007 (12:00-18:00 EST)	$(6.1\pm0.3)x10^{-13}$	0.82	North West
July 24, 2007 (12:00-18:00 EST))	$(7.8\pm0.3)x10^{-13}$	0.80	South West
June 30, 2007 (6:00-12:00 EST)	$(2.9\pm0.07)x10^{-13}$	0.90	North East
July 4, 2007 (6:00-12:00 EST)	$(4.4\pm0.06)x10^{-13}$	0.97	South West

During the morning of June 30 the wind directions were from the North East and gave the smallest apparent k value. Winds were from the South West during the morning of July 4 yielding an apparent k value of $(4.4\pm0.06) \times 10^{-13}$ $cm^3molec^{-1}s^{-1}$. These winds correspond to the Toledo region (South West).

In summary since the slopes of the correlations between chemical HONO production and the calculated HONO production from equation (Eq. 6) are changing it is very unlikely that this is a simple gas phase process. Days featuring similar wind direction, June 24th and July 4th, showed apparent rate constants which varied by a nearly a factor of two. Many laboratory studies have suggested efficient heterogeneous conversion of NO_2 on surfaces, enhanced by photo-excitation, which appears to be more consistent with the Harrow data than a homogeneous process.

4.2 Photolytic Production at a Forested Site

The same procedure of calculating the effective rate constants for the Borden data set is used with the Harrow data. A plot of the production rate versus the product of J_{NO2}*, the mixing ratio of NO_2 and the mixing ratio of H_2O for the hours of 10:00-16:00 from August 8-23 is shown in Figure 62.

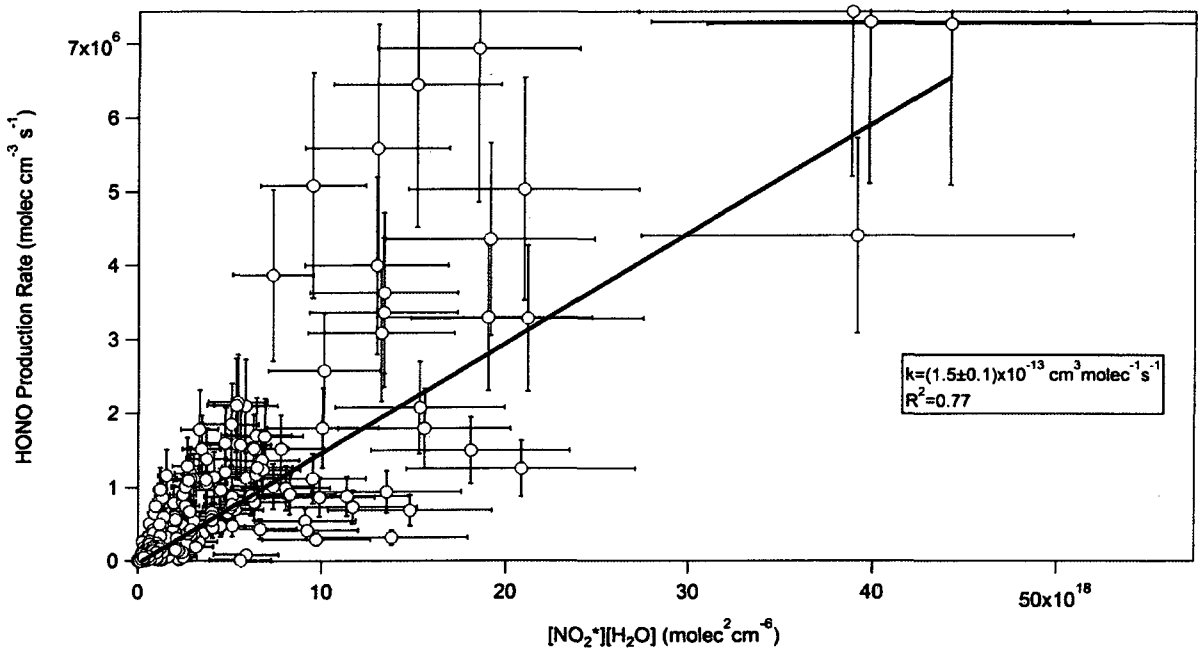

Figure 62: Measured HONO production as a function of calculated production rate for the month of August 2006.

The value of calculated rate constant was determined to be 1.5 x 10^{-13} cm^3 $mol^{-1}s^{-1}$. This is only slightly larger than that measured in the laboratory by Li et al., (2008) of 1.2 x 10^{-13} cm^3 $mol^{-1}s^{-1}$ for a gas phase process and certainly is much closer to that value than any of the apparent k value calculated during the BAQS-Met study.

Three days (Aug. 18-20th) were further examined, and excellent correlations of the chemical production rate and the product of J_{NO2}*, the mixing ratio of NO_2 and the mixing ratio of H_2O were found. They were further inspected to determine if there were large deviations in the apparent k values as was found to be the case at Harrow.. The time of day used for all three days was 10:00-16:00 EST when maximum amounts of light penetrated the forest canopy. Apparent rate constants for those days were calculated from the correlation plots in Figure 63, Figure 64 and Figure 65.

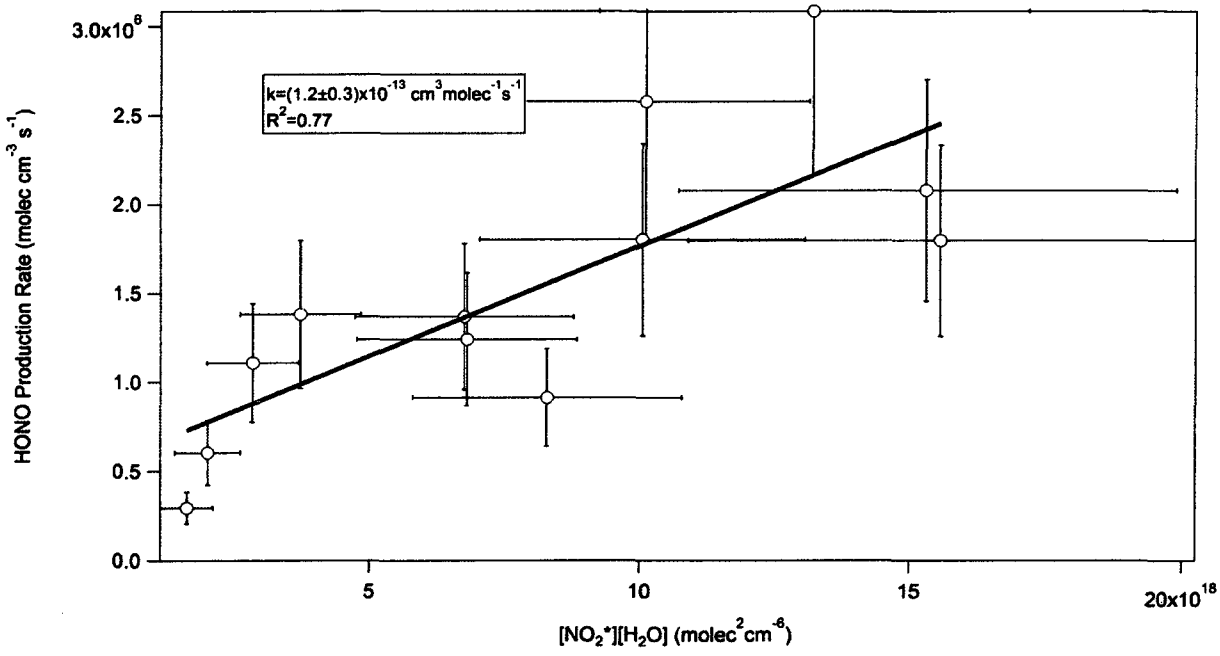

Figure 63: Measured HONO Production as a function of calculated HONO production rate for the day of August 18, 2006.

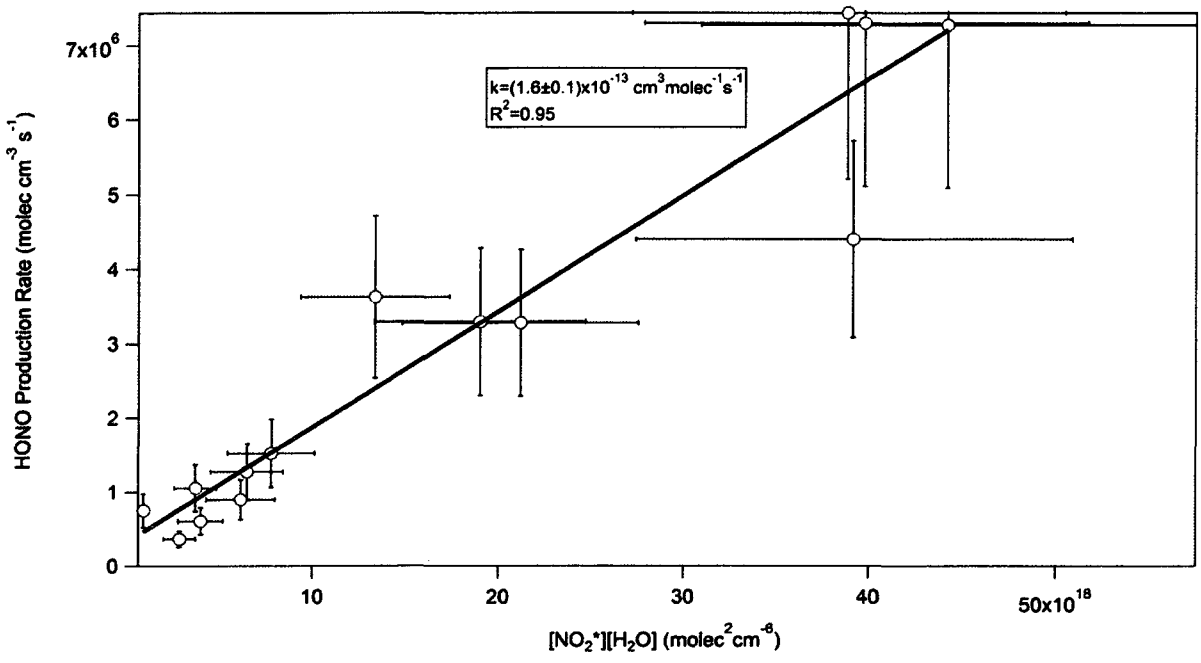

Figure 64: Measured HONO Production as a function of calculated HONO production rate for the day of August 19, 2006.

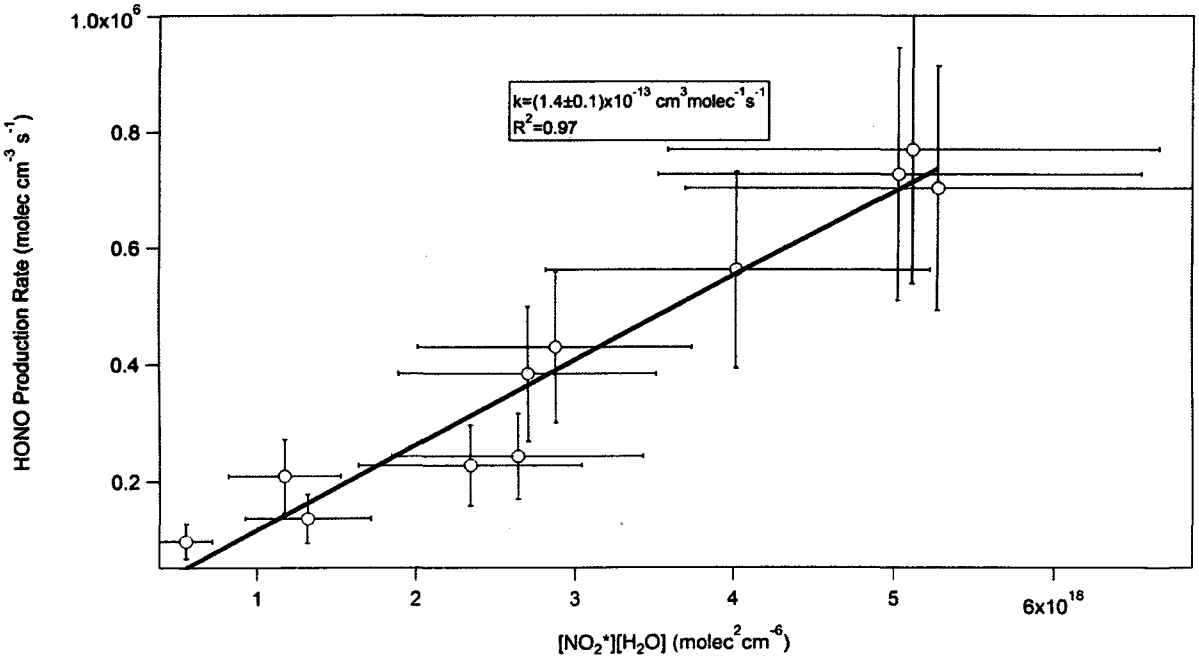

Figure 65: Measured HONO Production as a function of calculated HONO production rate for the day of August 20, 2006.

The difference in the calculated apparent k values was much smaller than that seen in the Harrow data and are shown in Table 11. The error value associated with the rate constant represents 1 standard deviation of the apparent rate constant value.

Table 11: Calculated HONO formation rate constants from Borden August 2006.

Date	k (cm^3 $molec^{-1}s^{-1}$)	R^2	Dominant Wind Direction
August 2006	$(1.5\pm0.1) \times 10^{-13}$	0.77	-
August 18, 2006	$(1.2\pm0.3) \times 10^{-13}$	0.77	North to North East
August 19, 2006	$(1.6\pm0.1) \times 10^{-13}$	0.95	North to North East
August 20, 2006	$(1.4\pm0.1) \times 10^{-13}$	0.97	North to North East

The calculated apparent rate constants were unlike those determined from the Harrow data; where the apparent k values at Harrow varied by as much as a factor of 4, the apparent rates from the Borden data were rather constant. Also unlike Harrow, winds on the three days (August 18-20) were from approximately the same direction, North to North East, where there were no large point sources of pollution. This would also imply that the "fetch" on these three days was similar, yielding similar apparent rate constant values. The two days at Harrow which yielded the largest apparent rate constant values, July 21st and July 24th 2007, showed winds coming from very different areas of large pollution, the metropolitan Detroit area on July 21st and the Ohio Valley on July 24th. However, if one accepts the measurement of k_5 by Li et al., (2008) rather than the upper limit from Crowley and Carl, (1997) the possibility of a simple gas phase process for the production of HONO at the Borden site cannot be ruled out. While such a process appears unlikely to be the dominant route for daytime production at Harrow, it is possibly a contributing factor. When the numerous suggested daytime production mechanisms (almost all involve UV radiation, NO_2 and

humidity) are considered, it appears to be unlikely that the gas phase process suggested by Li et. al. (2008) is the most important, even at Borden. The Harrow site, with its open fields, frequent changes of air mass and nearby pollution sources are in contrast to the measurements below a forest canopy at the Borden site where the local "fetch" is less dependent on wind direction aloft.

5 Conclusions and Future Work

A long path absorption photometer (LOPAP) was successfully constructed and used to measure HONO in Southern Ontario. The instrument provided excellent sensitivity (3σ detection limit=5 pptv) and response time (5 minutes) for making high quality HONO measurements. Instrument interferences were examined and the only one of note found was that from NO_2. The second channel of the instrument is used to specifically correct for this interference. Particulate nitrite has been found to be an interference which the second channel will not correct as particles are taken up quantitatively in the first channel; however the effects of particulate nitrite are expected to be of minor importance to ambient measurements, where particle pH's are low.

Once the instrument was constructed and evaluated, three sites were chosen to perform field measurements. Each site provided a different characteristic with respect to HONO chemistry, (forested, semi-rural and urban). Higher daytime concentrations of HONO than predicted by "classical" HONO chemistry were measured at all 3 sites. Often more than 10 times the expected daytime HONO was measured at the Harrow site. Daytime production values were calculated for the Borden and Harrow sites which showed strong daytime sources. Correlations have shown that there is a strong dependence at both sites on the product of UV radiation, NO_2 and H_2O mixing ratio. While the Harrow data set produced a variety of apparent k values, ranging from 2.9-7.8 x 10^{-13} cm^3 $molec^{-1}s^{-1}$, suggesting a heterogeneous source, the Borden data set yielded more reproducible rate constants of 1.2-1.6 x 10^{-13} cm^3 $molec^{-1}s^{-1}$ leaving open the possibility of a simple gas phase reaction. At the urban site the measured HONO can be largely explained by automobile emissions from the nearby highway and heterogeneous hydrolysis of NO_2.

It is suggested in the future work that studies involving HONO measurement take place in conjunction with measurements of OH as well as high quality measurements of NO_x (specifically NO, since NO detection limits at the Harrow site were not optimal, ~1 ppbv) so that accurate photo stationary states can be calculated. Higher quality J_{HONO} measurements in conjunction with measurements of J_{O3} and J_{HCHO} would be of great value in determining the overall effect of HONO on the daytime OH budget. Faster measurements of HONO would also be of value, since they could allow for measurement of HONO fluxes using eddy correlation, which would help in determining the effect of deposition on the HONO budget as well as production at surfaces. While such high speeds are not possible with the LOPAP instrument, techniques such as PF-LIF and CIMS might be sufficiently powerful. Having accurate knowledge of daytime HONO chemistry has been shown in several studies to be important to the understanding of the overall OH budget [Alicke et al., (2003); Kleffmann et al., (2005); Elshorbany et al., (2009)]. While the exact contribution of HONO to the OH budgets in this work is uncertain, photolysis of larger than expected concentrations of daytime HONO would clearly have an effect on the apportionment of OH sources.

6 References

Acker, K., D. Möller, R. Auel, W. Wieprecht, and D. Kalaß (2005), CONCENTRATIONS OF NITROUS ACID, NITRIC ACID, NITRITE AND NITRATE IN THE GAS AND AEROSOL PHASE AT A SITE IN THE EMISSION ZONE DURING ESCOMPTE 2001 EXPERIMENT, *Atmospheric Environment, 74*, 507– 524.

Alicke, B., A. Geyer, A. Hofzumahaus, F. Holland, S. Konrad, H. W. Patz, J. Schafer, J. Stutz, A. Volz-Thomas, and U. Platt (2003), OH FORMATION BY HONO PHOTOLYSIS DURING THE BERLIOZ EXPERIMENT, *Journal of Geophysical Research, 108*, 8247-8264.

Alicke, B., U. Platt, and J. Stutz (2002), IMPACT OF NITROUS ACID PHOTOLYSIS ON THE TOTAL HYDROXYL RADICAL BUDGET DURING THE LIMITATION OF OXIDANT Production/Pianura PADANA PRODUZIONE DI OZONO STUDY IN MILAN, *Journal of Geophysical Research, 107*, 8196-8213.

Altkorn, R., I. Koev, and A. Gottlieb (1997), WAVEGUIDE CAPILLARY CELL FOR LOW-REFRACTIVE-INDEX LIQUIDS, *Applied Spectroscopy, 51*, 1554-1558.

Ammann, M., M. Kalberer, D. T. Jost, L. Tobler, E. Rössler, D. Piguet, H. W. Gäggeler, and U. Baltensperger (1998), HETEROGENEOUS PRODUCTION OF NITROUS ACID ON SOOT IN POLLUTED AIR MASSES, *Letters to Nature, 395*, 157-160.

ARL and NOAA (2005), NOAA ARL HYSPLIT MODEL (http://www.arl.noaa.gov/ready/hysplit4.html).

Barney, W. S. and B. J. Finlayson-Pitts (2000), ENHANCEMENT OF N_2O_4 ON POROUS GLASS AT ROOM TEMPERATURE: A KEY INTERMEDIATE IN THE HETEROGENEOUS HYDROLYSIS OF NO_2?, *Journal of Physical Chemistry A, 104*, 171-175.

Beine, H. J., A. Amoroso, G. Esposito, R. Sparapani, A. Ianniello, T. Georgiadis, M. Nardino, P. Bonasoni, P. Cristofanelli, and F. Dominé (2005), DEPOSITION OF ATMOSPHERIC NITROUS ACID ON ALKALINE SNOW SURFACES, *Geophysical Research Letters, 32*, doi: 10.1029/2005GL022589.

Bejan, I., Y. Abd-el-Aal, I. Barnes, T. Benter, B. Bohn, P. Wiesen, and J. Kleffmann (2006), THE PHOTOLYSIS OF ORTHO-NITROPHENOLS: a NEW GAS PHASE SOURCE OF HONO, *Physical Chemistry Chemical Physics, 8*, 2028-2035, doi: 10.1039/b516590c.

Belz, M., P. Dress, K. Klein, W. J. O. Boyle, H. Franke, and K. T. V. Grattan (1998), LIQUID CORE WAVEGUIDE WITH FIBER OPTIC COUPLING FOR REMOTE POLLUTION MONITORING IN THE DEEP ULTRAVIOLET, *Water Science and Technology, 37*, 279-284.

Belz, M., P. Dress, A. Sukhitskiy, and S. Liu (1999), LINEARITY AND EFFECTIVE OPTICAL PATHLENGTH OF LIQUID WAVEGUIDE CAPILLARY CELLS, *Internal Standardization and Calibration Architectures for Chemical Sensors, 3856*, 271-281, doi: 10.1117/12.371300.

Bröske, R., J. Kleffmann, and P. Wiesen (2003), HETEROGENEOUS CONVERSION OF NO_2 ON SECONDARY ORGANIC AEROSOL SURFACES: A POSSIBLE SOURCE OF NITROUS ACID (HONO) IN THE ATMOSPHERE?, *Atmospheric Chemistry and Physics, 3*, 469-474.

Cape, J. N., K. J. Hargreaves, R. Storeton-West, D. Fowler, R. N. Colville, T. W. Choularton, and M. W. Gallagher (1992), NITRITE IN OROGRAPHIC CLOUD AS AN INDICATOR OF NITROUS ACID IN RURAL AIR, *Atmospheric Environment. Part A, 26*, 2301-2307.

Cape, J. N., K. J. Hargreaves, R. L. Storeton-West, B. Jones, T. Davies, R. N. Colvile, M. W. Gallagher, T. W. Choularton, S. Pahl, A. Berner, C. Kruisz, M. Bizjak, P. Laj, M. C. Facchini, S. Fuzzi, B. G. Arends, K. Acker, W. Wieprecht, R. M. Harrison, and J. D. Peak (1997), THE BUDGET OF OXIDISED NITROGEN SPECIES IN OROGRAPHIC CLOUDS, *Atmospheric Environment, 31*, 2625-2636.

Carr, S., D. E. Heard, and M. A. Blitz (2009), COMMENT ON ATMOSPHERIC HYDROXYL RADICAL PRODUCTION FROM ELECTRONICALLY EXCITED NO2 AND H2O, *Science, 324*, 336b.

Cheung, J. L., Y. Q. Li, J. Boniface, Q. Shi, P. Davidovits, D. R. Worsnop, J. T. Jayne, and C. E. Kolb (2000), HETEROGENEOUS INTERACTIONS OF NO2 WITH AQUEOUS SURFACES, *The Journal of Physical Chemistry A, 104*, 2655-2662, doi: 10.1021/jp992929f.

Crowley, J. N. and S. A. Carl (1997), OH FORMATION IN THE PHOTOEXCITATION OF NO_2 BEYOND THE DISSOCIATION THRESHOLD IN THE PRESENCE OF WATER VAPOR, *Journal of Physical Chemistry A, 101*, 4178-4184.

Dallas, T. and P. K. Dasgupta (2004), LIGHT AT THE END OF THE TUNNEL: RECENT ANALYTICAL APPLICATIONS OF LIQUID-CORE WAVEGUIDES, *TrAC Trends in Analytical Chemistry, 23*, 385-392.

Dasgupta, P. K., Z. Genfa, S. K. Poruthoor, S. Caldwell, S. Dong, and S. Y. Liu (1998), HIGH-SENSITIVITY GAS SENSORS BASED ON GAS-PERMEABLE LIQUID CORE WAVEGUIDES AND LONG-PATH ABSORBANCE DETECTION, *Analytical Chemistry, 70*, 4661-4669.

Diemer, S., J. Meister, R. Jung, S. Klein, M. Haisch, W. Fuss, and P. Hering (1997), LIQUID-CORE LIGHT GUIDES FOR NEAR-INFRARED APPLICATIONS, *Applied Optics, 36*, 9075-9082, doi: 10.1364/AO.36.009075.

Dionex URG 9000A , AIR MONITORING, *2009* (http://www.dionex.com/en-us/interest/environmental/pollution-testing/lp74110.html).

Donnelly, V. M., D. G. Keil, and F. Kaufman (1979), FLUORESCENCE LIFETIME STUDIES OF NO_2. III. MECHANISM OF FLUORESCENCE QUENCHING, *The Journal of Chemical Physics, 71*, 659-673, doi: 10.1063/1.438417.

Dress, P., M. Belz, K. F. Klein, K. T. V. Grattan, and H. Franke (1998), WATER-CORE WAVEGUIDE FOR POLLUTION MEASUREMENTS IN THE DEEP ULTRAVIOLET, *Applied Optics, 37*, 4991-4997.

Dress, P. and H. Franke (1996), A CYLINDRICAL LIQUID-CORE WAVEGUIDE, *Applied Physics B: Lasers and Optics, 63*, 12-19.

Dress, P. and H. Franke (1997), INCREASING THE ACCURACY OF LIQUID ANALYSIS AND pH-VALUE CONTROL USING a LIQUID-CORE WAVEGUIDE, *Review of Scientific Instruments, 68*, 2167-2171.

Dress, P., M. Belz, K. Klein, K. T. V. Grattan, and H. Franke (1998), PHYSICAL ANALYSIS OF TEFLON COATED CAPILLARY WAVEGUIDES, *Sensors and Actuators B: Chemical, 51*, 278-284.

D'Sa, E. J., R. G. Steward, A. Vodacek, N. V. Blough, and D. Phinney (1999), DETERMINING OPTICAL ABSORPTION OF COLORED DISSOLVED ORGANIC MATTER IN SEA WATER WITH a LIQUID CAPILLARY WAVEGUIDE, *Limnology and Oceanography, 44*, 1142-1148.

Elshorbany, Y. F., R. Kurtenbach, P. Wiesen, E. Lissi, M. Rubio, G. Villena, E. Gramsch, A. R. Rickard, M. J. Pilling, and J. Kleffmann (2009), OXIDATION CAPACITY OF THE CITY AIR OF SANTIAGO, CHILE, *Atmospheric Chemistry and Physics, 9*, 2257-2273.

Environment Canada , FOREST FLUX RESEARCH STATION, *2008* (http://www.msc-smc.ec.gc.ca/arqp/borden_e.cfm).

Febo, A., P. Cinzia, M. Ghebardi, and R. Sparapani (1995a), EVALUATION OF a HIGH-PURITY AND HIGH-STABILITY CONTINUOUS GENERATION SYSTEM FOR NITROUS ACID, *Environmental Science & Technology, 29*, 2390-2395.

Febo, A., C. Perrino, and I. Allegrini (1995b), MEASUREMENT OF NITROUS ACID IN MILAN, ITALY BY DOAS AND DIFFUSION DENUDERS, *Atmospheric Environment, 30*, 3599-3609.

Finlayson-Pitts, B. J. and J. N. Pitts (2000), *Chemistry of the Upper and Lower Atmosphere : Theory, Experiments and Applications*, 969 pp., Academic Press, San Diego, Calif. ; London.

Fuentes, J. D., T. J. Gillespie, G. den Hartog, and H. H. Neumann (1992), OZONE DEPOSITION ONTO a DECIDUOUS FOREST DURING DRY AND WET CONDITIONS, *Agricultural and Forest Meteorology, 62*, 1-18.

Fuentes, J. D., D. Wang, G. Den Hartog, H. H. Neumann, T. F. Dann, and K. J. Puckett (1995), MODELLED AND FIELD MEASUREMENTS OF BIOGENIC HYDROCARBON EMISSIONS FROM a CANADIAN DECIDUOUS FOREST, *Atmospheric Environment, 29*, 3003-3017, doi: DOI: 10.1016/1352-2310(95)00120-N.

Genfa, Z., S. Sjaak, C. B. Boring, P. A. C. Jongejan, and P. K. Dasgupta (2003), CONTINUOUS WET DENUDER MEASUREMENTS OF ATMOSPHERIC NITRIC AND NITROUS ACIDS DURING THE 1999 ATLANTA SUPERSITE, *Atmospheric Environment, 37*, 1351-1364.

George, C., R. S. Strekowski, J. Kleffmann, K. Stemmler, and M. Ammann (2005), PHOTOENHANCED UPTAKE OF GASEOUS NO_2 ON SOLID ORGANIC COMPOUNDS: a PHOTOCHEMICAL SOURCE OF HONO?, *Faraday Discussions, 130*, 195-210; discussion 241-64, 519-24.

Gooijer, C., G. P. Hoornweg, T. de Beer, A. Bader, D. J. van Iperen, and U. A. T. Brinkman (1998), DETECTOR CELL BASED ON PLASTIC LIQUID-CORE WAVEGUIDES SUITABLE FOR AQUEOUS

SOLUTIONS: ONE-TO-TWO DECADES IMPROVED DETECTION LIMITS IN CONVENTIONAL-SIZE COLUMN LIQUID CHROMATOGRAPHY WITH ABSORPTION DETECTION, *Journal of Chromatography A, 824*, 1-5.

Grasshoff, K., M. Ehrhardt, and K. Kremling (1983), *Methods of Sea Water Analysis*, Verlag Chemie, Weinheim.

Gu, L., J. Fuentes, H. Shugart, R. Staebler, and T. Black (1999), RESPONSES OF NET ECOSYSTEM EXCHANGES OF CARBON DIOXIDE TO CHANGES IN CLOUDINESS: RESULTS FROM TWO NORTH AMERICAN DECIDUOUS FORESTS, *Journal of Geophysical Research, 104*, 31421-31434.

Gutzwiller, L., F. Arens, U. Baltensperger, H. W. Gaggeler, and M. Ammann (2002), SIGNIFICANCE OF SEMIVOLATILE DIESEL EXHAUST ORGANICS FOR SECONDARY HONO FORMATION, *Environmental Science & Technology, 36*, 677-682.

Hanst, P. L., J. W. Spence, and M. Miller (1977), ATMOSPHERIC CHEMISTRY OF N-NITROSO DIMETHYLAMINE, *Environmental Science & Technology, 11*, 403-405.

Harris, G. W., W. P. L. Carter, A. M. Winer, J. N. Pitts, U. Platt, and D. Perner (1982), OBSERVATIONS OF NITROUS ACID IN THE LOS ANGELES ATMOSPHERE AND IMPLICATIONS FOR PREDICTIONS OF OZONE-PRECURSOR RELATIONSHIPS, *Environmental Science & Technology, 16*, 414-419.

Harrison, R. M., J. D. Peak, and G. M. Collins (1996), TROPOSPHERIC CYCLE OF NITROUS ACID, *Journal of Geophysical Research, 101(D9)*, 14,429-14,439.

Harrison, M. A. J., S. Barra, D. Borghesi, D. Vione, C. Arsene, and R. Iulian Olariu (2005), NITRATED PHENOLS IN THE ATMOSPHERE: a REVIEW, *Atmospheric Environment, 39*, 231-248.

Harrison, R. M. and A. -. N. Kitto (1994), EVIDENCE FOR a SURFACE SOURCE OF ATMOSPHERIC NITROUS ACID, *Atmospheric Environment, 28*, 1089-1094.

Hecht, E. (1998), Fiberoptics, in , 3rd edn.Anonymous , pp. 195-198, Addison-Wesley, Reading, Mass.

Heland, J., J. Kleffmann, R. Kurtenbach, and P. Wiesen (2001), A NEW INSTRUMENT TO MEASURE GASEOUS NITROUS ACID (HONO) IN THE ATMOSPHERE, *Environmental Science & Technology, 35*, 3207-3212.

Hirokawa, J., T. Kato, and F. Mafuné (2009), IN SITU MEASUREMENTS OF ATMOSPHERIC NITROUS ACID BY CHEMICAL IONIZATION MASS SPECTROMETRY USING CHLORIDE ION TRANSFER REACTIONS, *Analytical Chemistry, 81*, 8380-8386, doi: 10.1021/ac901117b.

Huang, G., X. Zhou, G. Deng, H. Qiao, and K. Civerolo (2002), MEASUREMENTS OF ATMOSPHERIC NITROUS ACID AND NITRIC ACID, *Atmospheric Environment, 36*, 2225-2235.

Jarvis, D. L., B. P. Leaderer, S. Chinn, and P. G. Burney (2005), INDOOR NITROUS ACID AND RESPIRATORY SYMPTOMS AND LUNG FUNCTION IN ADULTS, *Thorax, 60*, 474-479, doi: 10.1136/thx.2004.032177.

Jenkin, M. E. and R. A. Cox (1987), KINETICS OF THE GAS-PHASE REACTION OF OH WITH NITROUS ACID, *Chemical Physics Letters, 137*, 548-552, doi: DOI: 10.1016/0009-2614(87)80627-9.

Jenkin, M. E., R. A. Cox, and D. J. Williams (1988), LABORATORY STUDIES OF THE KINETICS OF FORMATION OF NITROUS ACID FROM THE THERMAL REACTION OF NITROGEN DIOXIDE AND WATER VAPOUR, *Atmospheric Environment, 22*, 487-498, doi: DOI: 10.1016/0004-6981(88)90194-1.

Junkermann, W. and T. Ibusuki (1992), FTIR SPECTROSCOPIC MEASUREMENTS OF SURFACE BOND PRODUCTS OF NITROGEN OXIDES ON AEROSOL surfaces—implications FOR HETEROGENEOUS HNO_2 PRODUCTION, *Atmospheric Environment Part A, 26*, 3099-3103, doi: DOI: 10.1016/0960-1686(92)90466-X.

Kaiser, E. W. and C. H. Wu (1977), A KINETIC STUDY OF THE GAS PHASE FORMATION AND DECOMPOSITION REACTIONS OF NITROUS ACID, *The Journal of Physical Chemistry, 81*, 1701-1706.

Kirchstetter, T. W., R. A. Harley, and D. Littlejohn (1996), MEASUREMENT OF NITROUS ACID IN MOTOR VEHICLE EXHAUST, *Environmental Science & Technology, 30*, 2843-2849.

Kleffmann, J., K. H. Becker, and P. Wiesen (1998), HETEROGENEOUS NO_2 CONVERSION PROCESSES ON ACID SURFACES: POSSIBLE ATMOSPHERIC IMPLICATIONS, *Atmospheric Environment, 32*, 2721-2729.

Kleffmann, J., T. Gavriloaiei, A. Hofzumahaus, F. Holland, R. Koppmann, L. Rupp, E. Schlosser, M. Siese, and A. Wahner (2005), DAYTIME FORMATION OF NITROUS ACID: A MAJOR SOURCE OF OH RADICALS IN A FOREST, *Geophysical Research Letters, 32*, L05818, doi: 10.1029/2005GL022524.

Kleffmann, J., J. Heland, R. Kurtenbach, J. Lörzer, and P. Wiesen (2002), A NEW INSTRUMENT (LOPAP) FOR THE MEASUREMENT OF NITROUS ACID (HONO), *Environmental Science & Pollution Research*, 48-54.

Kleffmann, J., R. Kurtenbach, J. Lörzer, P. Wiesen, N. Kalthoff, B. Vogel, and H. Vogel (2003), MEASURED AND SIMULATED VERTICAL PROFILES OF NITROUS ACID-PART I: FIELD MEASUREMENTS, *Atmospheric Environment, 37*, 2949-2955.

Kleffmann, J., J. C. Lorzer, P. Wiesena, C. Kernb, S. Trickb, R. Volkamer, M. Rodenas, and K. Wirtz (2006), INTERCOMPARISON OF THE DOAS AND LOPAP TECHNIQUES FOR THE DETECTION OF NITROUS ACID (HONO), *Atmospheric Environment, 40*, 3640-3652.

Kraus, A. and A. Hofzumahaus (1998), FIELD MEASUREMENTS OF ATMOSPHERIC PHOTOLYSIS FREQUENCIES FOR O_3, NO_2, HCHO, CH_3CHO, H_2O_2, AND HONO BY UV SPECTRORADIOMETRY, *Journal of Atmospheric Chemistry, 31*, 161-180.

Kurtenbach, R., K. H. Becker, J. A. G. Gomes, J. Kleffmann, J. C. Lörser, M. Spittler, P. Wiesen, R. Ackermann, A. Geyer, and U. Platt (2001), INVESTIGATIONS OF EMISSIONS AND HETEROGENEOUS FORMATION OF HONO IN a ROAD TRAFFIC TUNNEL, *Atmospheric Environment, 35*, 3385-3394.

Lammel, G. and J. N. Cape (1996), NITROUS ACID AND NITRITE IN THE ATMOSPHERE, *Chemical Society Reviews*, 361-369.

Lammel, G. and D. Perner (1988), THE ATMOSPHERIC AEROSOL AS A SOURCE OF NITROUS ACID IN THE POLLUTED ATMOSPHERE, *Journal of Aerosol Science, 19*, 1199-1202.

Lee, Y. N. and S. E. Schwartz (1981), REACTION KINETICS OF NITROGEN DIOXIDE WITH LIQUID WATER AT LOW PARTIAL PRESSURE, *Journal of Physical Chemistry, 85*, 840-848, doi: 10.1021/j150607a022.

Li, S., J. Matthews, and A. Sinha (2008), ATMOSPHERIC HYDROXYL RADICAL PRODUCTION FROM ELECTRONICALLY EXCITED NO_2 AND H_2O, *Science, 319*, 1657-1660.

Li, S., J. Matthews, and A. Sinha (2009), RESPONSE TO COMMENT ON ATMOSPHERIC HYDROXYL RADICAL PRODUCTION FROM ELECTRONICALLY EXCITED NO2 AND H2O, *Science, 324*, 336.

Li, Y. Q., J. J. Schwab, and K. L. Demerjian (2008), FAST TIME RESPONSE MEASUREMENTS OF GASEOUS NITROUS ACID USING a TUNABLE DIODE LASER ABSORPTION SPECTROMETER: HONO EMISSION SOURCE FROM VEHICLE EXHAUSTS, *Geophysical Research Letters, 35*, L04803, doi: 10.1029/2007GL031218.

Liao, W., A. T. Case, J. Mastromarino, D. Tan, and J. E. Dibb (2006-05-10), OBSERVATIONS OF HONO BY LASER-INDUCED FLUORESCENCE AT THE SOUTH POLE DURING ANTCI 2003, *Geophysical Research Letters, 33*, 1-4.

Liao, W., A. Hecobian, J. Mastromarino, and D. Tan (2006), DEVELOPMENT OF a PHOTO-fragmentation/laser-INDUCED FLUORESCENCE MEASUREMENT OF ATMOSPHERIC NITROUS ACID, *Atmospheric Environment, 40*, 17-26, doi: DOI: 10.1016/j.atmosenv.2005.07.001.

Longfellow, C. A., T. Imamura, A. R. Ravishankara, and D. R. Hanson (1998), HONO SOLUBILITY AND HETEROGENEOUS REACTIVITY ON SULFURIC ACID SURFACES, *Journal of Physical Chemistry A, 102*, 3323-3332.

Makar, P., J. Fuentes, D. Wang, R. Staebler, and H. Wiebe (1999), CHEMICAL PROCESSING OF BIOGENIC HYDROCARBONS WITHIN AND ABOVE a TEMPERATE DECIDUOUS FOREST, *Journal of Geophysical Research, 104*, 3581-3603.

Manor, R., A. Datta, I. Ahmad, M. Holtz, S. Gangopadhyay, and T. Dallas (2003), MICROFABRICATION AND CHARACTERIZATION OF LIQUID CORE WAVEGUIDE GLASS CHANNELS COATED WITH TEFLON AF, *IEEE Sensors Journal, 3*, 687-692.

Mebel, A. M., M. C. Lin, and C. F. Melius (1998), RATE CONSTANT OF THE HONO + HONO → H_2O + NO + NO_2 REACTION FROM AB INITIO MO AND TST CALCULATIONS, *The Journal of Physical Chemistry A, 102*, 1803-1807.

Ndour, M., B. D'Anna, C. George, O. Ka, Y. Balkanski, J. Kleffmann, K. Stemmler, and M. Ammann (2008), PHOTOENHANCED UPTAKE OF NO_2 ON MINERAL DUST: LABORATORY EXPERIMENTS AND MODEL SIMULATIONS, *Geophysical Research Letters, 35*, L05812, doi: 10.1029/2007GL032006.

Neftel, A., A. Blatter, R. Hesterberg, and T. Staffelbach (1996), MEASUREMENTS OF CONCENTRATION GRADIENTS OF HNO_2 AND HNO_3 OVER a SEMI-NATURAL ECOSYSTEM, *Atmospheric Environment, 30*, 3017-3025.

Ontario Ministry of Transportation , **TORONTO (HIGHWAY 401) COMPASS SYSTEM**, *2009* (http://www.mto.gov.on.ca/english/traveller/trip/compass-sio.shtml).

Park, J. Y. and Y. N. Lee (1988), SOLUBILITY AND DECOMPOSITION KINETICS OF NITROUS ACID IN AQUEOUS SOLUTION, *Journal of Physical Chemistry A, 92*, 6294-6302.

Perner, D. and U. Platt (1979), DETECTION OF NITROUS ACID IN THE ATMOSPHERE BY DIFFERENTIAL OPTICAL ABSORPTION, *Geophysical Research Letters, 6*, 917-920.

Pitts, J. N., D. Grosjean, K. Van Cauwenberghe, J. P. Schmid, and D. R. Fitz (1978), PHOTOOXIDATION OF ALIPHATIC AMINES UNDER SIMULATED ATMOSPHERIC CONDITIONS: FORMATION OF NITROSAMINES, NITRAMINES, AMIDES, AND PHOTOCHEMICAL OXIDANT, *Environmental Science & Technology, 12*, 946-953.

Platt, U., D. Perner, G. W. Harris, A. M. Winer, and J. N. Pitts (1980), OBSERVATIONS OF NITROUS ACID IN AN URBAN ATMOSPHERE BY DIFFERENTIAL OPTICAL ABSORPTION, *Nature, 285*, 312-314.

Rasmussen, T., M. Brauer, and S. Kjaergaard (1995), EFFECTS OF NITROUS ACID EXPOSURE ON HUMAN MUCOUS MEMBRANES, *American Journal of Respiratory and Critical Care Medicine, 151*, 1504-1511.

Reisinger, A. R. (2000), OBSERVATIONS OF HNO_2 IN THE POLLUTED WINTER ATMOSPHERE: POSSIBLE HETEROGENEOUS PRODUCTION ON AEROSOLS, *Atmospheric Environment, 34*, 3865-3874.

Rogers, M. O. and D. D. Davis (1989), A UV-Photofragmentation/Laser-INDUCED FLUORESCENCE SENSOR FOR THE ATMOSPHERIC DETECTION OF HONO, *Environmental Science & Technology, 23*, 1106-1112.

Rohrer, F., B. Bohn, T. Brauers, D. Brüning, F. -. Johnen, A. Wahner, and J. Kleffmann (2005), CHARACTERISATION OF THE PHOTOLYIC HONO-SOURCE IN THE ATMOSPHERE SIMULATION CHAMBER SAPHIR, *Atmospheric Chemistry and Physics, 5*, 2189-2201.

Sakugawa, H. and J. N. Cape (2007), HARMFUL EFFECTS OF ATMOSPHERIC NITROUS ACID ON THE PHYSIOLOGICAL STATUS OF SCOTS PINE TREES, *Environmental Pollution, 147*, 532-534.

Schiller, C. L., S. Locquiao, T. J. Johnson, and G. W. Harris (2001), ATMOSPHERIC MEASUREMENTS OF HONO BY TUNABLE DIODE LASER ABSORPTION SPECTROSCOPY, *Journal of Atmospheric Chemistry, 40*, 275-293.

Schimang, R., A. Folkers, J. Kleffmann, E. Kleist, M. Miebach, and J. Wildt (2006), UPTAKE OF GASEOUS NITROUS ACID (HONO) BY SEVERAL PLANT SPECIES, *Atmospheric Environment, 40*, 1324-1335.

Staffelbach, T., A. Neftel, A. Blatter, A. Gut, M. Fahrni, J. Stähelin, A. Prévôt, A. Hering, M. Lehning, B. Neininger, M. Bäumle, G. L. Kok, J. Dommen, M. Hutterli, and M. Anklin (1997a), PHOTOCHEMICAL OXIDANT FORMATION OVER SOUTHERN SWITZERLAND. 1. RESULTS FROM SUMMER 1994, *Journal of Geophysical Research, 102*, 23345-23362, doi: 10.1029/97JD00933.

Staffelbach, T., A. Neftel, and L. W. Horowitz (1997b), PHOTOCHEMICAL OXIDANT FORMATION OVER SOUTHERN SWITZERLAND. 2. MODEL RESULTS, *Journal of Geophysical Research, 102*, 23363-23373, doi: 10.1029/97JD00932.

Stemmler, K., M. Ammann, C. Donders, J. Kleffmann, and C. George (2006), PHOTOSENSITIZED REDUCTION OF NITROGEN DIOXIDE ON HUMIC ACID AS a SOURCE OF NITROUS ACID, *Nature, 440*, 195-198, doi: 10.1038/nature04603.

Stemmler, K., M. Ndour, Y. Elshorbany, J. Kleffmann, B. D'Anna, C. George, B. Bohn, and M. Ammann (2007), LIGHT INDUCED CONVERSION OF NITROGEN DIOXIDE INTO NITROUS ACID ON SUBMICRON HUMIC ACID AEROSOL, *Atmospheric Chemistry and Physics, 7*, 4237-4248.

Stutz, J., B. Alicke, R. Ackermann, A. Geyer, S. Wang, A. B. White, E. J. Williams, C. W. Spicer, and J. D. Fast (2004), RELATIVE HUMIDITY DEPENDENCE OF HONO CHEMISTRY IN URBAN AREAS, *Journal of Geophysical Research, 109*, D03307, doi: 10.1029/2003JD004135.

Stutz, J., B. Alicke, and A. Neftel (2002), NITROUS ACID FORMATION IN THE URBAN ATMOSPHERE: GRADIENT MEASUREMENTS OF NO_2 AND HONO OVER GRASS IN MILAN, ITALY, *Journal of Geophysical Research, 107*, 8192-8208.

Stutz, J., E. S. Kim, U. Platt, P. Bruno, C. Perrino, and A. Febo (2000), UV-VISIBLE ABSORPTION CROSS SECTIONS OF NITROUS ACID, *Journal of Geophysical Research, 105*, 14,585-14,592.

Svensson, R., E. Ljungström, and O. Lindqvist (1987), KINETICS OF THE REACTION BETWEEN NITROGEN DIOXIDE AND WATER VAPOUR, *Atmospheric Environment (1967), 21*, 1529-1539, doi: DOI: 10.1016/0004-6981(87)90315-5.

Thornton, J. A., P. J. Wooldridge, and R. C. Cohen (2000), ATMOSPHERIC NO_2: IN SITU LASER-INDUCED FLUORESCENCE DETECTION AT PARTS PER TRILLION MIXING RATIOS, *Analytical Chemistry, 72*, 528.

Vecera, Z. and P. K. Dasgupta (1991), MEASUREMENT OF ATMOSPHERIC NITRIC AND NITROUS ACIDS WITH a WET EFFLUENT DIFFUSION DENUDER AND LOW-PRESSURE ION CHROMATOGRAPHY-POSTCOLUMN REACTION DETECTION, *Analytical Chemistry, 63*, 2210-2216.

Vione, D., V. Maurino, C. Minero, M. Duncianu, R. Olariu, C. Arsene, M. Sarakha, and G. Mailhot (2009), ASSESSING THE TRANSFORMATION KINETICS OF 2- AND 4-NITROPHENOL IN THE ATMOSPHERIC AQUEOUS PHASE. IMPLICATIONS FOR THE DISTRIBUTION OF BOTH NITROISOMERS IN THE ATMOSPHERE, *Atmospheric Environment, 43*, 2321-2327, doi: DOI: 10.1016/j.atmosenv.2009.01.025.

Vogel, B., H. Vogel, J. Kleffmann, and R. Kurtenbach (2003), MEASURED AND SIMULATED VERTICAL PROFILES OF NITROUS ACID-PART II: MODEL SIMULATIONS AND INDICATIONS FOR a PHOTOLYTIC SOURCE, *Atmospheric Environment, 37*, 2957-2966.

Wall, K. J., C. L. Schiller, and G. W. Harris (2006), MEASUREMENTS OF THE HONO PHOTODISSOCIATION CONSTANT, *Journal of Atmospheric Chemistry, 55*, 31-54.

Wang, D., J. Li, X. Huang, C. Geng, and C. Sun (2007), OH + HONO REACTION: A THEORETICAL STUDY, *Journal of Molecular Structure: THEOCHEM, 847*, 10-22, doi: DOI: 10.1016/j.theochem.2007.08.037.

Wang, L. and J. Zhang (2000), DETECTION OF NITROUS ACID BY CAVITY RING-DOWN SPECTROSCOPY, *Environmental Science & Technology, 34*, 4221-4227.

Wisthaler, A., A. Hansel, J. Kleffmann, T. Brauers, F. Rohrer, and A. Wahner (2003), Nitrous acid (HONO) measurements by PTR-MS, 1st International Conference on Proton Transfer Reaction Mass Spectrometry and Its Applications , Institut für Ionenphysik der Universität Innsbruck Technikerstrasse 25, 6020 Innsbruck, Austria, January 18 – 23, 2003.

Zhou, X., Y. He, G. Huang, T. D. Thornberry, M. A. Carroll, and S. B. Bertman (2002), PHOTOCHEMICAL PRODUCTION OF NITROUS ACID ON GLASS SAMPLE MANIFOLD SURFACE, *Geophysical Research Letters, 29*, 1681-1685.

Zhou, X., H. Qiao, G. Deng, and K. Civerolo (1999), A METHOD FOR THE MEASUREMENT OF ATMOSPHERIC HONO BASED ON DNPH DERIVATIZATION AND HPLC ANALYSIS, *Environmental Science & Technology, 33*, 3672-3679.